AFGL-TR-87-0134

AD-A201 039

Report on Results of Borehole Tilt Measurements From the Charlevoix Observatory, Quebec

John Peters
Christopher Beaumont

Dalhousie University
Oceanography Department
Halifax, Nova Scotia, CANADA B3H 4J1

30 November 1986

Final Report
9 February 1983-9 August 1986

AIR FORCE GEOPHYSICS LABORATORY
AIR FORCE SYSTEMS COMMAND
UNITED STATES AIR FORCE
HANSCOM AIR FORCE BASE, MASSACHUSETTS 01731-5000

Unclassified

SECURITY CLASSIFICATION OF THIS PAGE *(When Data Entered)*

REPORT DOCUMENTATION PAGE

READ INSTRUCTIONS BEFORE COMPLETING FORM

1. REPORT NUMBER AFGL-TR-87-0134	2. GOVT ACCESSION NO. A201-039
3. RECIPIENT'S CATALOG NUMBER	
4. TITLE *(and Subtitle)* Report on Results of Borehole Tilt Measurements from the Charlevoix Observatory, Quebec	5. TYPE OF REPORT & PERIOD COVERED Final Report 9 Feb 1983 - 9 Aug 1986
	6. PERFORMING ORG. REPORT NUMBER
7. AUTHOR(s) John Peters and Christopher Beaumont	8. CONTRACT OR GRANT NUMBER(s) F19628-83-K-0023
9. PERFORMING ORGANIZATION NAME AND ADDRESS Oceanography Department, Dalhousie University, Halifax, Nova Scotia, Canada, B3H 4J1	10. PROGRAM ELEMENT, PROJECT, TASK AREA & WORK UNIT NUMBERS 61102F 2309G2AN
11. CONTROLLING OFFICE NAME AND ADDRESS Air Force Geophysics Laboratory Hanscom A.F.B. MA 01731 Monitor / J. Cipar / LWH	12. REPORT DATE Nov. 31, 1986 30 13. NUMBER OF PAGES 76
14. MONITORING AGENCY NAME & ADDRESS *(if different from Controlling Office)*	15. SECURITY CLASS. *(of this report)* Unclassified 15a. DECLASSIFICATION DOWNGRADING SCHEDULE

16. DISTRIBUTION STATEMENT *(of this Report)*

Approved for public release; distribution unlimited

17. DISTRIBUTION STATEMENT *(of the abstract entered in Block 20, if different from Report)*

18. SUPPLEMENTARY NOTES

19. KEY WORDS *(Continue on reverse side if necessary and identify by block number)*

Earth tides, tiltmeters, tidal loading, seismic activity, linear and nonlinear tides, groundwater.

20. ABSTRACT *(Continue on reverse side if necessary and identify by block number)*

See reverse for abstract.

DD FORM 1 JAN 73 1473 EDITION OF 1 NOV 65 IS OBSOLETE

Unclassified

SECURITY CLASSIFICATION OF THIS PAGE *(When Data Entered)*

This report comprises four papers that discuss the results of our borehole tilt observations from the Charlevoix region of Québec, Canada. It should be read in conjunction with our 1983 report from contract F19628-80-C-0032.
The papers are:
1) 'Borehole Tilt Measurements from Charlevoix, Québec'
by J. Peters and C. Beaumont.
2) 'Tidal and Secular Tilt from an Earthquake Zone: Threshold Baselines for Detection of Regional Anomalies'
by J. Peters and C. Beaumont.
3) 'Non-linear Tilt Tides from the Charlevoix Seismic Zone in Québec'
by J. Peters and H.-J. Kümpel.
4) 'Nontidal Tilt and Water Table, Variations in a Seismically Active Region in Québec, Canada'
by H.-J. Kümpel, J.A. Peters, and D.R. Bower.

The array of three tiltmeters is arranged as an equilateral triangle of approximately 80 m side. Two of the Bodenseewerk Gbp tiltmeters operate at a depth of 47 m and the third at 110m. The Charlevoix region is one of high intraplate seismicity and the tiltmeter array was designed to investigate the relationship between earthquake activity, the tectonic stress that induces it, and the tilting of the Earth's surface under the combined effects of the earth tide, marine tidal loading, and tectonic stress.

Paper 1 describes the site, installation procedures, and preliminary analysis of the linear tidal data and drift characteristics for the 1981/1982 time interval for two tiltmeters.

Paper 2 extends the analysis of the data to include data from all three tiltmeters to the end of the experiment, March 1986. The highly coherent admittance variations in both the linear and nonlinear tides are shown to be largely due to temporal variations in the tidal loading from the St. Lawrence River estuary. No variations that are unequivocally 'tectonic' in origin were detected. This is not surprising because the level of seismicity in the immediate vicinity of the tiltmeter site was low during the observation period.

Paper 3 comprises a detailed analysis of a subset of the data for the mean and variations of the nonlinear tidal constituents, in particular M_4 and M_6. The mean values can be attributed to tidal loading by these constituents in the St. Lawrence estuary. Similarly, the high variability is also considered to result from the variability in the marine tides, although this cannot be proven due to the lack of a detailed knowledge of the spatial aspects of the marine tide time variations during the period of observation.

Paper 4 contains a discussion of the nontidal aspects of the tilt signal and its correlation with seasonal and transient water table fluctuations. A model is presented in which the distortion of the rock mass, as measured by the tiltmeters, can be attributed to the pressure from groundwater variations through Biot's consolidation theory for porous media.

Table of Contents

4) NON-TIDAL TILT AND WATER TABLE VARIATIONS IN A SEISMICALLY ACTIVE REGION IN QUÉBEC, CANADA

JOURNAL OF GEOPHYSICAL RESEARCH, VOL. 90, NO. B14, PAGES 12,791–12,806, DECEMBER 10, 1985

Borehole Tilt Measurements From Charlevoix, Québec

JOHN PETERS AND CHRISTOPHER BEAUMONT

Oceanography Department, Dalhousie University, Halifax, Nova Scotia, Canada

An array of three borehole tiltmeters near Québec City in eastern Canada is designed to study the tidal and secular response of the crust in the Charlevoix seismic zone. The objectives of this study of the first year of data from two boreholes of the array are to investigate the spatial coherency of the tidal observations and determine whether there are time variations in the tidal amplitudes and phases and to describe the main features of the secular tilt signal. The tidal analysis was done using a modified version of the HYCON harmonic analysis program with which the time-varying tidal amplitudes and phases were determined by the sequential analysis of overlapping 2-monthly subsets of the data. The admittance observed for the major semidiurnal (M_2) and diurnal (O_1) constituents varies by up to 10 and 30%, respectively, and is strongly correlated between boreholes. Comparison with admittance variations determined from two nearby tide gauges indicates a strong correlation in the amplitude fluctuations, pointing to a predominantly marine loading source for the time-varying tilt admittance. Differences of up to 20% in amplitude and 5° in phase were found between the mean M_2 results determined from boreholes 1 and 2, located only 80 m apart, indicating small-scale distortion of the local tilt field by lateral inhomogeneities. The secular tilt from both boreholes correlates strongly with transient and seasonal water table fluctuations, suggesting the dominant influence of pore pressure effects on the nontidal tilt. A preliminary estimate of the detectability of long-term regional trends in tilt is 0.4 μrad yr.

1. INTRODUCTION

An array of three borehole tiltmeters has been installed in the Charlevoix region of Québec (Figure 1), one of the most seismically active areas in eastern North America. The tilt observations are being made at the Charlevoix Geophysical Observatory of the Canadian Department of Energy, Mines and Resources and are intended to investigate the behavior of crustal rocks in an earthquake zone. Specifically, the measurements are designed to sample the earth tide response as a possible indicator of changing crustal conditions and, by monitoring secular and transient tilts, to directly detect regional crustal deformations associated with processes occurring at depth.

This first analysis of the borehole tilt data from the Charlevoix Observatory provides an explanation of the first-order properties of the secular tilt, establishes a methodology for determining the real variations in the tidal admittance, and applies this approach to the Charlevoix data. On the basis of our results we then assess the potential of using the time-varying tidal admittance at Charlevoix as an indicator of changes in crustal response and of using the secular component to detect long-term tilts of tectonic origin.

The first study of tidal response in relation to earthquake activity was reported by *Nishimura* [1950] who recorded fluctuations of up to 75% in monthly amplitude determinations of the M_2 constituent using quartz pendulums installed in Makimine copper mine, Japan. More recent results from the same station [*Tanaka*, 1976] indicated amplitude variations not exceeding a range of 20%, suggesting that the extraordinary amplitude changes seen by Nishimura included instrumental effects. Other studies have indicated less dramatic but physically more reasonable effects: measured tidal response variations generally not exceeding 15%. Monthly M_2 strain amplitudes recorded at Kamitakara from 1968 to 1972 [*Mikumo et al.*, 1978] showed a steady rise of 15% during the 11 months prior to the 1969 Gifu ($M = 6.6$) earthquake. *Kato* [1979] measured 2.4% amplitude fluctuations in M_2 from observations recorded by a water tube tiltmeter, also at Kamitakara, from September 1977 to October 1978. *Agnew* [1979] has studied the time variation of M_2 in strain data recorded on the 800-m laser strain meter at Piñon Flat, California. From 1973 to 1978 fluctuations were confined within 2% of the mean amplitude. Given the high signal to noise ratio (45dB) of the estimates and the fact that Piñon Flat is locally an aseismic region, this result establishes an experimental baseline upon which to evaluate the significance of time variations in admittance in active seismic zones.

Beaumont and Berger [1974] suggested that if V_p, V_s seismic velocity anomalies are indicative of changes in crustal elastic properties, then they should be accompanied by tidal response anomalies. Tilt anomalies would be the result of contrasts in the elastic properties of an anomalous crustal inclusion with the surrounding normal crust. For example, a 15% reduction in V_p within the crustal inclusion would be accompanied by a maximum 30–40% change in amplitude at the edge of the inclusion, decreasing rapidly with distance away from it. *Tanaka* [1976] used a similar approach to predict the modification of the marine load tide response due to a dilatant zone near a coastline. *Beaumont* [1978*a*] expanded on the work of *Beaumont and Berger* [1974] by considering the effect on the tidal response of the superposition of tidal and increasing tectonic stress regimes in the crust. Appealing to laboratory results which showed that hysteresis occurs in intact rock samples as they approach failure, he outlined ways in which linear and nonlinear anomalies in the tidal response may be generated depending on the rate of change of stress in the crust. *Agnew* [1981] considered different types of nonlinearities and searched without success for their signature in strain records at Piñon Flat.

There have been many attempts to measure meaningful subtidal tectonic tilts and strains (see, for example, *Wyatt et al.* [1982], *McConnell and Lewkowicz* [1978], *Herbst* [1976], and *Mortensen and Johnston* [1975]). Few have been demonstrably successful, for the most part because such measurements are carried out near the surface where they are severely polluted

Paper number 4B5073.
0148-0227/85/004B-5073$05.00

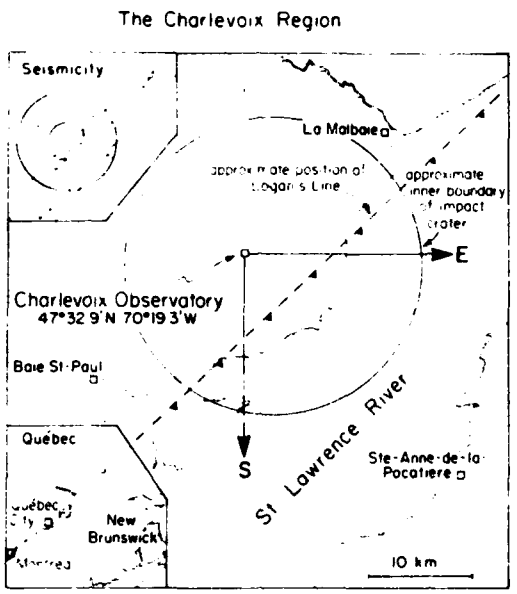

Fig. 1. Location of the Charlevoix Observatory. The lower inset shows the observatory area in relation to the St. Lawrence river valley. The upper inset shows the spatial relationship of recent seismicity in the region to the zone of deformation associated with the Charlevoix crater [after *Lyons et al.*, 1980]. The two circles define the inner and outer boundaries of the crater.

by other, inseparable signals usually of meteorological origin. It is clear that any hope of success lies in an approach which either ensures the isolation of the measurement from these sources of noise (by deep enough burial) or one which utilizes a spatial average of the near-surface signal. This second approach may involve a network of instruments and subsequent statistical elimination of noise [*Mortensen and Johnston*, 1975], or the use of long-baseline instruments [*Wyatt et al.*, 1982]. These methods assume that the spatial scales of the meteorological and other sources of noise are less than that of true tectonic tilt anomalies. *Wyatt et al.* [1982], in an important comparative experiment at Piñon Flat, demonstrated the relative potential for secular tilt studies of measurements performed over a long baseline (535 m), at moderate depth (26 m), and in shallow (5 m) borehole installations. Their results, for data spanning a 5-month period, indicate successive order of magnitude increases in the drift rates from the long-baseline tiltmeter (0.07 μrad/month) to the 26-m-deep borehole tiltmeter (0.4 μrad/month) to the shallow installations (up to 7 μrad/month). However, the most encouraging results to date are those of *Cabaniss* [1978], who measured a net secular drift of 0.3 μrad in a 120-m-deep borehole at Bedford, Massachusetts over a 3-year period.

The Charlevoix region has a history of large earthquakes occurring roughly every 60 to 90 years. The last major earthquake was a magnitude 7 which struck in 1925. Seismicity surveys in 1968, 1970, and 1974 [*Milne et al.*, 1970; *Leblanc et al.*, 1973; *Leblanc and Buchbinder*, 1977] show that the earthquake zone covers a 70 by 40 km region centered on the St. Lawrence River 150 km northeast of Québec City (Figure 1, inset). Almost all the earthquakes were shown to have occurred within the Precambrian rocks of the Grenville Province, at an average depth of 11 km. The nodal plane solutions are compatible with pure thrusting, the planes dipping on average 40° to the west and 50° to the east [*Leblanc and Buchbinder*, 1977] with the direction of the pressure axis not in disagreement with what *Sbar and Sykes* [1973] found in other parts of North America. Seismic crustal studies [*Lyons et al.*, 1980] indicate that the contact between the Grenville basement and the base of the Ordovician overthrusts outcrops at Logan's Line along the north shore of the river and dips beneath the river to the southeast at an average angle of 20°. It appears that the length of the seismic zone parallel to the river is related to the conjunction of Logan's Line and the 350-Ma Charlevoix impact crater [*Leblanc and Buchbinder*, 1977]. Presumably, either the structures represent a zone of weakness, remaining from crustal damage caused during the impact, in which tectonic stress is released by earthquakes, or the structures focus the tectonic stress in some way causing a higher rate of seismicity in an otherwise normal crust.

Since 1972, geophysical measurements have been made in the Charlevoix area by the Earth Physics Branch of the Department of Energy, Mines and Resources, in addition to geodetic and leveling surveys conducted by the Geological Survey of Canada. The present measurements [*Buchbinder et al.*, 1983] comprise first-order leveling along the north and south shores of the St. Lawrence River; a precise gravity network consisting of 15 stations and 22 connections; a triangulation network consisting of 12 points and 26 connections spanning the St. Lawrence River; two permanent tide gauges; a permanent seismic observatory at La Pocatière on the south shore; an array of four magnetotelluric stations; and tilt, strain, seismic and magnetotelluric installations located at the Charlevoix Observatory and operating in conjunction with the borehole tiltmeter program discussed in this study.

In the following sections, we briefly describe the borehole tiltmeter experiment and discuss the methods and procedures used in analyzing the data. Results are presented for the M_2 and O_1 mean and time-varying admittances and for the behavior of the secular tilt component.

2. The Borehole Tiltmeter Array

The borehole array consists of three holes, two of which (boreholes 1 and 2) are 47 m deep and the third of which (borehole 3, only recently instrumented) is 110 m deep [*Peters*, 1983]. Each is cased with a 20-cm-diameter mild steel casing terminated by a 6-m-long stainless steel pod of the same diameter which houses the tiltmeter. All of the holes are dry, but only the shorter two are straight. Figure 2 is a diagram of the experimental configuration, showing a plan view of the observatory and the tiltmeter installation in section (see figure caption for details). Adjacent to each of the boreholes is a well (referred to as A, B, or C) in which manual and continuous measurements of water level are made. A vault containing three Auckland Nuclear Accessory Company (ANAC) mercury level tiltmeters is situated near the centre of the borehole array [*Peters et al.*, 1983*a*].

The borehole tiltmeters are Bodenseewerk Gbp 10 (formerly Askania) vertical pendulums [*Flach and Rosenbach*, 1971] chosen because of their proven performance [*Zschau*, 1976; *Edge et al.*, 1979, 1983; *Flach et al.*, 1975] and, not least, because they are the only high-quality tiltmeters commercially available and supported. The most important feature of the instrument is the accurate in situ calibration absent in most other instruments but essential for the study of time variations in tidal admittance from which the effects of sensitivity changes of the tiltmeter and the recording system must be eliminated. The calibration takes the form of a sequence of repeated 150-nrad offsets caused by electromechanically

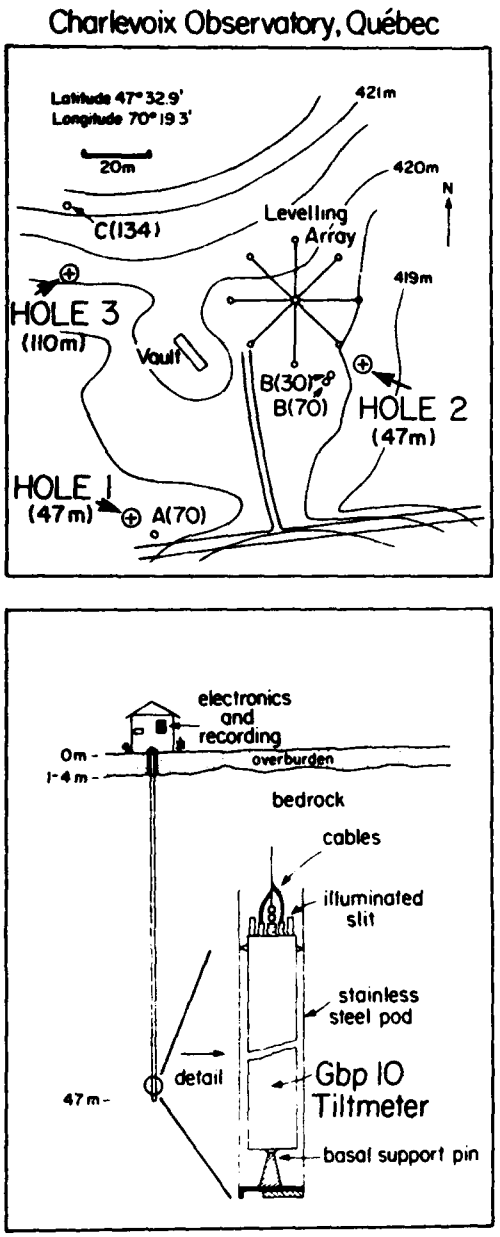

Fig. 2. (Top) Plan view of the Charlevoix Observatory showing the locations of the three boreholes; water wells A (70 m deep), B (two wells 30 and 70 m deep), and C (134 m deep); the tilt and strain observatory vault; and the 40-m baseline leveling array. (Bottom) Cross-sectional view of the borehole layout. The tiltmeter rests on a stainless steel support pin attached 1.5 m above the base of the casing and is held vertical by three spring-loaded pins near the top of the instrument [*Bodenseewerk Geosystem*, 1979].

moving a small metal ball back and forth between two fixed locations on the tiltmeter pendulum, thereby displacing its center of mass and causing a tilt [*Grosse-Brauckmann*, 1976]. The absolute value and accuracy of the calibration are determined by the manufacturer on the basis of the geometry of the arrangement. In this experiment it is the repeatibility of the calibration that is most important. Changes in the mean of the calibration sequences serve to calibrate the sensitivity of the transducer, the electronics, and the recording system. It is assumed that a stable amplitude response of the system to calibration pulses is also indicative of a stable phase response.

The tiltmeters in boreholes 1 and 2 are oriented photographically [*Peters et al.*, 1983*b*]. A reference line over the borehole at the surface is photographed using a short focal length lens. A second exposure on the same frame is then taken, with a telephoto lens, of illuminated slits located on top of the instrument and aligned with the measuring axes. The tiltmeter azimuth is determined graphically by measuring the angle between the reference line and slit images on a photographic print. The precision achievable with this approach is limited by the quality of the exposure and the size of the print. In the present case, the azimuth is determined to better than 0.25 degrees.

3. Data Analysis

Data Preparation

The data analyzed in this study were recorded during the periods: September 27, 1980, to June 29, 1981 (tiltmeter 105 in borehole 1); November 27, 1981, to December 31, 1982 (tiltmeters 107 and 106 in boreholes 1 and 2, respectively, and tide gauge St. Joseph de la Rive); and January 24, 1982, to December 31, 1982 (tide gauge Tadoussac). The tilt data were recorded on strip chart recorders at a recording speed of 30 mm per hour and at a sensitivity of approximately 0.2 mm/nrad. Hourly time marks were superimposed on the recordings and the data digitized at these marks. Spurious points, resets, and short thermal trends were removed, and a few gaps of under 24 hours duration were manually interpolated on the basis of data before and after the gap. This was possible because the long-period trends in the data change slowly in comparison with the tide.

The data were scaled using calibration factors derived from twice-weekly in situ calibration sequences (see section 2). Each sequence consisted of 12 to 18 individual offsets which, when averaged, showed a typical standard deviation of 0.1 mm (equivalent to 0.5 nrad), limited by the resolution of the digitizing table. The population of calibration means was homogeneous at the 95% confidence level, allowing a single scale factor to be determined with a precision of 0.1% for each of the analyzed tilt time series.

Prior to analysis the data were digitally filtered to separate the tides from the long-period and secular components of the signal. For the harmonic analysis a 61-point symmetrical bandpass filter designed to pass the diurnal and semidiurnal bands was used. The response of the filter was computed for each tidal frequency in the harmonic analysis and the computed amplitudes corrected for the small effects, typically 0.1%, of the filtering. A high-pass filter was used to prewhiten the data prior to the power and high-resolution spectral analyses, and the estimates were subsequently corrected for its effect.

Harmonic Analysis

The aim of harmonic analysis of the tilt data is to determine accurately the amplitudes and phases of tidal constituents of known frequency within the data. For this study the constituents of interest are those of astronomical origin which either contain sufficient energy to be recognizable above the noise or are unresolved in the analysis yet must be included to avoid significant modulation of the adjacent spectral components. This consideration is particularly important in the study of time variations in the constituents where it is necessary to distinguish between actual changes in the earth response or the tidal forcing, and apparent admittance changes due to

modulation when finite samples of the data are analyzed. We have used the HYCON method of *Schüller* [1977] (see appendix) in which the original 505 astronomical frequencies have been reduced to 73 having theoretical earth tide amplitudes (ignoring tidal loading) greater than 0.1 nrad. This represents a compromise between the cost of computation and the precision required of the analysis, and is justified later by comparison with the background noise level. Since constituents closely spaced in frequency cannot be resolved for the data window used, those clustered around each of the 10 main constituents are assumed to have the same admittance.

The HYCON program computes the theoretical earth tide, forms and solves the normal equations separately for overlapping subsets of the data, and outputs a time series of estimates of the admittance of the observed data to the body tide input. The associated error for each of the estimates is computed for each tidal species (diurnal and semidiurnal) on the basis of the frequency dependent residual variance determined from Fourier analysis of the residual time series [*Schüller*, 1977].

One of the chief advantages of the HYCON method is that it combines the spectral analysis technique of windowing the data, using the Hanning window, with the least squares analysis for the admittance of the tidal frequencies. The approach recognizes that the effects of the spectral side lobes associated with the rectangular window are operative even in regression analysis when the model does not exactly describe the data, a situation we normally encounter when we try to fit a deterministic model to a signal comprising mixed periodic, aperiodic, and random components. Because the Hanning spectral window broadens the spectral peaks by comparison with those given by the equivalent rectangular window, the minimum data window must be increased to 2 months in order to avoid the leakage of energy between the major tidal groups, especially M_2 and N_2. This correspondingly reduces the number of independent estimates of the admittance for the 1981/1982 data sets to six.

Our approach to the analysis of potentially nonstationary tidal signals is to assume that admittance changes are sufficiently slow that 2-month samples may be considered to be stationary. By analyzing samples that overlap in time we expect to detect variations in the Earth's tidal response, or the tidal forcing, as changes in the average admittance from one sample to the next. In practice, the sequence of average admittances (which we will refer to as the admittance function) may reflect apparent but unreal time variations which result either from the inaccuracy of the assumption that the admittance does not vary within a tidal group or from the effects of nonlinear or other constituents of a nonastronomical origin that are not modeled by the theory. In both cases, periodicities will be induced which result in a time-varying admittance function due to intermodulation. Considerable care is required to properly detect such modulation and to distinguish it from real time variations in the earth response or the tidal forcing.

As pointed out by *Schüller* [1977], the admittance functions are equispaced time series, and care must be taken to avoid aliasing. The Nyquist frequency is given by $\omega_c = \pi/\Delta T$, where ΔT is the time shift of the sequential epochs. The maximum frequency present in the admittance function is determined by the bandwidth of the Hanning window, $B_h = 4\pi/T$, where T is the length of the sample epoch. Thus the condition $\Delta T < T/4$ determines the maximum time shift required to avoid aliasing in the sequential analysis. The sample epoch for the present analysis was chosen to be 1440 hours in order to separate the main tidal groups, and the time shift was set to 288 hours, which satisfies the above condition.

Apart from the fact that a continuous record is desirable if we hope to reliably detect departures from a stable admittance function, it is also logistically necessary if we wish to perform the type of analysis described above. Gaps exist in our data and after filtering, with attendant loss of data, amount to approximately 18% for 106 and 12% for 107 of the total recording period. Gaps can be interpolated within the HYCON program using the synthesized tide based on the mean admittance of the total data set. Any interpretation of the results must take this into account, since the degree of interaction of the Hanning data window with the synthesized data depends on the position of the filled gap within the sample epoch. The relative contribution of the synthesized data, in terms of its weighting by the Hanning window, to the analysis of each overlapping sample epoch has been computed and each sample estimate coded according to whether the contribution is less than 10%, between 10 and 20%, or greater than 20%. We consider that estimates affected at a level greater than 20% are not reliable. Although this treatment is not an ideal solution, it goes further than most in dealing with the difficult problem of data continuity and represents an attempt to get the most out of what amounts to an average working data set.

A representative estimate of the mean tidal admittance is necessary for comparison of the average coherency among the three borehole tiltmeters and the vault measurements and for comparison of the observations with the theoretical tilt based on a marine loading model (section 4). *Schüller* [1977] argues that the best, unbiased estimate of the mean admittance is derived from the means of the in-phase and quadrature components of the time-varying admittance function determined as above, since any bias due to aliasing is avoided. The error in the estimate is derived from the variance of the time-varying admittance function.

Fourier Analysis of the Tidal Residuals

Power spectra of the tilt tidal residuals, with the Hanning window applied, were computed to determine an upper limit of the signal to noise ratio for the main tidal constituents. The ensemble average of five independent 2-month sets covering the 13 months of data studied was calculated to increase the stability of the estimates.

With a view to examining the detailed spectral content of the tidal residuals, a high-resolution Fourier amplitude spectrum was calculated, with the Hanning window applied, for the tilt time series, after subtracting the mean tidal estimates resulting from the sequential harmonic analyses. Our main objective in this high-resolution analysis was to identify unresolved and unaccounted for constituents (resulting, for example, from shallow water, nonlinear interactions) which possess enough energy to influence the major groups in the 2-month analyses. In addition, there is the possibility that unresolved astronomical constituents, forced to have the same admittance as the rest of their group under the constant admittance assumption, are modeled poorly and can therefore modulate one of the principal constituents.

4. THE MARINE TIDAL LOADING MODEL

The load tilt calculations were made by the same method as those of *Beaumont and Lambert* [1972], *Beaumont* [1978*b*], and *Beaumont and Boutilier* [1978], using the Farrell Gutenburg Bullen (FGB) earth model [*Farrell*, 1972]. The Green functions for the point load response of the earth model were computed and the integrated effect of the ocean tide distribution found by convolving the Green functions with the in-

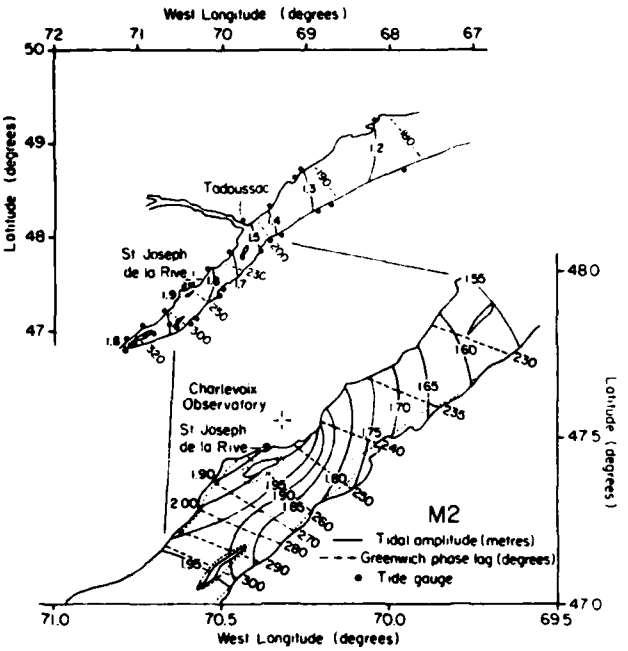

Fig. 3. Empirical M_2 cotidal chart for the St. Lawrence estuary, with detail of the area adjacent to the Charlevoix site. Dots mark the location of the tide gauge installations.

phase and quadrature components of the tidal distribution. The cotidal charts were divided into triangular areas in which the amplitude and phase of the tides could be regarded as being constant in order that the convolution could be evaluated numerically [*Bower*, 1971]. A more detailed representation of the tides in the St. Lawrence estuary and Saguenay river is used here than in the earlier work because most of the load tilt is generated close to the Charlevoix Observatory. The cotidal charts for this region (Figures 3 and 4) are empirical and based on observations from the coastal sites indicated

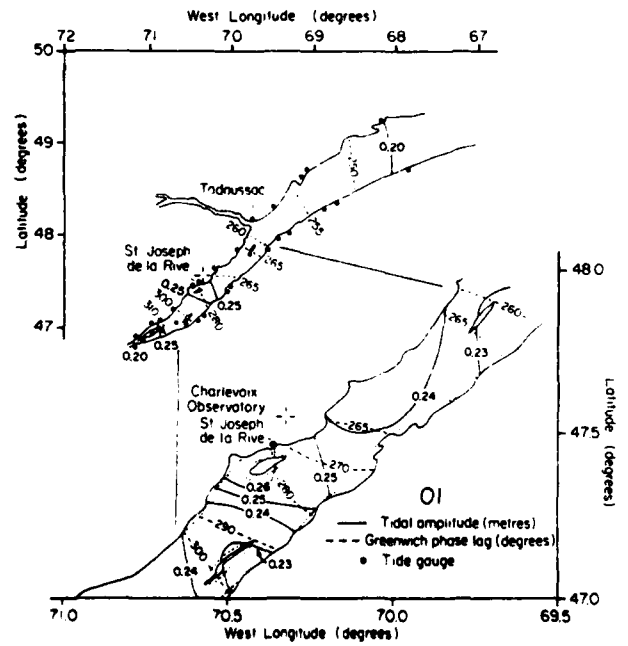

Fig. 4. Empirical O_1 cotidal chart for the St. Lawrence estuary, with detail of the area adjacent to the Charlevoix site. Dots mark the location of tide gauge installations.

and on numerical calculations of the M_2 and O_1 constituents [*El-Sabh et al.*, 1979]. We suspect that the largest errors in the marine tidal loading model arise from areas that "dry" during the tidal cycle (outlined by the fine dashed lines in Figures 3 and 4). For this reason the computation has been done for two extreme cases in which there is no drying and in which areas that dry remain permanently dry.

5. Results

Correlation of Secular Tilt With Water Level Changes

Figures 5*a* and 5*b* show the low pass filtered observations (decimated to 48 hours) for tiltmeter 105 operating in borehole 1 during 1980/1981 and tiltmeters 107 and 106 operating concurrently in boreholes 1 and 2 during 1981/1982. Also shown are hand-measured water level data observed in well B(70) near borehole 2. The east and south components of 105 show similar behavior, both in the short and the long term. The total range of the 105 drift in each direction over the 260-day interval is 1.5 μrad. Although the water level is not adequately sampled to show short-term fluctuations, there is a strong long-term correlation with the tilt. A similar correlation exists between water level and tilt for tiltmeters 106 and 107. Furthermore, the directions of highest correlation with water level changes are similar for each of the boreholes. This can best be

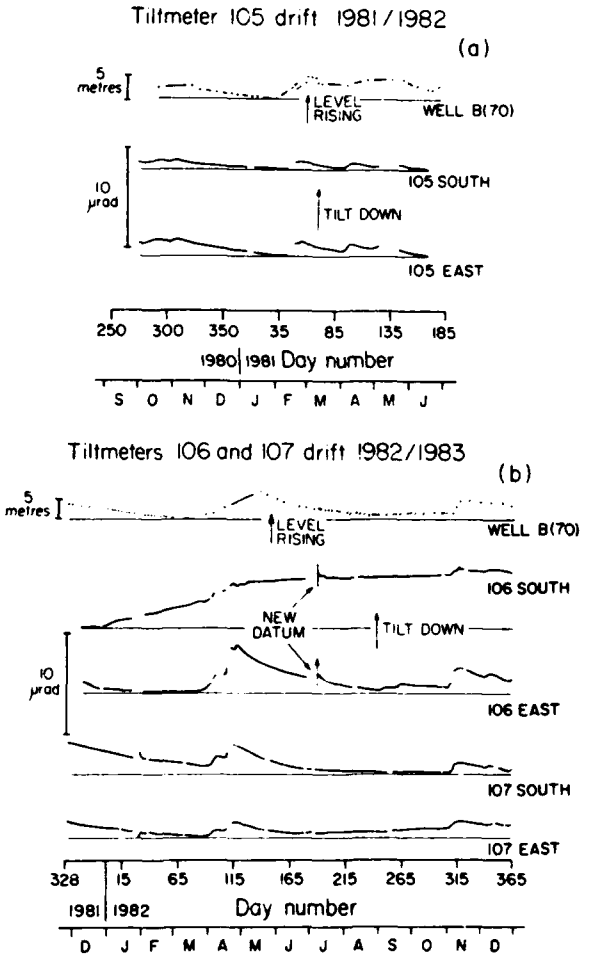

Fig. 5. Plots versus time of secular tilt for (*a*) tiltmeter 105 operating in borehole 1 from September 1980 to June 1981; (*b*) tiltmeters 107 and 106 operating in boreholes 1 and 2, respectively, from November 1981 to December 1982. Also shown for both periods are manual measurements of water level taken from well B (70).

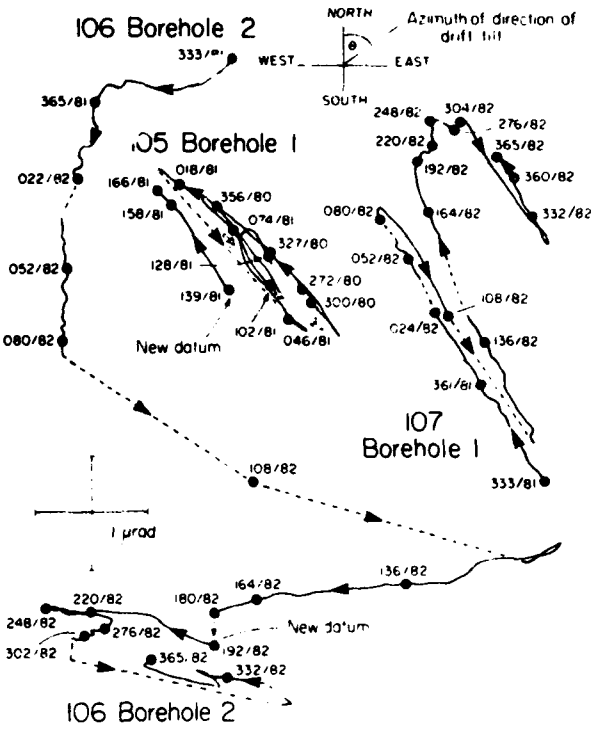

Fig. 6. Secular tilt trajectories of tiltmeter 105 operating in borehole 1 and tiltmeters 107 and 106 operating in boreholes 1 and 2 for the same periods indicated in Figure 5. Each trajectory describes the path taken by the bottom of the freely hanging pendulum relative to the instrument body. Reference times are marked by full circles and show the Julian day number and year.

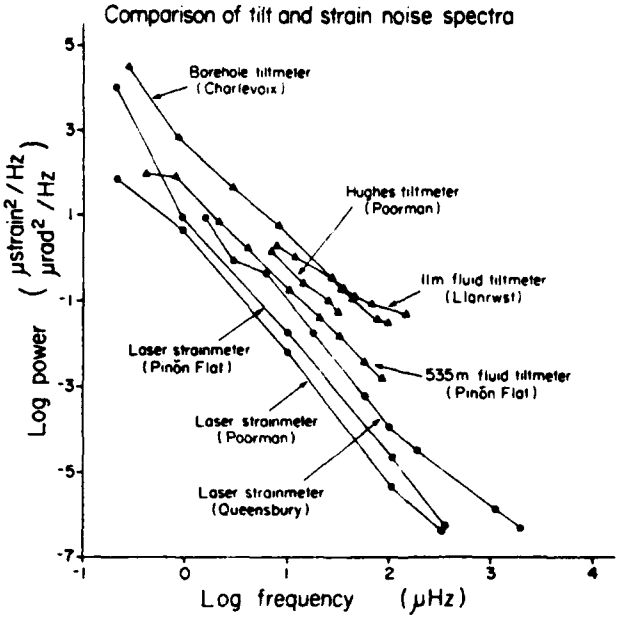

Fig. 8. Comparison plot of tilt and strain background noise spectra taken from various sites: Piñon Flat, California: laser strainmeter [*Berger and Levine*, 1974], fluid tiltmeter [*Wyatt et al.*, 1982]; Queensbury, U.K.: laser strainmeter [*Beavan and Goulty*, 1977]; Poorman mine, Colorado: laser strainmeter [*Berger and Levine*, 1974]. Hughes bubble tiltmeter [*Harrison*, 1976]; Llanrwst, U.K.: fluid tiltmeter [*Peters*, 1978]; Charlevoix, Québec: borehole tiltmeter (this study). The sampled points are represented by solid circles in the case of strain and solid triangles for the tilt measurements. Logarithms are to base 10.

seen in the tilt trajectories plotted in Figure 6. The predominant drift direction, θ, for 105 has an azimuth of 135°, and for 107, operating in the same borehole one year later, the drift azimuth is 145°. The situation for 106 is more complicated. We believe that from the time of installation in 1981 to day 180 (June 29) of 1982, tiltmeter 106 was not well seated in the borehole and was unstable. After day 180, 106 was reinstalled, and from this time, tilt in the 100° azimuth correlated closely with the water level changes. This indicates a difference between the two boreholes in the direction of the water level effect of about 40°. Also, the amplitude of the tilt apparently induced by the water level changes is different for each borehole. Tiltmeters 105 and 107 in borehole 1 yielded an average 0.4 μrad per meter of water level change, while tiltmeter 106 in borehole 2 yielded approximately 0.7 μrad per meter. It is not surprising that in an area of fracture-dominated permeability (on the evidence from drilling operations), water level induced tilts vary in direction and amplitude on a scale of 80 m, since we expect the fractures in the immediate vicinity of each borehole to dominate the local response.

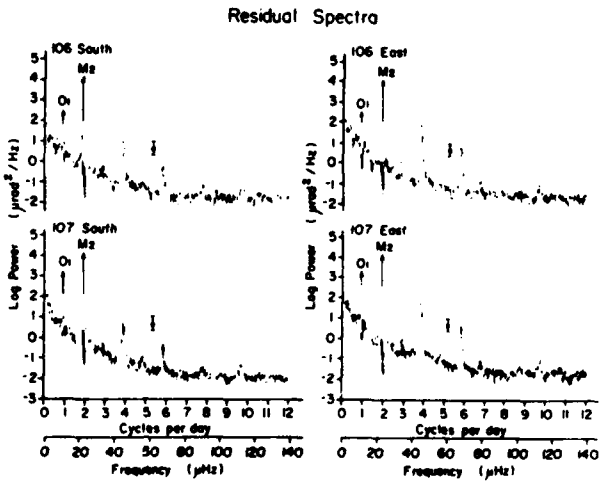

Fig. 7. Residual power spectra of the south and east components of tiltmeters 107 and 106 operating in boreholes 1 and 2, respectively. The observed M_2 and O_1 power levels are indicated by the tip of the arrows. The error bars represent 95% confidence bounds on the randomness of the background noise. Logarithms are to base 10.

There is a very clear monotonic drift in 107 of 1.2 μrad to the northeast ($\theta = 45°$) in addition to the first-order ($\theta = 135°$) cyclical effect that correlates with the water level. There is evidence of a similar but smaller trend in 106, although the direction may be reversed. The sense of the residual drift in the case of 105 is not certain because the annual water level related cycle was not completed. The origin of this component of the long-term tilt is not known.

Power Spectrum of the Residual Time Series

The accuracy of the tidal estimates depends upon the residual energy in the tidal bands. Before discussing the tidal results, we will examine the residual power spectra shown in Figure 7 for both components of tiltmeters 106 and 107.

The residuals in all components share a number of common features. First, there is a strong presence of quarter, sixth and tenth diurnal energy, most likely generated by loading from

shallow water nonlinear interactions [*Baker*, 1980; *Agnew*, 1981], since similar energy resides in the St. Lawrence tide gauge spectra [*Godin*, 1973]. Otherwise, the spectra consist of a statistically featureless background which decreases in power with increasing frequency but flattens out beyond 70 μHz (6 cpd) at a level of 0.025 nrad^2/μHz (power spectral density). Last, there is a distinct "hole" in the semidirunal band, as expected, where most of the energy has been removed in the least squares analysis for the tidal constituents. However, there is also significant residual energy, more prominent in 106, remaining in that band, suggesting that the linear tidal model cannot account for all of the signal.

It is interesting to compare the residual background noise, after removal of the tides, among different measurements which cover a range of techniques and geographical locations. In Figure 8, we compare the published background noise spectra from three strain and four tilt measurements, including that of 107 east from borehole 1 as representative of the Charlevoix experiment (see figure caption for details). The spectra are plotted on a log-log scale, and all show the characteristic "red noise" linear trend typical of geophysical spectra plotted in this way. Interestingly, the slopes among the strain spectra and among three of the tilt spectra are remarkably consistent. In the case of strain the relationship between noise power P and frequency f is $P \propto f^{-2.9}$. For each of the tilt measurements, $P \propto f^{-2.3}$, excepting Llanrwst, where the noise level decays more slowly. There is a clear geographical relationship evident among the spectral characterisitics. Those measurements which are most strongly influenced by marine loading effects (Queensbury, Llanrwst, and Charlevoix) possess the highest background noise persisting over the entire spectrum. It is apparent that in coastal locations the lower limits to ground noise are determined by dynamical effects in the oceans. It is not clear whether this is also the case for inland sites.

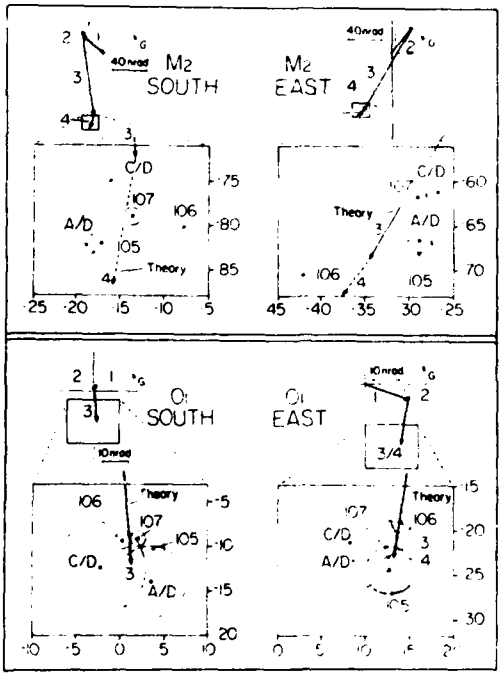

Fig. 9. Polar diagrams showing the comparison with theory of the mean M_2 and O_1 admittances observed for the south and east components of tiltmeters 105 (borehole 1), 107 (borehole 1), 106 (borehole 2), and the ANAC tiltmeters operating in the observatory vault. G is the Greenwich phase lag. The ANAC results are taken from *Peters et al.* [1983*a*] and rotated into their south and east components by combining the redundant A and C measurements with the single orthogonal D measurement. The theory is represented in the upper part of each diagram by the sum of the body tide (vector 1), the far-field load (vector 2), and the local load (vectors 3 and 4; see text). The lower part of the diagrams shows the detailed comparison between the observations and theory. The circles represent 95% errors on the mean admittance estimates.

Comparison of Observed and Theoretical Tidal Tilts

Figure 9 shows polar diagrams of the observed and computed M_2 and O_1 mean admittances for tiltmeters 105 and 107 (borehole 1); tiltmeter 106 (borehole 2); and the ANAC measurements A/D and C/D [*Peters et al.*, 1983*a*] made in the shallow vault (Figure 2). Also shown are the loading model results based on the computations outlined in section 4. *Peters et al.* [1983*a*] concluded that owing to the geometry of the vault and the expected strain-tilt coupling effects the ANAC measurements are best approximated by the average of the two measurements. An error of 180° in the phase of the ANAC D component quoted in their paper has been corrected.

There are substantial differences in the observed M_2 results among all of the measurements. A 5–8% amplitude discrepancy in both directions between 105 and 107, operating at different times in borehole 1, exceeds the range of variability so far determined. The averaged ANAC results do, however, plot between the borehole 1 observations. Tiltmeter 106 in borehole 2 lags the other measurements by 4–5° in the south direction and leads by nearly 7° in the east direction. Furthermore, there is a 20% difference between the 106 and 107 amplitudes in the east. The M_2 results, therefore, tend to fall into two groups: 106 in borehole 2 and the others. Meanwhile, the modeled M_2 tide is consistent with the range of observations. In the south, where drying is important, the borehole 1 and ANAC results lie within the range of the total drying (3) and nondrying (4) model vectors and may constrain the model to the partial drying case which lies between the two extremes and is physically the most realistic. In the east, however, the two observation groups lie at extremes of the possible theoretical vector and do not help constrain the model. In any case, the layered Earth model (FGB, see section 4) used to compute the tilt Green functions does not take into account the regional structure which is dominated by Logan's contact (section 1), nor are corrections made for the effects of local topography and geological structure. The O_1 observations are in fairly good agreement both among themselves and with theory.

Time Variations in the Tidal Constituents

One aspect of this study is to identify "true" variability, or lack of it, in the tidal constituents. By "true" variability we mean fluctuations that require an interpretation in terms of time changes in the Earth's response to the tidal forcing or changes in the tidal forcing itself. Our aim is first to eliminate apparent variations which either are artifacts of the analysis procedure or are due to intermodulation between constituents not separable over the analysis epoch.

The results of the time variant HYCON analysis described in section 3 are presented in the form of polar diagrams in which variations in admittance trace out a path, or trajectory, with a surrounding swath of error estimates, in polar coordi-

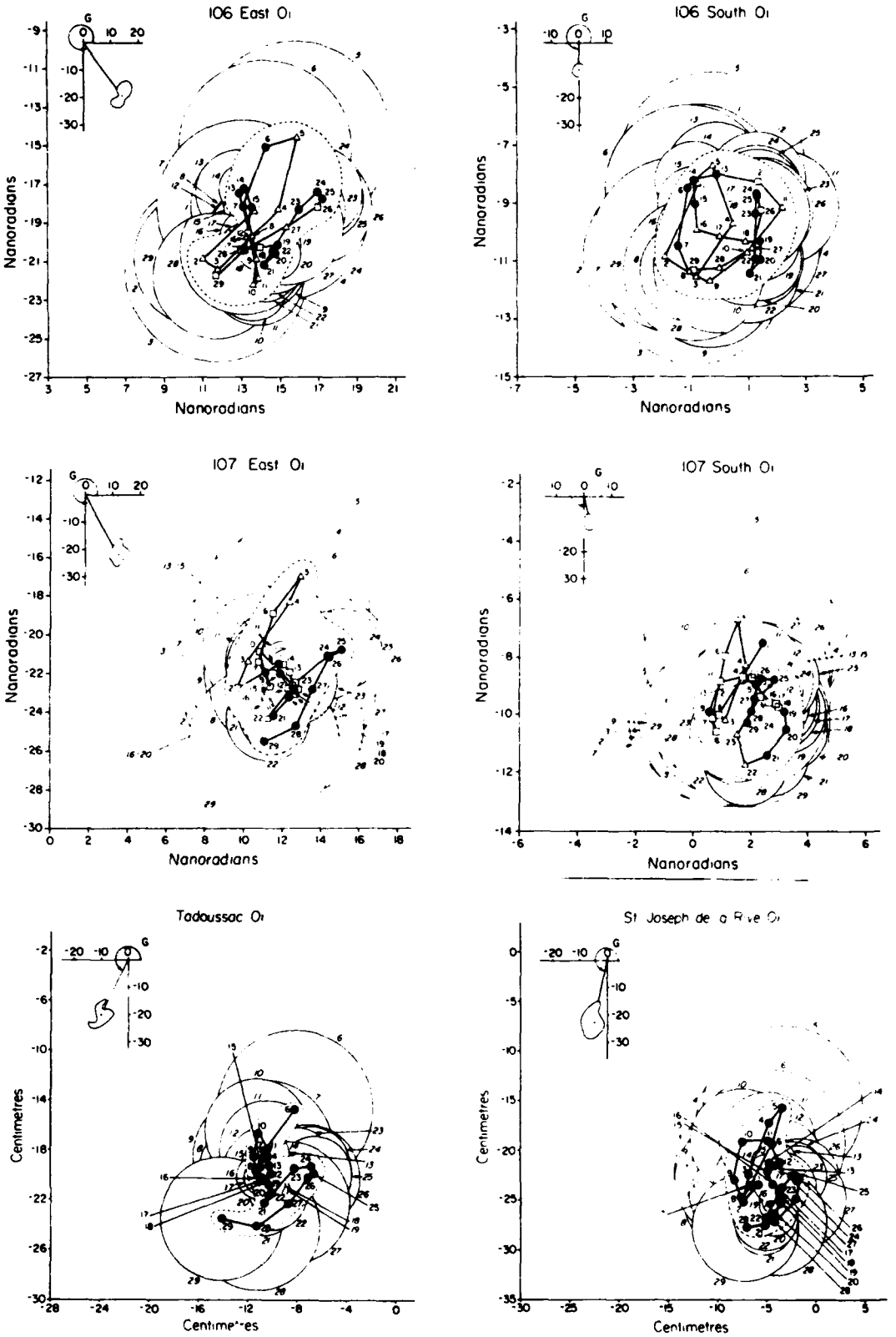

Fig. 10. Polar trajectory plots of the O_1 admittance for tiltmeters 106 and 107 south and east components and tide gauges St. Joseph de la Rive and Tadoussac, estimated from the HYCON sequential analysis. The observed mean admittance vector is shown in the upper part of each diagram. The shape surrounding the end point of the vector corresponds with the dashed curve surrounding the detailed trajectory plot. Each point on the trajectory is represented by a symbol indicating the degree to which that estimate is influenced by interpolated gaps (see text). Solid circles indicate an influence less than 10%, open squares less than 20%, and open triangles greater than 20%. Points associated with triangles are least reliable. Part of the 95% error circle associated with each estimate is indicated by a matching sequence number in sloping numerals.

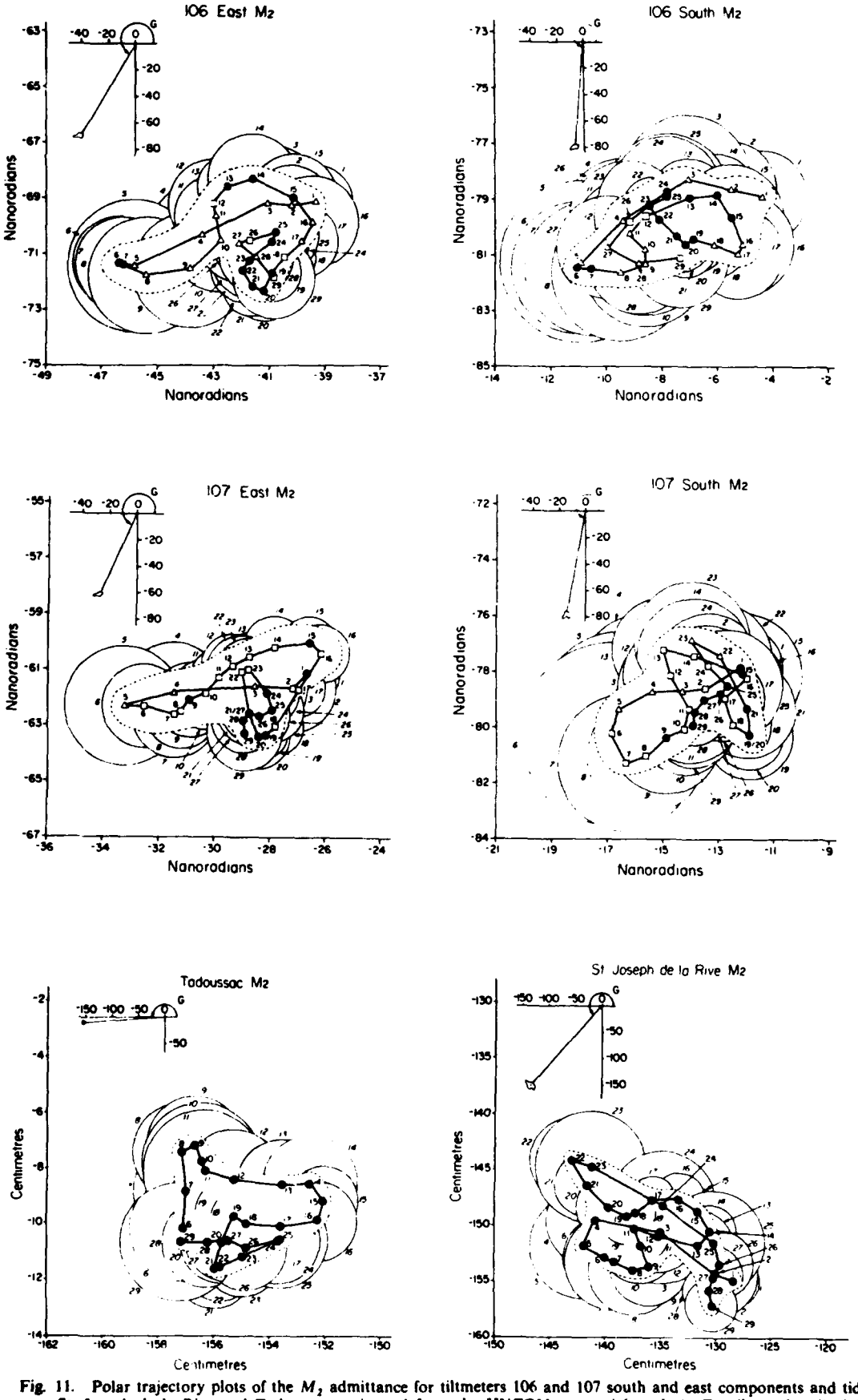

Fig. 11. Polar trajectory plots of the M_2 admittance for tiltmeters 106 and 107 south and east components and tide gauges St. Joseph de la Rive and Tadoussac, estimated from the HYCON sequential analysis. Details as described in Figure 10.

nates. The plots are shown in Figure 10 (O_1) and Figure 11 (M_2) for tiltmeters 107 (borehole 1) and 106 (borehole 2) south and east components and tide gauges St. Joseph de la Rive and Tadoussac. Each numbered point represents the admittance vector determined from that member of the sequence of overlapping 60-day subsets of the data. Ninety-five percent error circles have been plotted for each point and then, to avoid confusion, largely erased, leaving only a representative arc labeled by the analysis number. The reader can reconstruct the complete plot from the information shown.

The potential influence of interpolated gaps on the analysis results (see section 3) is indicated by identifying each plotted point with a symbol according to the level of the effect. The symbols are explained in the caption to Figure 10. The significance of admittance variations should be judged in the light of these qualitative confidence estimates because the effects of a poor interpolation model cannot be distinguished from an admittance variation. Less weight should be given to estimates from data subsets for which the interpolation effect is greater than 20% than those where the corresponding effect is less than 10%.

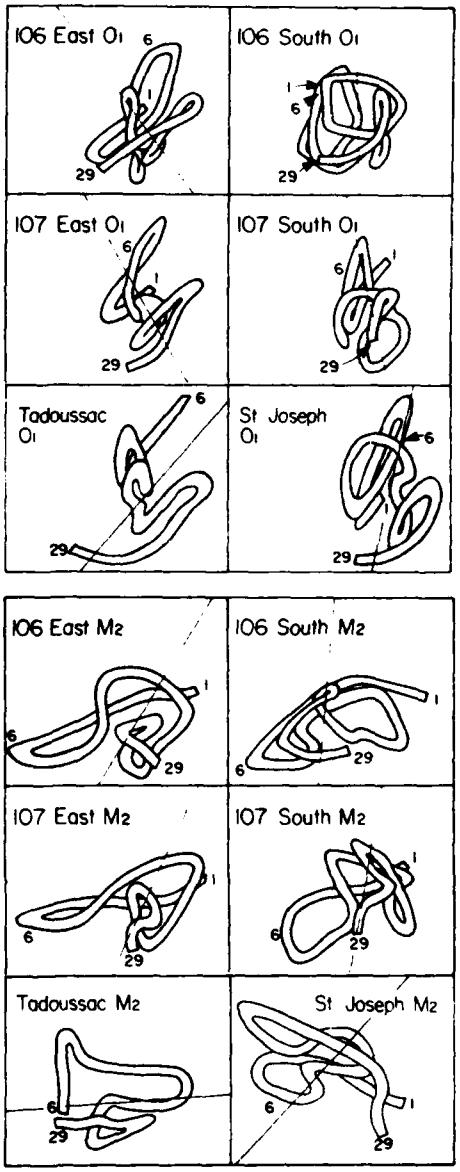

Fig. 12. Polar trajectory interpretation. Qualitative representation of the admittance time variations shown in Figures 10 and 11. The phase angle of the mean admittance vector is indicated by the fine line in each panel.

With this in mind, we have attempted to identify the most likely paths of the admittance variations. The interpretation is shown in Figure 12 which should be considered in conjunction with Figures 10 and 11. In general, for all components and both constituents, the variability of the estimates is hardly greater than the range of the 95% error circles, indicating that from a statistical point of view with respect to the residual noise the variations are barely significant. Despite this, there are distinct correlations between the trajectories, particularly for the redundant borehole measurements made in the same azimuth. Looking at O_1 first in Figures 10 and 12*a*, we see that while the trajectories are quite complex, they behave in much the same way in both tilt azimuths and in the same way as the tide gauges. The tilt variations are characterized by predominantly phase oscillations during the first and last 4 months of the data set (the winter months), and these are associated with the largest error circles. The middle (summer) estimates, which include analyses 14 to 22, represent a period of slowly increasing amplitude and reduced residual error. It should be noted that while we discuss admittance variations in terms of the physical concepts of amplitude and phase, it is more correct to compare variations in terms of the in-phase and quadrature components of the admittance. This can be important if the compared vectors are not aligned. For example, O_1 east and Tadoussac are nearly in quadrature, so that amplitude changes in the tide gauge are correlated with phase changes in the tilt.

For the M_2 estimates shown in Figures 11 and 12*b* the resemblence between the two east components is remarkable and is firmly based on the "under 10%" interpolation effect data. Even the early data (analyses 1 to 5), where 106 suffers from large interpolation errors, correlate closely in their behavior. The strong trend from analyses 6 to 15 occurs during the spring and comprises a combined amplitude decrease of about 5% and phase lag increase to 3°. From mid-June to mid-August (analyses 15 to 20), only the amplitude changes, increasing by 3.5% in 106 and 4.5% in 107. This is followed by a period of greater stability in analyses 21 to 25, which are well determined, and in 26 to 29, which are less well determined in tiltmeter 106.

In the south direction, the resemblence between the two M_2 trajectories is less impressive. However, an early, predominantly phase, trend (analyses 1 to 5) and its well-determined reversal during the spring (6 to 15), show the same level of variation as in the east direction. The fluctuations after this time are relatively small and are not well correlated between the instruments. Certainly, the period covered by analyses 21 to 29 is one of greater stability for both components, and it is probable that statistical uncertainties in the analysis results obscure any correlation between trajectory paths.

Unlike the diurnal case, there is not an obvious correlation between the St. Joseph de la Rive and Tadoussac tide gauge admittance variations. This is also true for the comparison between the tilt and the tide gauges. However, the differences, both among the gauges and the tilt, are almost entirely in the phase variations. Figure 13 is a plot of the M_2 amplitudes as a function of time for each of the components (see figure caption for details). Clearly, all the series are strongly correlated, especially in the apparent approximately 6-month cycle that

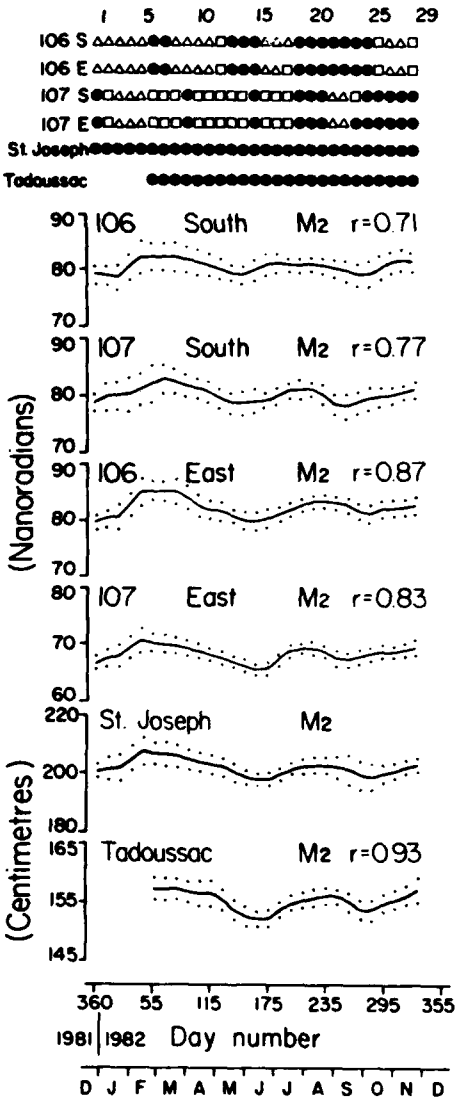

Fig. 13. Plots versus time of the M_2 amplitude for tiltmeters 106 and 107 south and east components and tide gauges St. Joseph de la Rive and Tadoussac, estimated from the HYCON sequential analysis. The solid curves join points representing the amplitudes, while the dotted curves inidcate the 95% error envelopes. The points are positioned in time in the middle of each analysis epoch. Symbols at the top of the diagram indicate the degree to which the individual estimates are influenced by interpolated gaps, following the scheme outlined in Figure 10. The correlation coefficient r between the amplitude at St. Joseph de la Rive and each of the other series is also shown.

dominates the amplitude signal. Thus, as in the diurnal case, there is strong evidence for a cause and effect relationship between tilt and marine tide variations.

While these interpretations cannot be regarded as definitive, they represent in our estimation the most obvious trends in the time-varying admittances. It is important to note that by comparison with the confidence estimates, only the maximum excursions are even marginally significant at the 95% level and that with only one instrument we would have difficulty in producing convincing arguments for variability. The close correlation between the two instruments suggests that our error estimates, based on noise estimates over a whole frequency band, are overly pessimistic. The importance of observations from two or more instruments is again confirmed.

High-Resolution Fourier Analysis of the Residuals

It is clear that the interaction between the Hanning window and gaps in the data is not responsible for the main features of the time varying admittances. The main concern now is the effect of any systematic modulation from constituents, within 0.39 μHz (tidal analysis bandwidth) around the major constituents, that were ignored or poorly modeled in the harmonic analysis.

The diurnal and semidiurnal portions of the high-resolution Fourier spectrum of the residuals (section 3) for both components of tiltmeters 106 and 107 are plotted in Figures 14 and 15 with a linear amplitude scale. The "background" noise in the diurnal band for all four components is essentially flat with an approximate level of 1 nrad. In the semidiurnal band, however, the residual noise rises, for each component, from a background of 0.3 nrad to a broad peak spanning the interval 21–23 μHz with a particular concentration of energy, in the south components, around $2N_2$. This broad feature resembles the "cusp" commonly observed in marine tides [*Munk et al.*, 1965] and tilt and strain observations affected by marine tidal loading (for example, *Peters* [1978] and *Beavan and Goulty* [1977]). It is attributed [*Munk et al.*, 1965] to nonlinear interactions between the strong tidal constituents and the low-frequency continuum and shallow water nonlinear interactions among the tidal constituents themselves. The cusp rises to a level around 0.75 nrad in the east and 1 nrad in the south

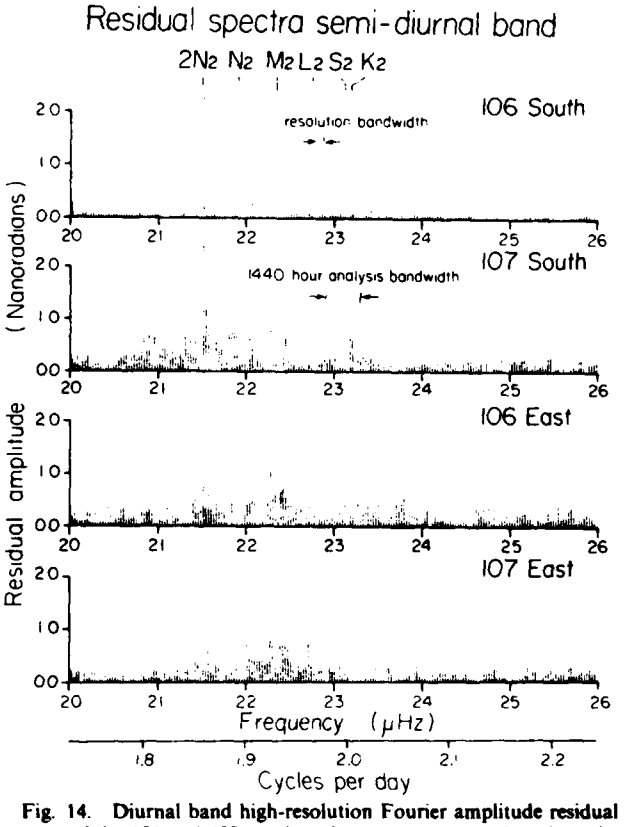

Fig. 14. Diurnal band high-resolution Fourier amplitude residual spectra of the 106 and 107 south and east components, based on the mean tidal admittance determined from the HYCON sequential analysis. Spectral estimates are plotted at intervals of 30 nHz, approximately half the resolution bandwidth of 58.5 nHz, in order to provide a visually clearer representation of closely spaced constituents. The location of the principal constituents in the band are indicated.

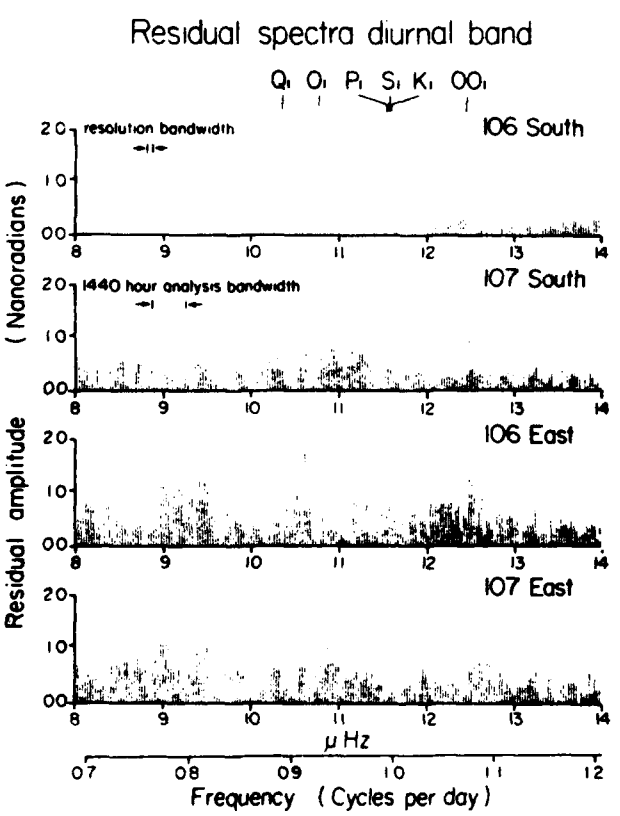

Fig. 15. Semidiurnal band high-resolution Fourier amplitude residual spectra of the 106 and 107 south and east components. Details as described in Figure 14.

and is consistent with the M_2 constituent rms errors derived from the sequential harmonic analyses. At this point we see the justification for choosing a subset of the original 505 astronomical constituents for the HYCON analysis. We chose a cutoff for the body tide amplitude of 0.1 nrad (leaving 73 constituents in the analysis), and few, if any, of the neglected constituents appear to be significant in the residual spectrum. These constituents are sufficiently below the observed background noise to make interconstituent modulation insignificant, even for a signal augmented by marine loading. The effect of the general background noise level has already been included in the error analysis for the 2-monthly data sets.

A closer inspection of the semidiurnal spectrum (Figure 15) shows holes in the vicinity of the main tidal lines which result from the least squares removal of energy at those frequencies. Rising significantly above the background in all four components but most pronounced in 106 is a pair of peaks located at a distance of one resolution bandwidth either side of M_2. This is the spectral representation of the observed, "around 6-month" cycle identified in the M_2 amplitude variations and may be a manifestation of the nonlinear interactions MKS_2 and MSK_2, also observed by *Baker and Alcock*, [1983] in their study of tilt and tide gauge admittance variations.

The prominent peak in the south direction (near 21.5 μHz) coincides with the $2N_2$ and μ_2 constituents which are included in the linear harmonic analysis. *Godin* [1973], in his analysis of marine tides at Québec, has, however, identified μ_2 as a double constituent, sharing its frequency with the nonlinear interaction $2M_2 - S_2$. He has also detected the nonlinear constituent O_2 between $2N_2$ and μ_2. A similar effect may occur in the loading near the Charlevoix site. If this is so, the nonlinear part will remain because the $2N_2$ group cannot be realistically modeled with a constant admittance.

6. Discussion

Spatial coherency of tilt observations is essential if they are to be interpreted in terms of regional crustal properties and processes. The general lack of spatial coherency among measurements within a region (or even beside one another) is related to the ubiquitous presence of meteorological noise and the departure on all length scales of the crust from lateral homogeneity. The advent of borehole and long-baseline measurements has increased the potential for achieving interpretable results. However, most of the traditional objectives of earth tide research such as refining global Love numbers, discriminating between crustal models, and solving the inverse marine loading problem, require, as *Baker* [1978] points out, regionally representative tidal response estimates accurate to better than 2–5%. It is considered unlikely that locally generated tilt perturbations and associated model corrections will, in general, be reduced to those levels. Our experience at Charlevoix provides a dramatic demonstration of the problem. The borehole installations were designed with a view to minimizing the sensitivity of the measurements to local strain-tilt coupling effects. Yet the mean M_2 tidal amplitudes differ by 20% between boreholes 1 and 2, separated by only 80 m, with no observable discontinuity present in the terrain. Further evidence of a subsurface discontinuity in the vicinity of boreholes 1 and 2 is provided by the observation of a 90° shift in the electric field polarization angle (determined from magnetotelluric measurements) in this part of the Charlevoix site (R. Kurtz, personal communication, 1983). Effects of this magnitude are rare but disturbing and serve to emphasize the difficulties associated with determining absolute response estimates with confidence.

In studies of time variations in the tidal admittance we are no longer shackled to the need for a structurally interpretable measurement. There remains, however, the need for spatial coherency of the relative changes in admittance over length scales smaller than the prospective active area. It is therefore essential, as in all regional studies using point observation, that redundant measurements be made. We have observed remarkable agreement between the time-varying admittances determined in two boreholes, lending credence to a regional interpretation. Nevertheless, the study of relative changes in the tidal parameters introduces a new set of interpretation problems and ambiguities.

There are few acknowledgements in published studies of time-varying tidal admittance of the inherent difficulties in fitting a stationary, deterministic regression model to a finite length, gappy representation of a nonstationary, partly deterministic collection of processes. *Schüller* [1977] has made an important contribution to the treatment of this problem, allowing for a "piecewise stationary" model and using the Hanning data window to avoid modulation due to spectral leakage. Complications arising from the interaction of interpolated gaps with the data window have been addressed in the present study as well as the importance of verifying the absence of intermodulation through detailed examination of the mean admittance residual spectrum.

It is clear that the tilt admittance variations observed at Charlevoix are largely due to changes in the marine loading input. In the diurnal band the integrated loading effect variations (as manifest in the tilt) correlate strongly with the tide gauge admittance variations, which suggests that we are concerned here with large-scale dynamical effects in the estuary.

In the semidiurnal band the relationship between the tilt and marine tide is more complex. The total lack of correlation between the phase variations of the two tide gauges suggests the influence of local, or site specific, effects superimposed on larger-scale processes dominating the amplitude response. One explanation may be the influence of timing errors in the marine data (which are known to be large at times) which affect the phase more than the amplitude. *Baker and Alcock* [1983] observed coherent seasonal variations in the M_2 amplitude from tide gauges around the British Isles which correlated with near-coastal tilt measurements. However, they too failed to observe systematic phase variability for this constituent (T. Baker, personal communication, 1984). Although we have established qualitatively a strong relationship between the tilt and tide gauge admittance variations, we cannot easily correct for the effects of the nonstationary loading input. First, gaps in the data lead to a distorted admittance function which furnishes a poorly determined regression equation between tilt and tide gauge. Second, in the case of the M_2 constituent, since a single tide gauge does not describe the loading tilt, a more refined model of the time-varying load is required before "true" crustal variations can be isolated. When these problems are overcome (or when we move to a midcontinental seismic region) we will be better able to establish a tectonic admittance baseline from which to detect crustal anomalies.

The prominent features in the borehole secular tilt correlate with the transient and seasonal behavior of the water table. Although the tilt series are not long enough to indicate established long-term trends, we can estimate the lower limit of the detectability of regional signals from the difference in the long-term drift rates between the redundant 106 and 107 measurements. A crude estimate, based on the 5 months of data following the reinstallation in July 1982 of tiltmeter 106, is 2 μrad/yr in the south direction and 0.4 μrad/yr in the east. By comparison, *Buchbinder et al.* [1983] conclude that after the reduction of groundwater effects in the 40-m baseline leveling array at the Charlevoix site, the uncertainty with which tectonic tilts could be detected falls within a range of 4–6 μrad. In terms of drift rate their data suggest that a persistent trend over a year or more of 4 μrad/yr would be detectable. This is considerably worse than the borehole results and arises from the dominance of groundwater (and probably thermal) effects which are at least 5 times larger than in the boreholes. At Piñon Flat, *Wyatt et al.* [1982] measured a long-term drift rate of 0.7 μrad/yr using the surface 535-m-baseline fluid tiltmeter, the same order as the difference tilt between the boreholes. These results suggest that the baseline of a surface tiltmeter needs to be an order of magnitude greater than the borehole depth to achieve comparable performance.

7. CONCLUSIONS

An array of three borehole tiltmeters has been established at Charlevoix Observatory, Québec, to study the tidal and secular response of the crust within the Charlevoix seismic zone. Differences in the M_2 tidal results as larger as 20% in amplitude and 5° in phase were found between two boreholes 80 m apart. The observations in the east direction, in particular, disagreed with the theoretical M_2 amplitudes and phases computed from the tidal loading model of the St. Lawrence River, indicating that local geological strain-tilt coupling effects, in addition to regional departures in crustal structure from a plane-layered model, which were ignored in the modeling, are to some extent distorting the response. The O_1 mean admittances were consistent among the different observations and in reasonable agreement with theory.

Time variations in the tidal admittance were observed for the major diurnal (O_1) and semidiurnal (M_2) constituents. Although the variations were not in general statistically significant at the 95% level (based on the least squares residual variance), they were remarkably consistent between the two boreholes, indicating that errors based on the residual variance tend to overestimate the uncertainty of the admittance determination. Fluctuations in the loading tide input are largely responsible for the observed behavior. However, it is important to note that the physical significance of the variations would have remained undetected if there had been measurements only from a single borehole. Once again the importance of redundant measurements is confirmed.

The borehole secular tilt is correlated with water table fluctuations, the typical transfer coefficient being approximately 0.5 μrad/m. A preliminary estimate of the lower detectable limit of long-term regional anomalies, using the difference between simultaneous measurements from two boreholes, is 0.4 μrad/yr, comparable with the lowest rates so far reported.

APPENDIX. TIDAL ANALYSIS USING THE HYCON METHOD

Tidal observations are of the form

$$o(t) = x(t) + r(t) \tag{1}$$

and can be represented as a superposition of N periodic components,

$$o(t) = 0.5 \sum_{n=-N}^{N} |x_n| e^{i(\omega_n t + \Phi_n)} + r(t) \tag{2}$$

where $|x_n|$ is the amplitude of the component with frequency ω_n, Φ is its phase, and $r(t)$ is the nontidal residual.

Following *Yaramanci* [1978*a*, *b*] we use the Wiener-Hopf condition for optimizing linear systems (in the sense of minimizing the residual variance) [*Jenkins and Watt*, 1968] to derive the normal equations used in the solution for the system response or admittance. The Wiener-Hopf integral equation is given by

$$c_{xo} = \int_{-\tau}^{\tau} s(u) c_{xx}(\tau - u)\, du \tag{3}$$

where c_{xo} is the cross correlation of $o(t)$ with $x(t)$, c_{xx} is the time lagged autocorrelation of $x(t)$, and $s(u)$ is the system response or admittance.

Expanding (3) into the explicit form of the cross correlation and autocorrelation and introducing the harmonic representation of the tidal input from (2), we have, after rearranging terms and reordering the integrals,

$$\lim_{T\to\infty} \frac{1}{T} \int_{-T/2}^{T/2} \left\{ \left[o(t) - 0.5 \sum_{n=-N}^{N} |x_n| e^{i(\omega_n t + \Phi_n)} \cdot \int_{-\tau}^{\tau} s(u) |x_n| e^{-i\omega_n u}\, du \right] 0.5 \sum_{m=-N}^{N} |x_m| e^{i(\omega_m (t-\tau) + \Phi_m)} \right\} dt = 0 \tag{4}$$

We recognize the integral over du as the Fourier transform $S(\omega)$ of $s(u)$. Taking the summation over m outside the integral, the summation will be zero if each of the m parts is zero. Dividing through by the constant $0.5e^{-i\omega_m \tau}$, we arrive at the complex normal equations,

$$\lim_{T\to\infty} \frac{1}{T} \int_{-T/2}^{T/2} \left[o(t) - 0.5 \sum_{n=-N}^{N} S_n |x_n| e^{i(\omega_n t + \Phi_n)} \right] \cdot |x_m| e^{i(\omega_m t + \Phi_m)}\, dt = 0 \qquad m = -N, -N+1, \cdots, N \tag{5}$$

Note that (5) is a special form of the Wiener-Hopf integral equation (3) for periodic inputs and is not applicable to nonperiodic components [*Yaramanci*, 1978*a*].

The normal equations are applied in their noncomplex form. Expressing S_n in terms of its real and imaginary parts a_n and b_n, respectively, and writing the cos and sin terms of the tidal input as

$$x_n^c = |x_n| \cos(\omega_n t + \Phi_n)$$

and

$$x_n^s = |x_n| \sin(\omega_n t + \Phi_n)$$

Yaramanci [1978*a*] derives the noncomplex form of the normal equations.

$$\lim_{T\to\infty} \frac{1}{T} \int_{-T/2}^{T/2} \left\{ o(t) x_m^c - \sum_{n=-N}^{N} [a_n x_n^c x_m^c + b_n x_n^s x_m^c] \right\} dt = 0$$
$$m = -N, -N+1, \cdots, N \tag{6}$$

$$\lim_{T\to\infty} \frac{1}{T} \int_{-T/2}^{T/2} \left\{ o(t) x_m^s - \sum_{n=-N}^{N} [a_n x_n^c x_m^s + b_n x_n^s x_m^s] \right\} dt = 0$$
$$m = -N, -N+1, \cdots, N$$

As explained in section 3, tidal frequencies that cannot be resolved in the data interval are grouped together in HYCON and forced to have the same admittance. To form the normal equations as they are used in HYCON, we rewrite (6) for finite and digitized data and to include the grouping of the frequencies.

$$\sum_{r=-R}^{R-1} o(t_r) \sum_{l=1}^{G_k} x_{kl}^c = \sum_{r=-R}^{R-1} \sum_{i=1}^{H} \left[a_i \sum_{j=1}^{G_i} x_{ij}^c \sum_{l=1}^{G_k} x_{kl}^c + b_i \sum_{j=1}^{G_i} x_{ij}^s \sum_{l=1}^{G_k} x_{kl}^c \right] \qquad k = 1, 2, \cdots, H \tag{7}$$

$$\sum_{r=-R}^{R-1} o(t_r) \sum_{l=1}^{G_k} x_{kl}^s = \sum_{r=-R}^{R-1} \sum_{i=1}^{H} \left[a_i \sum_{j=1}^{G_i} x_{ij}^c \sum_{l=1}^{G_k} x_{kl}^s + b_i \sum_{j=1}^{G_i} x_{ij}^s \sum_{l=1}^{G_k} x_{kl}^s \right] \qquad k = 1, 2, \cdots, H$$

where the digitized time base t_r is given by $t_r = r\Delta t$, $\Delta t = 1$ hour, H is the number of groups, and G_i is the number of frequencies in the ith group.

In matrix form, (7) may be written [*Yaramanci*, 1978*a*; *Schüller*, 1977]

$$\mathbf{A}^T\mathbf{o} = \mathbf{A}^T\mathbf{A}\mathbf{s} \tag{8}$$

where $\mathbf{A}$ is the matrix of $2R$ rows and $2H$ columns whose elements are

$$A_{rp} = \sum_{l=1}^{G_k} x_{kl}^c \qquad \text{odd } p$$

$$A_{rp} = \sum_{l=1}^{G_k} x_{kl}^s \qquad \text{even } p$$

k is the integer part of $\frac{p+1}{2}$

$\mathbf{o}$ is the vector containing $2R$ digitized values of the signal $o(t)$, $\mathbf{s}$ is the vector containing the $2H$ unknown real and imaginary parts of the admittance.

$$s_p = a_i \qquad \text{odd } p$$

$$s_p = b_i \qquad \text{even } p$$

i is the integer part of $\frac{p+1}{2}$

and T denotes the transpose matrix. The normal equation system (8) can be written

$$\mathbf{w} = \mathbf{N}\mathbf{s} \tag{9}$$

with the solution

$$\mathbf{s} = \mathbf{N}^{-1}\mathbf{w} \tag{10}$$

where

$$\mathbf{w} = \mathbf{A}^T\mathbf{o}$$

and

$$\mathbf{N} = \mathbf{A}^T\mathbf{A}$$

As noted earlier, the normal equations are a special case of the Wiener-Hopf integral equation and are applicable to the idealized situation in which the observations contain only the periodic components specified in the input plus white noise. In reality, the observed tidal signal contains periodic and aperiodic components which are not modeled within this scheme. These unmodeled components are treated by *Schüller* [1977] as a perturbation $z(t)$ on the tidal part of the signal. We add to $r(t)$ in (1), which is assumed to be normal and white, the perturbation $z(t)$ containing unmodeled deterministic components. Thus

$$o(t) = x(t) + z(t) + r(t) \tag{11}$$

and introducing this into (8), we have

$$\mathbf{A}^T(\mathbf{o} + \mathbf{z}) = \mathbf{A}^T\mathbf{A}(\mathbf{s} + \Delta\mathbf{s}) \tag{12}$$

or from (9)

$$\mathbf{w} + \Delta\mathbf{w} = \mathbf{N}(\mathbf{s} + \Delta\mathbf{s}) \tag{13}$$

where $\Delta\mathbf{w} = \mathbf{A}^T\mathbf{z}$.
Thus

$$\Delta\mathbf{s} = \mathbf{N}^{-1}\Delta\mathbf{w} \tag{14}$$

is the perturbation on the true solution $\mathbf{s}$. The elements of $\Delta\mathbf{w}$ are of the form

$$\Delta w_{kl}^c = \sum_{r=-R}^{R-1} \sum_{l=1}^{G_k} x_{kl}^c z(t_r) \qquad k = 1, 2, \cdots, H$$
$$\Delta w_{kl}^s = \sum_{r=-R}^{R-1} \sum_{l=1}^{G_k} x_{kl}^s z(t_r) \qquad k = 1, 2, \cdots, H \tag{15}$$

As pointed out by *Schüller* [1977], the influence of $z(t)$ on $\Delta\mathbf{w}$ is difficult to predict in the time domain. We can transform (15) into the frequency domain using the convolution theorem [*Bath*, 1974] and examine the influence of the perturbation components on the tides. In this case we have to take account of the finite data length. Thus

$$\Delta w_{kl}^c = \sum_{r=-\infty}^{\infty} \sum_{l=1}^{G_k} x_{kl}^c z(t_r)\, d(t_r) \qquad k = 1, 2, \cdots, H$$
$$\Delta w_{kl}^s = \sum_{r=-\infty}^{\infty} \sum_{l=1}^{G_k} x_{kl}^s z(t_r)\, d(t_r) \qquad k = 1, 2, \cdots, H \tag{16}$$

where

$$d(t_r) = 1 \qquad -R \le t_r \le R - 1$$

$$d(t_r) = 0 \qquad \text{otherwise}$$

The Fourier transform of (16) is given by [*Schüller*, 1977]

$$\Delta w_{kl}{}^c = c \sum_{l=-G_k}^{G_k} X_{kl}{}^c \int_{-\omega_v}^{\omega_v} Z(-\lambda) D(\lambda - \omega_{kl})\, d\lambda \qquad k = 1, 2, \cdots, H \tag{17}$$

$$\Delta w_{kl}{}^s = c \sum_{l=-G_k}^{G_k} X_{kl}{}^s \int_{-\omega_v}^{\omega_v} Z(-\lambda) D(\lambda - \omega_{kl})\, d\lambda \qquad k = 1, 2, \cdots, H$$

where X, Z, and D are the Fourier transforms of x, y, and d, respectively, ω_v is the Nyquist frequency of the band-limited Fourier transform, and c is a constant.

It is clear from (17) that the influence of $z(t)$ on Δw and hence Δs, the perturbation on the solution, is governed by the properties of the window function $d(t_r)$ acting as a weighting function in the frequency domain. The essence of the HYCON method is therefore

1. the use of the Hanning window to reduce to an acceptable level (2.3% maximum) side-lobe leakage of energy into the tidal constituents from unmodeled components outside the window bandwidth, and

2. the sequential analysis of overlapping data subsets sufficiently sampled to detect, without aliasing, interacting components within the window bandwidth. The resulting time-varying admittance function will contain information on unmodeled periodic and nonperiodic signal components due either to their presence in the input or resulting from nonstationarity in the system response.

Acknowledgments. This project was supported by the Air Force Geophysics Laboratory, Hanscom AFB (under contracts F19628-80-C-0032 and F19628-83-K-0023), the Natural Sciences and Engineering Research Council through Operating and Equipment grants and the Gravity, Geothermics and Geodynamics Division of the Earth Physics Branch. The Marine Environment Data Service provided the tide gauge data. We would like to thank Ross Boutilier for the loading calculations and invaluable computing and field assistance. We are grateful to Gerry Cabannis, Tony Lambert, and Don Bower for their interest and support throughout the program and to Jacques Labrecque for his assistance in operations at the Charlevoix Observatory. The careful criticisms of an anonymous reviewer are greatly appreciated. Benoit Dostaler and Josée Laurion maintained the array on a day to day basis, and Jim Covill assisted with data reduction and analysis. Terry Collins skillfully drafted the diagrams.

REFERENCES

Agnew, D. C., Strain tides at Piñon Flat: Analysis and interpretation, Ph.D. thesis, Univ. of California, San Diego, 1979.

Agnew, D. C., Nonlinearity in rock: Evidence from earth tides, *J. Geophys. Res.*, *86*, 3969–3978, 1981.

Baker, T. F., What can Earth tide measurements tell us about ocean tides and crustal structure?, in *Applications of Geodesy to Geodynamics*, edited by I. Mueller, Ohio State University Press, Columbus, pp. 299–307, 1978.

Baker, T. F., Tidal tilt at Llanrwst, North Wales: Tidal loading and Earth structure, *Geophys. J. R. Astron. Soc.*, *62*, 269, 1980.

Baker, T. F., and G. A. Alcock, On the time variation of ocean tides, in *Proceedings of the Ninth International Symposium on Earth Tides*, edited by J. T. Kuo, E. Schweizerbart'sche Verlagsbuchhandlung, Stuttgart, Federal Republic of Germany, 1983.

Bath, M., *Spectral Analysis in Geophysics*, p. 79, Elsevier, New York, 1974.

Beaumont, C., Linear and nonlinear interactions between the earth tide and a tectonically stressed earth, in *Applications of Geodesy to Geodynamics*, edited by I. Mueller, Ohio State University Press, Columbus, pp. 313–318, 1978*a*.

Beaumont, C., Tidal loading: Crustal structure of Nova Scotia and the M_2 tide in the northwest Atlantic from tilt and gravity observations, *Geophys. J. R. Astron. Soc.*, *53*, 27–53, 1978*b*.

Beaumont, C., and J. Berger, Earthquake prediction: Modification of the earth tide tilts and strains by dilatancy, *Geophys. J. R. Astron. Soc.*, *39*, 111–121, 1974.

Beaumont, C., and R. Boutilier, Tidal loading in Nova Scotia: Results from improved ocean tide models, *Can. J. Earth Sci.*, *15*, 981–993, 1978.

Beaumont, C., and A. Lambert, Crustal structure from surface load tilts, using a finite element model, *Geophys. J. R. Astron. Soc.*, *29*, 203–226, 1972.

Beavan, R. J., and N. R. Goulty, Earth-strain observations made with the Cambridge laser strainmeter, *Geophys. J. R. Astron. Soc.*, *48*, 293–305, 1977.

Berger, J., and J. Levine, The spectrum of earth strain from 10^{-8} Hz to 10^{2} Hz, *J. Geophys. Res.*, 79, 1210–1214, 1974.

Bodenseewerk Geosystem, Borehole Tiltmeter Gpb10, *Tech. Bull. 19*, Bodenseewerk Geosystem GmbH, Überlingen, Federal Republic of Germany, 1979.

Bower, D. R., The measurement of the earth tide and regional heterogeneity due to the ocean tide, Ph.D. thesis, Univ. of Durham, Durham, England, 1971.

Buchbinder, G., R. Kurtz, and A. Lambert, A review of time-dependent geophysical parameters in the Charlevoix Region, Québec, *Earthquake Prediction Res.*, *2*, 149–166, 1983.

Cabannis, G. H., The measurement of long period and secular deformation with deep borehole tiltmeters, in *Applications of Geodesy to Geodynamics*, edited by I. Mueller, Ohio State University Press, Columbus, pp. 165–169, 1978.

Edge, R. J., T. F. Baker, and G. Jeffries, Earth Tides: Tilt in the English Lake District, in *Proceedings of the International Workshop on Monitoring Crustal Dynamics in Earthquake Zones*, F. Vieweg und Sohn Verlag, Weisbaden, Federal Republic of Germany, 1979.

Edge, R. J., T. F. Baker, and G. Jeffries, Some results from simultaneously recording tiltmeters, in *Proceedings of the Ninth International Symposium on Earth Tides*, edited by J. T. Kuo, E. Schweizerbart'sche Verlagsbuchhandlung, Stuttgart, Federal Republic of Germany, 1983.

El-Sabh, M. I., T. S. Murty, and L. Levesque, Mouvements des eaux indiuts par la marée et le vent dans l'estuaire du Saint-Laurent, *Le Naturaliste Can.*, *106*, 89–104, 1979.

Farrell, W. E., Deformation of the Earth by surface loads, *Rev. Geophys.*, *10*, 761, 1972.

Flach, D. and O. Rosenbach, The Askania borehole tiltmeter (tide pendulum) of A. Graf at the Zellerfeld-Muhlenhohe testing station, *Bull. Inf. Marees Terr.*, *60*, 2934–2943, 1971.

Flach, D., W. Grosse-Brauckmann, K. Herbst, G. Jentzsch, and O. Rosenbach, Results of long-term recordings with Askania borehole tiltmeters—Comparative analysis with respect to the tide parameters and long period portions and instrumental investigations, Rep. *B211*, *Dtsch. Geod. Komm.*, 72–95, Munich, 1975.

Godin, G., Eight years of observations on the water level at Québec and Grondines 1962–1969, *Manuscript Rep. Ser. 31*, Mar. Sci. Directorate, Dep. Environ., Ottawa, Ontario, Canada, 1973.

Grosse-Brauckmann, W., High precision ball calibration of the Askania borehole tiltmeter, *Proceedings of the Seventh International Symposium on Earth Tides, Sopron 1973*, E. Schweizerbart'sche Verlagsbuchhandlung, Stuttgart, Federal Republic of Germany, 1976.

Harrison, J. C., Tilt observations in the Poorman mine near Boulder, Colorado, *J. Geophys. Res.*, *81*, 329, 1976*a*.

Herbst, K., Interpretation of tilt measurements in the period range above that of the tides (in German), Ph.D. thesis, Tech. Univ. Clausthal, Clausthal-Zellerfeld, Federal Republic of Germany, 1976. (English translation, *Tech. Rep. AFGL-TR-77-0162*, Air Force Geophys. Lab., Bedford, Mass. 1979.)

Jenkins, G. M., and D. G. Watt, *Spectral Analysis and Its Applications*, Holden-Day, San Francisco, 1968.

Kato, M., Observations of crustal movements by newly-designed horizontal pendulum and water-tube tiltmeters with electromagnetic transducers, 2, *Bull. Disaster. Prev. Res. Inst. Kyoto Univ.*, *29*, *Part 2*, 83–97, 1979.

Leblanc, G., and G. Buchbinder, Second microearthquake survey of the St. Lawrence Valley near La Malbaie, Québec, *Can. J. Earth Sci.*, *14*, 2278–2789, 1977.

Leblanc, G., A. E. Stevens, R. J. Wetmiller, and R. DuBerger, A microearthquake survey of the St. Lawrence valley near La Malbaie, Québec, *Can. J. Earth Sci.*, *10*, 42–53, 1973.

Lyons, J. A., D. A. Forsyth, and J. A. Mair, Crustal studies in the La Malbaie region, Québec, *Can. J. Earth Sci.*, *17*, 478–490, 1980.

McConnell, R. K., Jr., and J. Lewkowicz, Research on the nature of ground tilts in the period range 10^3 to 10^7 seconds, *Tech. Rep. AFGL-TR-78-0105*, Air Force Geophys. Lab., Bedford, Mass., 1978.

Mikumo, T., M. Kato, H. Doi, Y. Wada, T. Tanaka, R. Shichi, and A. Yamamoto, Possibility of temporal variations in earth tidal strain amplitudes associated with major earthquakes, in *Earthquake Precursors: Proceedings of the U.S.-Japan Seminar on Theoretical and Experimental Investigations of Earthquake Precursors, Tokyo, 1977*, edited by C. Kisslinger and Z. Suzuki, pp. 123–136, Central Academic Publishers of Japan, Tokyo, 1978.

Milne, W. G., W. E. T. Smith, and G. C. Rogers, Canadian seismicity and microearthquake research in Canada, *Can. J. Earth Sci.*, *7*, 591–601, 1970.

Mortenson, C. E., and M. J. S. Johnston, The nature of surface tilts along 85 km of the San Andreas Fault—Preliminary results from a 14 instrument array, *Pure Appl. Geophys.*, *113*, 237, 1975.

Munk, W. H., B. Zetler, and G. W. Groves, Tidal cusps, *Geophys. J. R. Astron. Soc.*, *10*, 211–219, 1965.

Nishimura, E., On earth tides, *Eos Trans. AGU*, *31*, 357–375, 1950.

Peters, J. A., Tidal measurements using a new long baselength tiltmeter, Ph.D. thesis, Univ. of Liverpool, Liverpool, England, 1978.

Peters, J. A., The construction of a cased borehole facility for the purpose of tilt observations at Charlevoix Observatory, Québec, *Earth Phys. Branch Open File rep.*, *83-21*, 1983.

Peters, J. A., D. R. Bower, and A. Lambert, Tidal tilt response at Charlevoix, Québec, in *Proceedings of the Ninth International Symposium on Earth Tides*, edited by J. T. Kuo, E. Schweizerbart'sche Verlagsbuchhandlung, 1983*a*.

Peters, J., C. Beaumont, and R. Boutilier, Borehole tilt measurements at the Charlevoix Observatory, Québec, *Tech. Rep. AFGL-TR-83-0027*, Air Force Geophys. Lab., Bedford, Mass., 1983*b*.

Sbar, M. L., and R. L. Sykes, Contemporary compressive stress and seismicity in Eastern North America: An example of intra-plate tectonics, *Geol. Soc. Am. Bull.*, *84*, 1861–1881, 1973.

Schüller, K., Tidal analysis by the hybrid least squares frequency domain convolution method, Proceedings of the *Eighth International Symposium on Earth Tides*, edited by M. Bonatz and P. Melchior, Institut für Theoretische Geodesie Der Universität Bonn, Federal Republic of Germany, 1977.

Tanaka, T., Effect of dilatancy on ocean load tides, *Pure Appl. Geophys.*, *114*, 415–423, 1976.

Wyatt, F., G. Cabaniss, and D. C. Agnew, A comparison of tiltmeters at tidal frequencies, *Geophys. Res. Lett.*, 9, 743–746, 1982.

Yaramanci, U., A unified approach to signal analysis in earth tides, Ph.D. thesis, Univ. of Liverpool, Liverpool, England, 1978*a*.

Yaramanci, U., Tidal analysis and optimal linear system approximation, *Bull. Inf. Marees Terr.*, *78*, 1978*b*.

Zschau, J., Tidal sea load tilt of the crust, and its application to the study of crustal and upper mantle structures, *Geophys. J. R. Astron. Soc.*, *44*, 577–593, 1976.

C. Beaumont and J. Peters, Department of Oceanography, Dalhousie University, Halifax, Nova Scotia, Canada B3H 4J1.

(Received April 11, 1984;
revised July 8, 1985;
accepted July 11, 1985.)

Earth and Planetary Science Letters, 84 (1987) 263–276
Elsevier Science Publishers B.V., Amsterdam – Printed in The Netherlands

[3]

Tidal and secular tilt from an earthquake zone: thresholds for detection of regional anomalies

John Peters * and Christopher Beaumont

Oceanography Department, Dalhousie University, Halifax, Nova Scotia B3H 4J1 (Canada)

Received December 10, 1986; revised version accepted April 25, 1987

Tiltmeter data from an array of three boreholes at the Charlevoix observatory in the Charlevoix seismic region of Québec have been analysed for evidence of tectonically related signals. The secular tilt is dominated by water table induced effects which can be substantially removed by linear regression of the water level on the tilt. Short-term (days to months) anomalies are shown to be detectable at the 0.3 μrad to 1 μrad level depending on the depth of the measurement. Long-term changes in the linear drift as small as 0.1 μrad/yr would be detectable in all of the boreholes.

Large spatial anomalies in the mean tidal admittance among boreholes preclude its use in refining either models of the regional crustal structure or the adjacent marine tide distribution. Strongly coherent time variations in the tidal admittance among the observations of all the major tidal constituents are shown to be generated by corresponding variations in marine tidal loading in the St. Lawrence estuary. Diurnal band variations are closely correlated with the tide gauge data. The semi-diurnal constituents show a weaker correlation because of the complex spatial pattern within the estuary of time variations in this band. Inspection of the residual admittance variations for the M_2 and O_1 constituents demonstrates that the thresholds for detecting tectonic tidal tilt anomalies are ±2% and ±5–8%, respectively.

The level of earthquake activity in the Charlevoix seismic zone throughout the period of the borehole tiltmeter experiment was sufficiently low that no significant tilt anomalies were expected or were undeniably detected.

1. Introduction

Tiltmeters, which can detect tilts as small as 1 nrad, have the potential to measure tilts induced by changes in stress and properties of the Earth's crust that are precursory to earthquakes. Current research is concerned with reducing noise levels and with detecting small signals in noisy data through redundant measurements in the belief that tectonic signals are more coherent than the noise.

The limited number of reliable tilt experiments designed to detect tectonically related tilts may be divided into two main types: long baseline horizontal installations (> 250 m); and, deep borehole studies (> 20 m). The advantage of these measurement techniques is that they attenuate near-surface meteorologically induced tilts by distance integration or by depth isolation. Recent comparative studies [1–3] permit an evaluation of these techniques and provide a threshold on the detectability of regional anomalies from a comparison of redundant observations. This threshold is essential to the unambiguous detection of anomalous tilts.

The principal source of the remaining noise in high-quality tilt records is apparently caused by groundwater effects [3,4]. A number of different mechanisms, depending on the nature of the local rocks, have been proposed to explain water level related tilts. Experience using borehole instruments in fractured hard rock at different sites has suggested a common mechanism, namely the opening and closing of fractures in response to either differential or hydrostatic pressure variations [5,6]. Installations in incompetent rock appear to be most sensitive to changes in the gradient of the water table [7].

Tidal tilt anomalies prior to earthquakes have been reported a number of times (see for example [8–10]). None of these reports has been convincing because of the poor quality of the data, questionable analysis, and the lack of a detection threshold. Theoretical studies [11–13] predict significant tidal tilt anomalies if there are precursory

* Now at Earth & Ocean Research Ltd., 22 Waddell Avenue, Dartmouth, Nova Scotia B3B 1K3, Canada.

0012-821X/87/$03.50

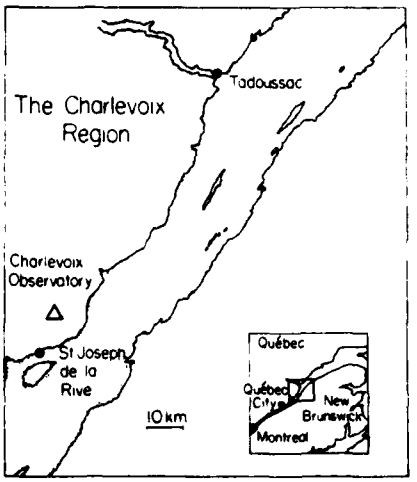

Fig. 1. Map of the Charlevoix region.

constitutive property changes in the rockmass surrounding earthquake source regions. A simple example in which a 15% reduction in seismic P-wave velocity is interpreted as a change in elastic properties of a crustal inclusion, results in a simultaneous 30–40% change in the tidal amplitude [11].

This study extends our analysis of the time variation of the tidal admittance of data from the three Charlevoix borehole tiltmeters [3] to include: four years of data from two tiltmeters; two years data from a third, deeper installation, and; the variability of the marine tide constituents from the St. Lawrence estuary tide gauge data. A comparison of the variations is essential to determine whether marine tidal loading is the cause of the undeniable changes in the tilt admittance.

Corrections are applied to the secular tilt for groundwater effects and to the observed tidal admittance for variations in the marine loading input. The residuals, which comprise the unexplained part of the observations and set a threshold for the detection of tectonic anomalies, are compared with occurrence times of earthquakes from the Charlevoix seismic zone (Fig. 1).

2. The experiment and data analysis

The Charlevoix borehole tiltmeter array [3,14] comprises three boreholes that form a triangle of approximately 80 m side. Holes 1 and 2 were drilled in October 1979 to a depth of 47 m and were instrumented for the interval November 1981 to March 1986. The third hole, completed in July 1982, was instrumented continuously from September 1983 until the completion of the experiment in March 1986. Hole 3 is 110 m deep and was added to the array to study the attenuation of environmental noise with depth.

The tiltmeters are Bodenseewerk Gbp10 (formerly Askania) biaxial borehole instruments [3,15] which use proportional feedback capacitive sensors and in situ calibration. Data were recorded on analogue strip chart recorders, digitized and calibrated as described in [3].

The data sets analysed in this study (Table 1) include two sets of tide gauge data. Sea level observations recorded during the period 1981–1985 at the nearby St. Joseph de la Rive and Tadoussac stations were analysed in parallel with the tilt observations. A second sea level data set, from tide gauges distributed over the whole of the St. Lawrence estuary, and recorded during 1972–1974, was analysed with the aim of gaining insight into the time variant behaviour of the tidal loading. The HYCON program [16] was used for the time variant analyses [3]. The data were divided into overlapping 60 day subsets with starting offsets of 10 days. Output from the analysis of the subsets is a sequence of amplitude and phase estimates for each tidal harmonic. The time sequence of results for each data set from a time varying admittance function.

TABLE 1

Data used in this study

Tilt		
Borehole 1	Gbp 107 [a]	26 Nov 1981–31 Mar 1986 [b]
Borehole 2	Gbp 106	26 Nov 1981–31 Mar 1986
Borehole 3	Gbp 105	25 Sep 1983–31 Mar 1986
Tide gauges		
St. Joseph de la Rive		26 Nov 1981–31 Dec 1984 [b]
Tadoussac		24 Jan 1982–31 Dec 1985
St. Anne des Monts	1	18 Aug 1972–31 Mar 1974 [b]
Baie Comeau	2	
Pointe au Père	3	
Rivière du Loup	4	
Tadoussac	5	18 Aug 1972–18 Jul 1974 [b]
St. Joseph de la Rive	6	
St. Jean-Port-Joli	7	
St. François	8	

[a] Tiltmeter; [b] data interval.

3. Secular tilt

The long-term tilt measured from each of the boreholes correlates strongly with water table fluctuations (Fig. 2). The water level fluctuations are characterized by strong transients near the beginning of May of each year, which reflect the recharge of the aquifer at the time of the spring thaw. A second, smaller annual event occurs near the end of the year in response to rainfall. The remainder of the water level variation appears to be dominated by a slow, exponential recovery from these transient events.

Linear regression of the water level on the tilt accounts for approximately 85% of the variance, excluding the linear trend, in most of the series. That the residual tilt signal is concentrated at the steep, leading edge of the water level transients (Fig. 2) suggests that a rate-dependent term could be added to the model. The large residual tilts that occur near the gaps in the water level record (dotted lines, Fig. 2) are a consequence of the interpolation and should be disregarded. Table 2 lists the regression coefficients relating tilt to water level, the linear drift of each of the series and, where available, data from comparable experiments.

The directions of maximum water level related tilt for all these boreholes are in the same quadrant: borehole 1 near azimuth 150°, borehole 2 near 110° and borehole 3 near 200°, where the azimuth is measured clockwise from north through east direction. The regression coefficients in the maximum directions are 0.30, 0.54 and 0.09 μrad/m, respectively. The hydrology at the Charlevoix site is dominated by fracture permeability and the range of the water table variations is very large (see Fig. 2, WELL). Despite this large variation, the water table effect on tilt is small and apparently decreases with depth. Edge et al. [2] and Herbst [5] describe similar measurements made respectively in slate in Cumbria, England and fractured greywacke in Clausthal, West Germany. In both of these cases strong short-term transients, attributed to direct rainfall effects, complicated the response. It therefore appears that increasing depth of burial may reduce the water level related tilt component, though not in [2] (R. Edge, personal communication). Our results support the need for maximising the depth of installation to enhance the regional tilt signal to noise ratio and simplify the response to water level related tilt.

With a single set of observations long-term regional tilts are inseparable from locally generated tilts and instrumental effects. Only by making redundant measurements in different boreholes can a basis for detecting regional signals be established. The Charlevoix tiltmeter data from each of the component axes were analysed separately so that channel-dependent instrumental effects may more easily be identified. It is especially clear from the difference in the south component residual drift for holes 1 and 2 (Fig. 2) that local effects dominate in at least one of the boreholes because the drift components tilt in opposite directions. This result demonstrates an inherent disadvantage of borehole tiltmeters by comparison with long baseline tiltmeters; any mechanical instability in the sensor or of the instrument/rock interface produces proportionately larger tilts because the instrument baseline is short. The drift rate and direction of data from holes 2 and 3 is similar, suggesting that the local effects may be confined to borehole 1. In fact, the south component in borehole 1 is the only one of the six measured that is inconsistent. Furthermore, this component is in line with one of the three support pins used to fix the tiltmeter to the borehole wall

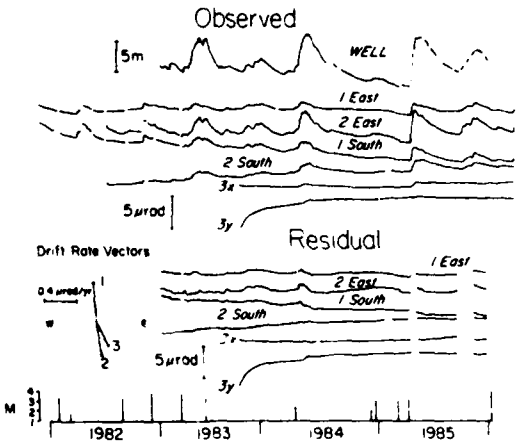

Fig. 2. Plot of the observed long-term tilt from the three boreholes (middle) compared with water well level data (top), and the residual tilt after regression of the well level on the tilt (lower). Lower left shows the linear drift rate of the residual tilt in each of the boreholes. The Charlevoix earthquakes listed in Appendix 3 are shown at the bottom of the diagram.

TABLE 2

Characteristics of the secular tilt

Borehole	Component	Tilt/water table correlation coefficient μrad/m)	Linear drift (μrad/yr)	Standard deviation of residual tilt (μrad)
Charlevoix borehole tiltmeters				
1	East	0.15	−0.07	0.21
2	East	0.50	0.12	0.35
3	X (120°)	0.02	0.52	0.28
1	South	0.26	−0.95	0.17
2	South	0.20	0.73	0.23
3	Y (210°)	0.09	0.28	0.14
Comparison measurements				
Long baseline tiltmeters				
CAMB [a]			0.26	
LDGO [a]			0.49	
USCD [a]			0.28	
Borehole tiltmeters				
Maynard, Mass, U.S.A.,	100 m deep [b]		0.1	
Clausthal, W. Germany,	15 m deep [c]		1.4	
	30 m deep [c]		0.8	
Cumbria, U.K.,	12 m deep [d]	1		
	30 m deep [d]	1		

[a] Wyatt et al. [22]
[b] Cabaniss [23]
[c] Flach et al. [18]
[d] Edge et al. [2].

and is therefore particularly susceptible to any instability in the contact between the pin and the tiltmeter pod. The tilt drift rates in the east direction are very low, and are as good as those from long baselength tiltmeters. Despite these results, it is unlikely that continuous tiltmeter measurements can be used confidently to monitor the *absolute* regional long-term tilt, although measurements from more than one instrument may indicate an upper limit to long term tectonic deformations. However, coherent long term (years) *changes* in the background trend may be detectable at the 0.1 μrad/yr level, assuming that installation dependent drifts are constant or diminishing.

The limiting factor on the detection of short- to medium-term (days to months) regional tilt events is the standard deviation of the residual hydrological component (Table 2). On average, coherent anomalies greater than 1 μrad in data from boreholes 1 and 2 and greater than 0.3 μrad in the deep borehole data are greater than the residual groundwater noise level for these time intervals, and may have regional significance.

The occurrence times of earthquakes in the Charlevoix region of magnitude greater than 3, and those within 10 km of the observatory of magnitude larger than 2, are shown at the bottom of Fig. 2. Details are listed in Appendix 3. The December 4, 1982 magnitude 3.9 earthquake is the only large event which is close to the observatory. However, this earthquake occurred before we had reliable, continuous measurements of water level. The relevant part of the tilt record was compared with manual measurements of water level by Peters and Beaumont [3], who showed that the November tilt transient and recovery was associated with water level changes, typical for that time of year. The largest event during the entire period was the magnitude 4.0 January 11, 1986 earthquake with epicenter 23 km northeast of the observatory. There is a suggestion of a coherent change in the trend of the east residual tilt during the middle of 1985, particularly noticeable in borehole 3 *X*-direction (120° azimuth). No relationship to the January 11 event is claimed because corrections for water table changes at the end of 1985 are

poor and we expect precursors to earthquakes of this size to be confined within a few kilometers of the epicenter and to span the order of days.

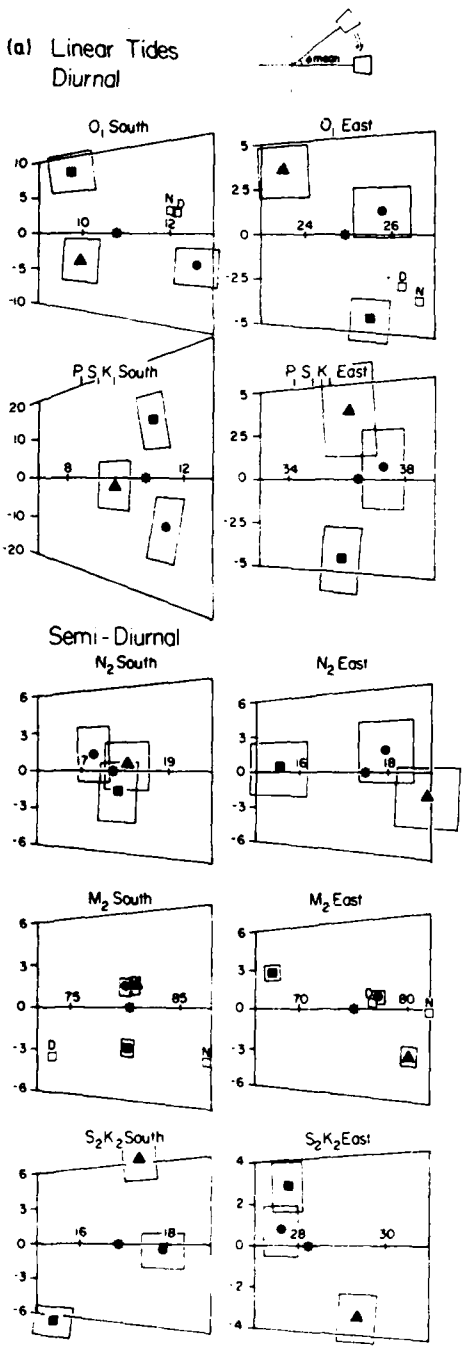

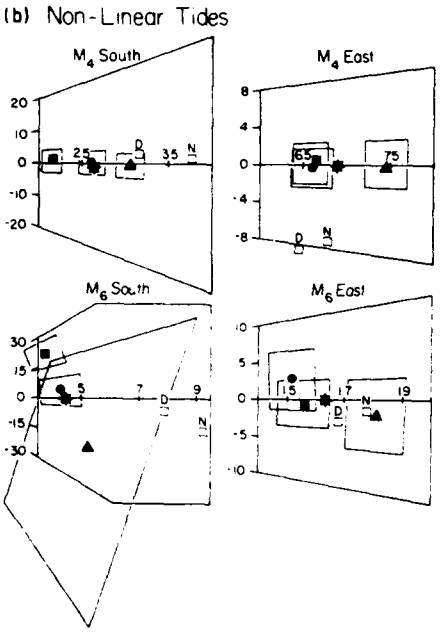

Fig. 3. Plot of the mean admittance vectors for: (a) the principal linear tides, and (b) the principal non-linear tides. Construction of the diagrams is indicated at the top right of Fig. 3a. The mean observed phase lag has been subtracted from the admittance for each constituent so that amplitude and phase differences among the different constituents can be compared directly. The scale along the zero phase line represents amplitude in nrad, and the vertical scale represents phase lag in degrees. The star (★) indicates the average amplitude among the 3 boreholes. The solid symbols indicate the observed data: a square (■) for borehole 1, a triangle (▲) for borehole 2 and a circle (●) for borehole 3. 95% confidence estimates in the observed data are represented by the box surrounding each symbol and are based on the temporal variability of the admittance. The star represents the mean of the admittance for the three boreholes, and the open squares show the theoretical tilt for O_1, M_2, M_4 and M_6 based on tidal loading calculations from Peters and Beaumont [3] and Peters and Kümpel [17]. D indicates the calculation in which known drying areas (see dotted areas in Fig. 1) always remain dry; N indicates the case in which there is no drying.

4. Mean tidal admittance

A comparison of the mean admittances for constituents M_2 and O_1 measured in boreholes 1 and 2 was made in [3]. We add here the linear tide constituents $P_1S_1K_1$, N_2 and S_2K_2 and non-linear constituents M_4 and M_6, and the new estimates from borehole 3. The analysis results (Fig. 3a, b) are compared with theoretical tilt calculations for

M_2 and O_1 [3] and for M_4 and M_6 [17]. The calculations are based on loading models of the St. Lawrence estuary. The analysis results for M_4 and M_6 are for a longer period than presented in Peters and Kümpel [17].

Although the azimuth of the tiltmeter in borehole 3 could not be measured directly, comparison of the borehole 3 diurnal and semi-diurnal amplitudes and phases with those of boreholes 1 and 2, allowed the recording direction to be determined with an uncertainty of $\pm 5°$. The M_2 constituent for the tiltmeter in borehole 3 was forced to agree as closely as possible with the south component M_2 estimate from borehole 2 in order to obtain a best estimate of the borehole 3 tiltmeter azimuth. We recognize that this choise was arbitrary, but it has little effect on the following discussion which emphasizes the lack of coherency among the mean tidal measurements.

The phasor plots (Fig. 3) reveal a surprisingly low level of coherency among the redundant measurements, a result which was quite unexpected from borehole measurements which have generally shown good agreement in adjacent installations [2,18,19]. Among the three sets of measurements, there is no systematic pairing of the results. Furthermore, the model data do not favour any one borehole, a result which is not surprising since the crustal model used in the calculations does not include the effects of the regional geology, and the load tide distribution in the vicinity of the observatory is poorly constrained by observation [3]. What do emerge, however, are patterns in the admittance results which are dependent on the tidal species and the component azimuth.

The east component diurnal observations differ mainly in phase, the phase lag increasing progressively in the results from hole 1 to holes 3 and 2 for both O_1 and $P_1S_1K_1$. For the south direction, the phase in hole 1 lags that from holes 2 and 3 in both constituents even when the uncertainty in azimuth of tiltmeter 3 is included. The semi-diurnals for the south component show a consistent pattern with the phase from borehole 1 leading that from borehole 2, while for the east component the borehole 2 result leads that from borehole 1 in phase and is the largest in amplitude. Apart from M_6 in the south, which is poorly determined because of its small amplitude, the non-linear constituents differ mainly in amplitude, hole 2 estimates in all cases being the largest.

As pointed out by Peters and Kümpel [17], the anomalies in the tidal tilt are not due to instrumental errors, but most be attributed to an inhomogeneous crustal response to the regional tidal forces. The major water bearing fractures that were encountered at different levels in each of the holes during drilling provide further evidence for inhomogeneities. When the amplitude and phase lag anomalies are characteristic of each of the tidal species, strain-tilt coupling may be the cause. The similarity of the M_2 and N_2 anomaly pattern (Fig. 3a) suggests that strain-tilt coupling may occur, but the O_1 and $P_1S_1K_1$ comparison (Fig. 3a) is less convincing, as is that for S_2K_2 by comparison with the other semi-diurnal constituents.

5. Time variations in the tidal admittance

The results of the time variant analysis of the tidal data are shown in the form of vector plots (Figs. 4–6) for constituents M_2, O_1, $P_1S_1K_1$, M_4 and M_6. The lower half of Fig. 4 shows how the plots should be interpreted. The level of agreement between boreholes for the time varying tilt admittance is remarkably high for all constituents except the south component of M_6 which is incoherent between boreholes, probably because of its small mean amplitude, about 0.5 nrad. Although we expect the tidal admittance to be stable, the fractional changes are surprisingly large—up to 10% for M_2 and 35–60% for the diurnal constituents. Small changes may not appear significant relative to the typical least squares error derived from individual analyses, but must be so because they are coherent among boreholes. As argued by Peters and Beaumont [3], the least squares error itself reflects the non-stationarity of the admittance and is therefore not a valid test of the significance of the variations. Clearly, the best measure of the significance of the time variations is the level of coherency between the redundant measurements. It is interesting that the time behaviour of the admittance variations is so similar despite the significant differences in the mean admittances.

Both components of the M_2 tilt are dominated by phase variations which are particularly clear in the 1984 and 1985 data during which there ap-

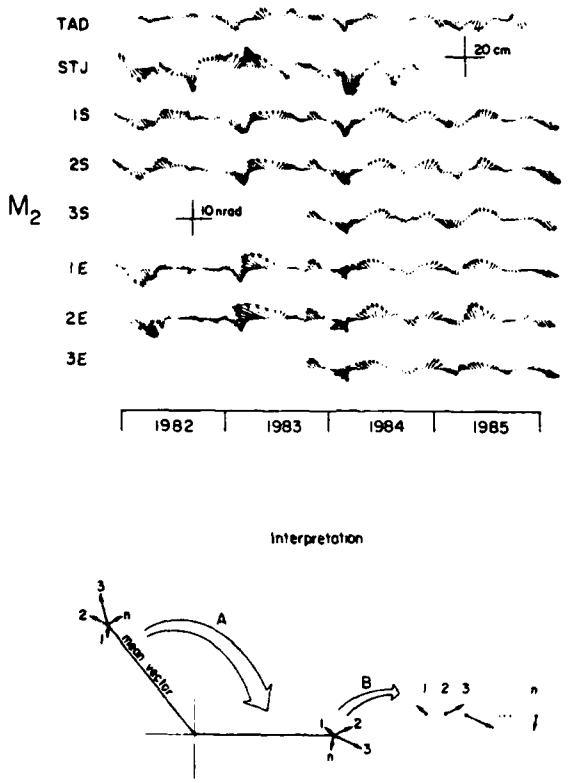

Fig. 4. Time variations of the M_2 admittance with respect to the mean from HYCON analyses of tilt data from boreholes 1, 2 and 3 and tide gauge data from stations Tadoussac and St. Joseph de la Rive. Interpretation of the diagram is shown in the lower half of the figure. The first diagram on the left represents the mean vector and associated difference vectors representing the variations from the mean. Step *A* involves the rotation to zero mean phase. Step *B* then shows the rotated difference vectors plotted as a function of time, each vector having as its origin the end point of the rotated mean vector. It is this series that is plotted for M_2 above and equivalently in Figs. 5, 6 and 8. Changes in the length of the vectors perpendicular to the time axis are primarily changes in phase. The component parallel to the time axis represents amplitude.

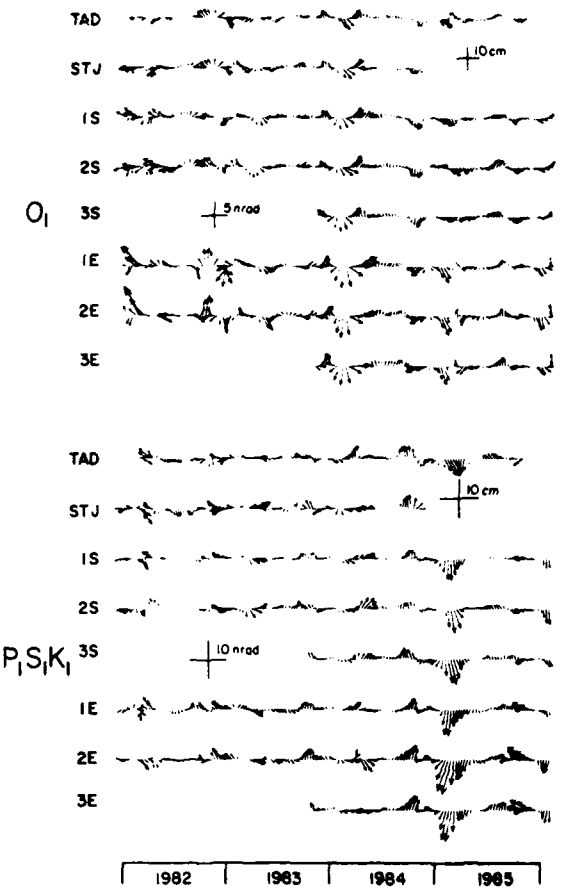

Fig. 5. Time variations of the O_1 and $P_1S_1K_1$ admittances with respect to their means. See Fig. 4 for details.

pears to be a cycle of about 6 months length. Each year begins with a period in which there is a phase lead followed by two periods of phase lag, of which the first is the most significant. This was also identified in the M_2 amplitude variations described by Peters and Beaumont [3] and may possibly be attributed to modulation by the non-linear interactions MKS_2 and MSK_2. While the apparent periodicity is not so obvious, there is a tendency for the M_4 and M_6 (east) data to show the same pattern as M_2 (Fig. 6), especially during intervals of strong change. This is expected since these constituents are non-linear interactions of M_2 with itself and, therefore, should be subject to the same fluctuations.

Both diurnal constituents show prominent amplitude changes together with variations in phase. There are minor systematic differences between the east and south component variations, but the three redundant measurements in each direction are highly coherent. Unlike the M_2 constituent, there is no clear periodicity in the variability of the O_1 or $P_1S_1K_1$ constituents. Instead, there is a tendency for the variance of the admittance fluctuations to be seasonal, most of the activity occurring near the turn of the year, in the middle of winter.

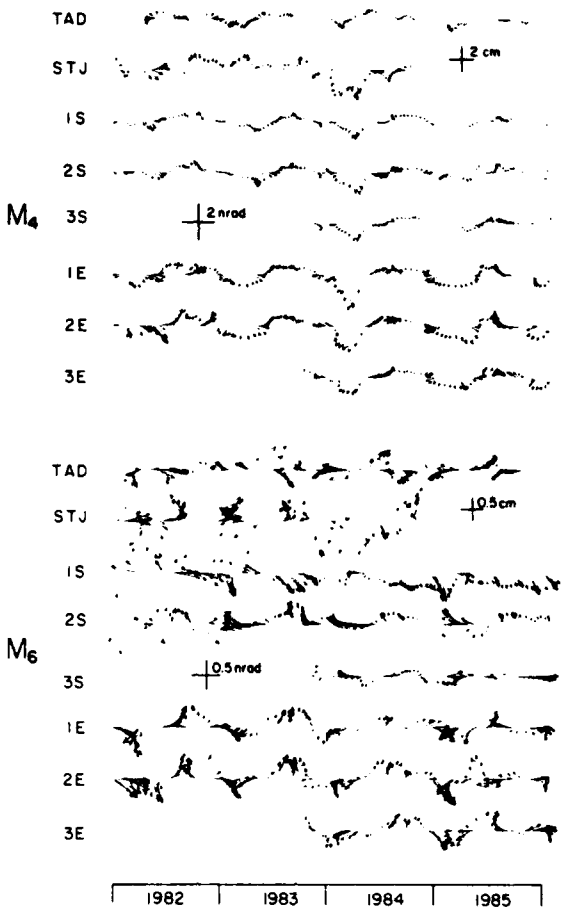

Fig. 6. Time variations of the M_4 and M_6 admittances with respect to their means. See Fig. 4 for details.

We know from our earlier work that variations in the tidal loading from the St. Lawrence river are responsible for much of the tilt behaviour. This is obvious for the diurnal constituents O_1 and $P_1S_1K_1$ which correlate well with equivalent variability in the St. Joseph de la Rive and Tadoussac tide gauge observations (Fig. 5), especially after 1982 when there were few gaps in the tilt data. The M_2 behaviour is more complex. Although not obvious from the data (Fig. 4), the amplitude variations of the tilt and both of the tide gauges correlate well, with correlation coefficients, r, between 0.8 and 0.9 in both the south and the east directions. The phase correlations, however, are low, r ranging from 0.1 to 0.5, except in the case of the south tilt and Tadoussac for which r is 0.75. The M_2 phase correlation between the two tide gauges is 0.15, a result which emphasizes the poor spatial coherency of this constituent within the estuary. The implication of this result is that prediction of the marine tides and correction of the tilt data for the time varying loading input may require more than the data from one or two tide gauges because the load is a spatially integrated effect.

6. Marine tides in the St. Lawrence estuary

An investigation of the way in which the marine tides in the St. Lawrence estuary change in space and time was carried out by analysing simultaneous recordings from a wide distribution of tide gauges (Fig. 7). Unfortunately, the only period in which all gauges were operating continuously was from August, 1972 to July, 1974, an interval that does not overlap with the tiltmeter observations. Fig. 8 shows the time varying part of the admittance (with the mean removed) for constituents M_2, N_2, S_2K_2, O_1 and $P_1S_1K_1$ plotted and interpreted in the same way as Figs. 4–6. O_1 and $P_1S_1K_1$ demonstrate remarkable spatial coherency, indicating that the whole estuary is responding coherently, with some enhancement upstream, to the mechanism responsible for their variability. Although the O_1 and $P_1S_1K_1$ variations are not congruent, they both show an apparent seasonal dependence in the variance of their modulation, as already seen in the tilt, which suggests seasonal storm surge activity as a driving force.

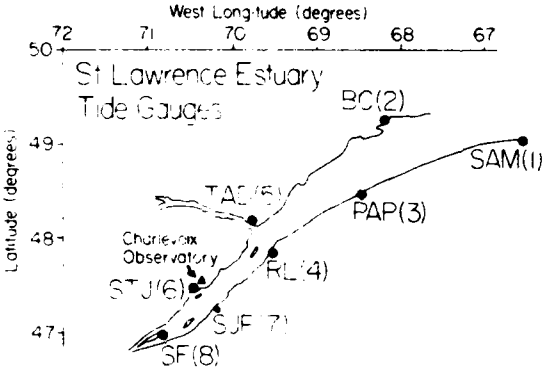

Fig. 7. Map of the St. Lawrence estuary showing the locations of tide gauges.

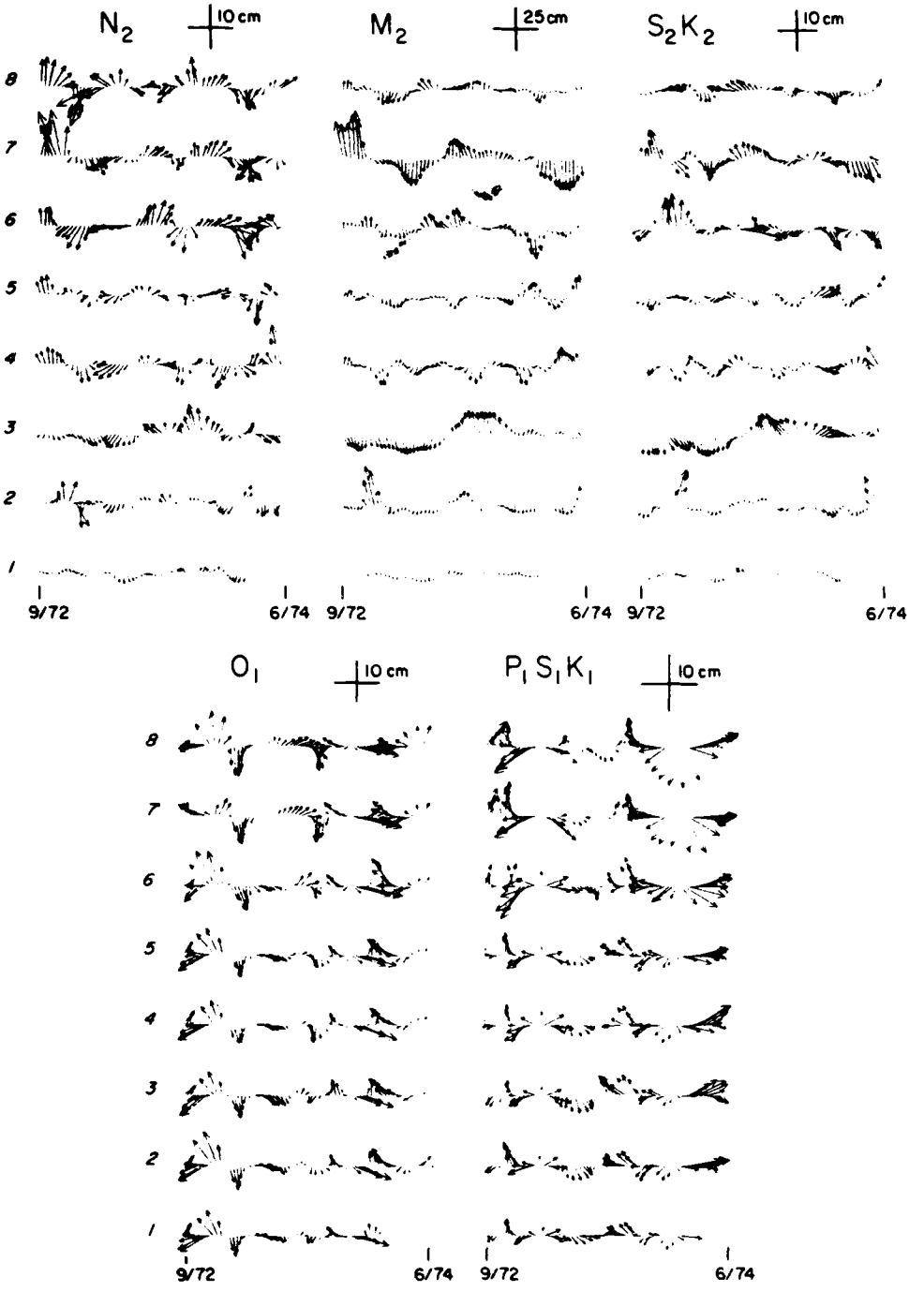

Fig. 8. Time variations of the admittance for St. Lawrence river tide gauge data for semi-diurnal constituents N_2, M_2 and S_2K_2 and diurnal constituents O_1 and $P_1S_1K_1$ with respect to their means. The series numbers correspond with the stations listed in Appendix 2 and shown in Fig. 7. The construction and interpretation of the diagrams is the same as described in Fig. 4.

In contrast, the best determined semi-diurnal constituent, M_2, shows little spatial coherency in its variations, although there sometimes appears to be local agreement among adjacent stations. For example, the series for Tadoussac (5) and St. Joseph de la Rive (6) correlate quite well in the amplitude changes (especially in the second half of the record), but not the phase (see Fig. 9). This is consistent with the kind of behaviour observed from 1982 to 1984 for those stations. This pattern persists for the station at St. Francois (8) further upstream, but is not apparent in the variations at St. Jean-Port-Joli (7) which is on the south shore directly opposite St. Joseph de la Rive.

Interestingly, the variations in N_2 and S_2K_2 show generally the same type of behaviour as those in M_2, a result that is especially obvious for the Pointe au Pere (3) and St. Jean-Port-Joli (7) gauges where the variations are almost entirely changes in phase. Unlike the variations in the two diurnal constituents, which behave somewhat differently from one another at each location but are individually uniform over the estuary, the semi-diurnal constituents have some coherence within a tidal species at some locations but are unrelated in space.

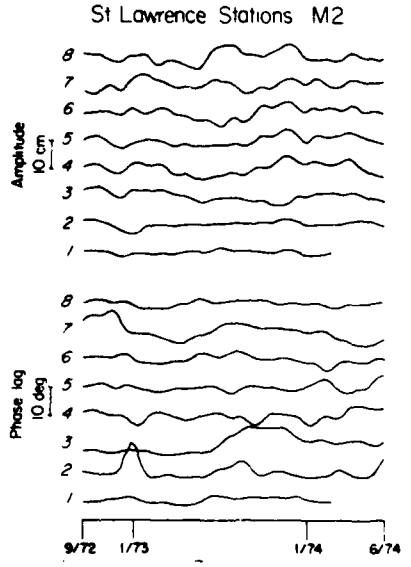

Fig. 9. M_2 amplitude and phase lag changes derived from the St. Lawrence river tide gauges plotted as a function of time. The series numbers correspond with the stations listed in Appendix 2 and shown in Fig. 7.

The task of modelling and compensating for the diurnal loading variations on the tilt observations is straightforward. Observations from a single tide gauge can be used to infer the integrated loading effect because the variations are highly coherent. For semi-diurnal M_2, the best determined and therefore most useful constituent for crustal response studies, some compensation can be made for the amplitude fluctuations of the load tide and, to some extent, the phase because the variations are somewhat correlated with the tide at Tadoussac. To establish a better resolved threshold for tectonic tidal variations will require a more complete model of the time varying load. That will require the identification of the process or processes driving the complex M_2 response.

7. Residual tide variations and a threshold for tectonic effects

The time varying marine loading effect on tilt at Charlevoix is particularly large. Our ability to correct for this variation limits our ability to detect any tectonic variations in tidal admittance. Fig. 10 shows plots of the residual tilt amplitude and phase variations for M_2 and O_1 from the three boreholes, having first removed the variations that are correlated with the Tadoussac tide gauge. Also plotted are the observed Tadoussac tidal amplitudes and phases, which are included to provide more control on the interpretation of possible tectonic effects, and the distribution of Charlevoix earthquakes.

The residual variations, especially for the M_2 constituent, are still strongly influenced by the loading. Therefore, the best we can do is to identify prominent deviations in the tilt response which are not accompanied by fluctuations in the marine tide. One convincing event of this kind occurs in the M_2 residuals. During the middle of 1985, the M_2 phase lag in both components increases above the background variations by about 3°. The effect of overlapping analyses is to broaden an event which perhaps lasted as little as a few days. The anomaly does not appear to be associated with any seismic activity. Anomalies of this size that lasted longer would certainly be detectable above the average residual load-induced fluctuations. The range of these residual loading effects determines the detectability of all tectonic effects.

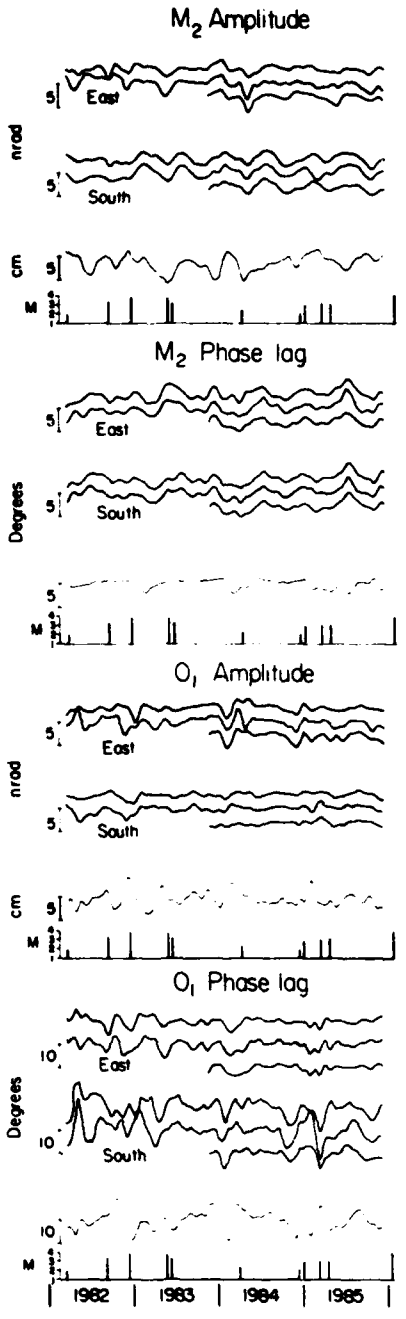

Fig. 10. M_2 and O_1 residual tilt amplitude and phase lag variations after regression against the tide gauge admittance variations observed at Tadoussac. The Tadoussac tide gauge admittance variations and the Charlevoix earthquakes, listed in Appendix 3, are shown below each of the residual tilt plots.

Coherent anomalies larger than ± 1.5 nrad ($\pm 2\%$) either in phase or quadrature for M_2 and ± 1 nrad for O_1 ($\pm 5\%$ and $\pm 8\%$ for the east and south components, respectively) would be detectable at Charlevoix. We suggest that in regions with minimal loading effect, or during intervals of stable marine tides, variations as small as ± 0.5 nrad could be detected using similar analysis techniques.

8. Discussion and conclusions

The borehole tiltmeter experiment has operated nearly continuously at Charlevoix for four years. We have concentrated during that period on observing the long-term non-tidal tilt and the linear and non-linear tidal response, with emphasis on the time variation of the tidal admittance.

The long-term tilt is dominated by the effects of groundwater level changes, presumably due to the opening and closing of cracks in response to changes in hydrostatic pressure [6]. A linear model of the water table effect leaves sufficient residual energy in recordings at 50 m depth to frustrate the search for regional, tectonic anomalies smaller than 1 μrad lasting from days to weeks. Additional attenuation of water table effects by at least a factor of three at 110 m depth, increases the detectability of regional, short-term anomalies to approximately 0.3 μrad over the same period range. The amplitude and direction of the maximum linear drift is nearly identical in boreholes 2 and 3 at less than 0.75 μrad/yr, and is comparable with the best measurements so far reported from continuous tilt measurements. It is, however, unlikely that the linear drift has a broad, regional significance. Buchbinder et al. [20] report elevation changes over 50 km baselines no greater than 2–3 cm since the 1920's when levelling measurements first began in the Charlevoix area. The corresponding implied average tilt rate over the period from 1977 to 1982 is less than 0.1 μrad/yr, an order of magnitude less than observed in the boreholes.

It is probably impossible to place significant constraints on the regional crustal structure or the marine tide distribution—traditional objectives of tidal research—at Charlevoix because of the overall lack of spatial coherency of the mean admittance among the redundant measurements. The

variation in the tidal anomalies among the constituents confirms that the rocks are locally heterogeneous.

Results for the time variation studies are more encouraging. The impressive agreement between boreholes, for all major constituents, of the time variations in the tidal admittance indicates a regional source for those variations. We have shown that a non-stationary marine load is largely responsible for the time varying tilt admittance. Similar time varying tides are discussed by Baker and Alcock [21]. Corrections can be made for the load tide fluctuations in the diurnal band because the effects are shown to be spatially coherent over the whole estuary, which permits the use of a single tide gauge to represent the loading. The semi-diurnal and related non-linear constituents cannot be corrected easily. There is little agreement in the tide gauge data from station to station, especially in the phase variations, although the pattern tends to be uniform across the semi-diurnal frequency band for a particular station. In the absence of a reasonable physical explanation for this unusual behaviour, we suggest that unsystematic timing errors in the tide gauge data could produce the observed phase behaviour. This argument is supported by the following observations.

(1) timing errors are known to occur in the tide gauge recordings,

(2) such errors will result in a predominantly phase modulation in which the semi-diurnal effect will be twice as large as that for diurnal constituents, and

(3) the effects would be less apparent in the diurnal band because the observed coherent phase changes are an order of magnitude larger than the expected timing-induced modulation.

Changes in the tidal admittance that are greater than ± 1.5 nrad would be detectable at Charlevoix. This threshold would be further reduced to about ± 0.5 nrad in the absence of load tide variations. The importance of the threshold to the detectability of changes depends on the amplitude of the constituent. In the case of M_2 at Charlevoix, ± 1.5 nrad is equivalent to $\pm 2\%$ in amplitude. In other areas, such as mid-continental regions with a small loading contribution, the M_2 amplitude is typically 40 nrad, and a ± 0.5 nrad threshold would result in a $\pm 1\%$ level of detectability. This level could, however, only be achieved under circumstances where high-quality long baselength or deep borehole instrumentation are used in installations where there is not a large response to aperiodic meteorological and groundwater effects.

Acknowledgements

This project was supported by the Air Force Geophysics Laboratory, Hanscom AFB (under contracts F19628-80-C-0032 and F19628-83-K-0023), the Natural Sciences and Engineering Research Council through operating and equipment grants and the Division of Geophysics, Geological Survey of Canada. The Marine Environment Data Service provided the tide gauge data. We would like to thank Keith Thompson and Dan Kelley for their suggestions regarding the causes of tide gauge admittance variations, Don Bower for providing the well level data, and Tony Lambert for his interest and support throughout the program. Jacques Labrecque provided invaluable field support, Benoit Dostaler, Dianne Lemieux and Josée Laurion maintained the array on a daily basis, and John Fahey and Peter Bugden assisted with data reduction and analysis. Constructive reviews by Bob Edge and Walter Zürn are gratefully acknowledged.

References

1 F. Wyatt, G. Cabaniss and D.C. Agnew, A comparison of tiltmeters at tidal frequencies, Geophys. Res. Lett. 9, 743–746, 1982.

2 R.J. Edge, T.F. Baker and G. Jeffries, Some results from simultaneously recording tiltmeters, in: Proceedings of the Ninth International Symposium on Earth Tides, J.T. Kuo, ed., pp. 9–16, E. Schweizerbart'sche Verlagsbuchhandlung, Stuttgart, 1983.

3 J. Peters and C. Beaumont, Borehole tilt measurements from Charlevoix, Québec, J. Geophys. Res. 90, 12791–12806, 1985.

4 R.J. Edge, T.F. Baker and G. Jeffries, Borehole tilt measurements: aperiodic crustal tilt in an aseismic area, Tectonophysics 71, 97–109, 1981.

5 K. Herbst, Interpretation of tilt measurements in the period range above that of the tides (in German), Ph. D. Thesis, Tech. Univ. Clausthal, Clausthal-Zellerfeld, 1976 (English translation, Tech. Rep. AFGL-TR-77-0162, Air Force Geophys. Lab., Bedford, Mass., 1979.).

6 K. Evans and F. Wyatt, Water table effects on the measurement of earth strain, Tectonophysics 108, 323–337, 1984.

7 H.-J. Kümpel, The effect of variations on the groundwater table on borehole tiltmeters, in: Proceedings of the Ninth International Symposium on Earth Tides, J.T. Kuo, ed., pp.

APPENDIX 1

Charlevoix tilt—mean admittance from HYCON

Constituent			South		East	
			amp. (nrad)	phase lag (deg)[a]	amp. (nrad)	phase lag (deg)[a]
O_1	Observed	1	10.1 ± 0.5	(280.6 ± 2.5)	25.5 ± 0.5	(298.3 ± 1.1)
		2	10.4 ± 0.4	(269.9 ± 2.8)	23.3 ± 0.6	(306.3 ± 1.4)
		3	12.6 ± 0.5	(270.4 ± 1.9)	25.5 ± 0.7	(304.1 ± 1.3)
	theory	D[b]	12.2	(276.6)	26.3	(300.3)
		N	12.0	(276.8)	26.7	(299.7)
$P_1S_1K_1$	observed	1	10.9 ± 0.5	(319.8 ± 4.7)	35.7 ± 0.7	(316.2 ± 1.7)
		2	9.7 ± 0.5	(310.0 ± 4.7)	35.6 ± 0.9	(324.3 ± 2.4)
		3	11.5 ± 0.5	(301.7 ± 5.4)	37.0 ± 0.7	(321.5 ± 2.0)
N_2	observed	1	17.9 ± 0.4	(227.5 ± 2.1)	15.5 ± 0.6	(196.0 ± 2.1)
		2	18.1 ± 0.5	(229.5 ± 1.7)	18.9 ± 0.7	(194.0 ± 2.0)
		3	17.3 ± 0.4	(230.3 ± 2.1)	18.0 ± 0.6	(197.2 ± 2.1)
M_2	observed	1	80.7 ± 0.6	(260.7 ± 0.6)	68.1 ± 0.7	(246.2 ± 0.6)
		2	81.7 ± 0.5	(264.6 ± 0.6)	80.3 ± 0.8	(240.6 ± 0.7)
		3	80.3 ± 0.6	(264.5 ± 0.6)	77.7 ± 0.7	(244.0 ± 0.5)
	theory	D[b]	73.5	(259.5)	76.8	(243.4)
		N	87.9	(259.8)	81.9	(242.9)
S_2K_2	observed	1	15.5 ± 0.4	(309.9 ± 1.2)	27.8 ± 0.3	(309.7 ± 1.2)
		2	17.5 ± 0.4	(322.6 ± 1.5)	29.4 ± 0.4	(303.9 ± 1.1)
		3	17.9 ± 0.5	(315.9 ± 1.3)	27.6 ± 0.4	(307.7 ± 1.2)
M_4	observed	1	2.2 ± 0.1	(342.4 ± 3.3)	6.6 ± 0.2	(353.2 ± 2.0)
		2	3.1 ± 0.2	(340.3 ± 2.7)	7.5 ± 0.2	(353.2 ± 2.1)
		3	2.7 ± 0.2	(341.9 ± 2.9)	6.6 ± 0.2	(352.8 ± 1.9)
	theory	D[b]	3.2	(341)	6.5	(345)
		N	3.8	(340)	6.8	(346)
M_6	observed	1	0.4 ± 0.1	(91.8 ± 6.6)	1.6 ± 0.1	(24.8 ± 2.9)
		2	0.6 ± 0.2	(52.5 ± 35.9)	1.8 ± 0.1	(23.6 ± 3.8)
		3	0.4 ± 0.1	(73.7 ± 6.0)	1.5 ± 0.1	(27.8 ± 3.5)
	theory	D[b]	0.8	(68)	1.7	(23)
		N	0.9	(64)	1.8	(24)

[a] Greenwich phase lag in degrees. Error estimates are 95% confidence intervals.
[b] D and N are explained in Fig. 3.

APPENDIX 2

St. Lawrence River tide gauges—mean admittance from HYCON

Station	M_2		N_2	S_2K_2	O_1	$P_1S_1K_1$
1 SAM	92.9[a]	(162.9)[b]	19.2 (136.1)	29.2 (204.0)	19.9 (238.5)	20.9 (264.9)
2 BC	117.5	(164.0)	24.3 (136.1)	37.6 (204.6)	20.4 (236.7)	22.5 (262.6)
3 PAP	124.3	(173.1)	25.3 (146.1)	40.5 (214.4)	21.0 (239.4)	23.4 (266.0)
4 RL	153.0	(194.7)	31.3 (163.8)	49.7 (234.0)	21.7 (246.6)	24.1 (272.8)
5 TAD	155.0	(184.0)	31.0 (155.5)	50.2 (255.5)	21.8 (242.2)	24.0 (268.4)
6 STJ	202.0	(227.0)	37.2 (193.8)	61.6 (265.8)	23.3 (257.7)	26.1 (283.5)
7 SJP	184.8	(252.3)	31.2 (221.4)	49.9 (295.8)	23.0 (274.6)	25.5 (302.2)
8 SF	199.2	(274.2)	32.8 (243.7)	49.3 (321.5)	22.7 (287.2)	24.9 (314.6)

[a] Amplitude in cm;
[b] Greenwich phase lag in degrees.
Stations: SAM = St. Anne des Monts; BC = Baie Comeau; PAP = Pointe au Père; RL = Rivière du Loup; TAD = Tadoussac; STJ = St. Joseph de la Rive; SJP = St. Jean-Port-Joli; SF = St. François.

APPENDIX 3

Charlevoix earthquakes—September, 1982 to June, 1986 [a]

Data	Magnitude	Depth (km)	Distance (km)	Lat.	Long.
27 Jan 82	3.3	6	12	47.45	70.38
6 Mar 82	2.0	4	6	47.52	70.39
29 Aug 82	3.4	20	19	47.37	70.38
4 Dec 82	3.9	15	8	47.54	70.22
15 May 83	3.8	11	38	47.69	69.89
2 Jun 83	3.3	10	9	47.44	70.24
24 Mar 84	2.4	20	8	47.51	70.25
3 Dec 84	2.1	7	10	47.47	70.38
22 Dec 84	3.0	19	17	47.40	70.25
3 Mar 85	3.1	14	22	47.39	70.48
10 Apr 85	3.1	12	28	47.52	69.96
11 Jan 86	4.0	5	23	47.70	70.11

[a] Includes events $M = 2.0$ and greater within 10 km of the observatory and all events $M = 3.0$ and greater.

33–45, E. Schweizerbart'sche Verlagsbuchhandlung, Stuttgart, 1983.

8 E. Nishimura, On earth tides, EOS Trans. Am. Geophys. Union 31, 357–375, 1950.

9 T. Mikumo, M. Kato, H. Doi, Y. Wada, T. Tanaka, R. Shichi and A. Yamamoto, Possibility of temporal variations in earth tidal strain amplitudes associated with major earthquakes, in: Earthquake Precursors: Proceedings of the U.S.-Japan Seminar on Theoretical and Experimental Investigations of Earthquake Precursors, K. Kisslinger and Z. Suzuki, eds., pp. 123–136, Central Academic Publishers of Japan, Tokyo, 1978.

10 M. Kato, Observations of crustal movements by newly-designed horizontal pendulum and water-tube tiltmeters with electromagnetic transducers, 2, Bull. Disaster Prev. Res. Inst. Kyoto Univ., 29, Part 2, 83–97, 1979.

11 C. Beaumont and J. Berger, Earthquake prediction: modification of the earth tide tilts and strains by dilatancy, Geophys. J.R. Astron. Soc. 39, 111–121, 1974.

12 T. Tanaka, Effect of dilatancy on ocean load tides, Pure Appl. Geophys. 114, 415–423, 1976.

13 C. Beaumont, Linear and nonlinear interactions between the earth tide and a tectonically stressed earth, in: Applications of Geodesy to Geodynamics, I. Mueller, ed., pp. 313–318, Ohio State University Press, Columbus, Ohio. 1978.

14 J. Peters, C. Beaumont and R. Boutilier, Borehole tilt measurements at the Charlevoix Observatory, Québec, Tech. Rep. AFGL-TR-83-0027, Air Force Geophys. Lab., Bedford, Mass., 1983.

15 D. Flach and O. Rosenbach, The Askania borehole tiltmeter (tide pendulum) of A. Graf at the Zellerfeld-Muhlenhohe testing station, Bull. Inf. Marees Terr. 60, 2934–2943, 1971.

16 K. Schüller, Tidal analysis by the hybrid least squares frequency domain convolution method, in: Proceedings of the Eighth International Symposium on Earth Tides, M. Bonatz and P. Melchior, eds., Institut für Theoretische Geodesie Der Universität Bonn, 1977.

17 J.A. Peters and H.-J. Kümpel, Non-linear tides from the Charlevoix seismic zone in Québec, submitted to Geophys. J.R. Astron. Soc.

18 D. Flach, W. Grosse-Brauckmann, K. Herbst, G. Jentsch and O. Rosenbach, Results of long-term recordings with Askania borehole tiltmeters—comparative analysis with respect to the tide parameters and long period portions and instrumental investigations, Rep. B211, Dtsch. Geod. Komm., pp. 72–95, Munich, 1975.

19 J. Zschau, Tidal sea load tilt of the crust, and its application to the study of crustal and upper mantle structures, Geophys. J.R. Astron. Soc. 44, 577–593, 1976.

20 G. Buchbinder, R. Kurtz and A. Lambert, A review of time-dependent geophysical parameters in the Charlevoix region, Québec, Earthq. Predict. Res. 2, 149–166, 1983.

21 T.F. Baker and G.A. Alcock, Time variation of ocean tides, in: Proceedings of the Ninth International Symposium on Earth Tides, J.T. Kuo, ed., pp. 341–348, E. Schweizerbart'sche Verlagsbuchhandlung, Stuttgart, 1983.

22 F. Wyatt, R. Bilham, J. Beavan, A. Sylvester, T. Owen, A. Harvey, C. Macdonald, D. Jackson and D. Agnew, Comparing tiltmeters for crustal deformation measurement—a preliminary report, Geophys. Res. Lett. 11, 963–966, 1984.

23 G.H. Cabaniss, The measurement of long period and secular deformation with deep borehole tiltmeters, in: Applications of Geodesy to Geodynamics, I. Mueller ed., pp. 165–169, Ohio State University Press, Columbus, Ohio, 1978.

J Geophys (1988) 62:128–135

Journal of Geophysics

Investigation of non-linear tilt tides from the Charlevoix seismic zone in Quebec

J. Peters* [1] **and H.-J. Kümpel** [2]

[1] Oceanography Department, Dalhousie University Halifax, Nova Scotia, Canada, B3H 4J1
[2] Institute of Geophysics, Kiel University, D-2300 Kiel, Federal Republic of Germany

Abstract. Under certain conditions of crustal stress, non-linearities may be generated in the earth tide response. Non-linear constituents present in borehole tilt and tide gauge recordings from the Charlevoix seismic zone are studied in an attempt to discriminate between possible tectonically induced non-linear components and those resulting from non-linear interactions in the marine load tide. Mean tidal admittance estimates from harmonic analysis are compared with a loading model for constituents M_4 and M_6, and time-variant analysis is used to determine the temporal behaviour of the tilt and tide gauge admittances. Agreement between the model and mean admittance results, confirmed by some similarities in the tilt and tide gauge admittance time variations, indicates that crustal non-linearities are absent or undetectable. If laboratory observations of non-linear behaviour of highly stressed rocks are representative of in situ processes, then the apparent absence of non-linear tidal anomalies implies that the special situation in which the rate of change of the tectonic stress is equal to the mean tidal stress rate does not apply in the Charlevoix region. The experiments at Charlevoix have also allowed us to evaluate the spatial stability of non-linearities in the tidal tilt. Simultaneous recordings from two boreholes only 80 m apart show considerable discrepancies among many of the tidal constituents. It is speculated that local inhomogeneities in the granite country rock at the site are responsible for the anomalies.

Key words: Tidal tilt – Loading tides – Non-linear tides

Introduction

Most earth tide studies have been concerned with the linear response of the earth to the combined astronomical forcing and secondary tidal loading. In this study of borehole tiltmeter data from the Charlevoix seismic zone, we examine signal components in tidal data arising from non-linear processes either from a marine source (through loading) or resulting from possible non-linearity in the transfer function of the local crust. Our aim is to determine to what extent the observed non-linear components may be explained by: (a) crustal processes, (b) marine loading and (c) local inhomogeneities at the site.

The response of the earth to tidal forcing is generally described by infinitesimal linear elasticity theory. However, results from laboratory studies of brittle rock samples (Brace et al. 1966; Soga et al. 1978; Sobolev et al. 1978) have shown that at deviatoric stress greater than half the rock failure strength, volumetric strains arise due to the growth of microcracks (dilatancy). A number of models of non-linear elasticity have been proposed (Stuart, 1974; Mjachkin et al., 1975; Rice and Rudnicki, 1979) to explain both the laboratory results and field observations, in particular V_p/V_s precursors (Nersesov et al., 1969; Mjachkin et al., 1972; Whitcomb et al., 1973). As Beaumont (1978) points out, since the range of tidal stress (about 0.01 bar) is much smaller than the range of tectonic stress (about 5 kbar), the tidal response in this situation is essentially linear, though anisotropic, and governed by the state of the tectonic stress.

Scholz and Kranz (1974) showed in the laboratory that rocks subjected to cyclic loading at high deviatoric stress respond plastically and exhibit hysteresis; the energy loss is presumably due to the work against friction in opening and closing microcracks. Beaumont (1978) has described the possible effect on the tidal response where the tidal stress is superimposed on an accumulating tectonic stress field. In the case where the tectonic stress accumulation is either much less than or much greater than the mean tidal stress rate, the tidal response remains essentially linear. We should be able to distinguish between these two situations by examining the time dependence of the linear tidal response. If the response is constant then the tectonic stress, while possibly high, is only slowly varying or not varying at all. If the linear response is changing appreciably with time, this would imply that the tectonic stress rate is large and may be interpreted as being premonitory to rupture. Where the tectonic and mean tidal stress rates are approximately equal, the response is non-linear over the range of the tidal cycle. This would result in the generation of additional lines in the spectrum at sum and difference frequencies of the tidal constituents. These different styles of tidal response are therefore, in principle, diagnostic of the state of stress in the local crust. A study of time variations in the linear tidal response at Charlevoix (Peters and Beaumont, 1985) has not revealed an obvious tectonic signal, suggesting that the rate of tectonic stress accumulation is not large. It is among the aims of this study to determine

* *Present address:* Earth & Ocean Research Ltd., 22 Waddell Avenue, Dartmouth, Nova Scotia, Canada, B3B 1K3

Offprint requests to: H.-J. Kümpel

whether the tectonic stress rate is in the range of the tidal stress rate.

Agnew (1981) has studied the effect on the tidal response of intrinsic non-linearity in rocks based on evidence from seismic studies. He shows that for non-dissipative materials the strongest effect would occur at the second harmonic of the tidal constituents (for example M_4, the second harmonic of M_2), whereas for dissipative materials the effects would be generated at the odd harmonics (for example M_6, the third harmonic of M_2). The predicted non-linear strains (or tilts), however, are too small to be detected at the significance level of this study. It should be emphasized that this is a different problem from that described by Beaumont (1978). Whereas Agnew considers the intrinsic non-linearity of the rock, Beaumont is looking at non-linearity generated in response to applied stress close to the failure strength of the rock.

We must additionally consider the non-linear content of the tidal input. There have been numerous studies of non-linear harmonics in the marine tide (see, for example, Zetler and Cummings, 1967; Rossiter and Lennon, 1968; Gallagher and Munk, 1971). The prominent sources of these components are velocity and friction-dependent interactions in shallow water. Godin (1973) has made a detailed analysis of 8 years of tide gauge data from Québec City (150 km upstream from Charlevoix) showing the importance of the non-linear harmonics in the estuary. Since the observed tidal signal at Charlevoix is dominated by loading from the St. Lawrence estuary, there is abundant energy at the higher-order tidal harmonics (Peters and Beaumont, 1985), at least part of which must arise from shallow-water interactions. Another source of harmonics in the loading arises from rectification of the linear tide over drying areas (Zschau, 1979). This is not generally reflected in the tide gauge data since they are recorded in deep water.

Cavities, topography or geological inhomogeneities may produce strain-induced tilt anomalies that vary over short distances (Harrison, 1976). For example, Flach et al. (1975) reported an 8° phase difference in M_2 between two Askania borehole pendulums recording simultaneously in 15-m and 30-m boreholes located 10 m apart. Characteristics of the temporal variation of non-linear tides due to tectonic stress build-up or marine loading should not be masked by these local effects. They will merely result in constant phase shifts and/or constant amplitude differences between installations at various locations.

In this study we compare the mean amplitudes and Greenwich phase lags of M_4 and M_6 determined from the borehole tilt recordings taken at Charlevoix Observatory, with theoretical estimates based on a loading model of the St. Lawrence estuary. Time-variant analysis results of the tilt and nearby tide gauge data are compared to see to what extent the stability of the tidal tilt response is determined by the loading input. Finally, we consider local effects that distort the crustal tilt response in the vicinity of the site.

Data and analysis

The tilt data were recorded in two boreholes 80 m apart and 47 m deep, using Bodenseewerk (formerly Askania) borehole pendulums (Peters and Beaumont, 1985). The study was done in two parts: one using tide gauge data available from May 1, 1981 to December 31, 1982 and tilt-meter data from November 27, 1981 to July 24, 1983 for determining the spectral characteristics of the non-linear constituents; and the second using tilt and tide gauge data for all of 1983 for the mean admittance and time-variant analysis. The 1983 data set was used for the time-variant analysis because of the small number of gaps during that period, a factor which has considerable influence on the accuracy of the results. Table 1 lists details of the data analysed; Fig. 1 shows the relevant locations.

Table 1. Data used in this study

Tilt	
Borehole 1	Nov. 27, 1981–Dec. 31, 1983
Borehole 2	Nov. 27, 1981–Dec. 31, 1983
Tide Gauge	
St. Joseph de la Rive	May 1, 1981–Dec. 31, 1983
Tadoussac	Jan. 1, 1983–Dec. 31, 1983

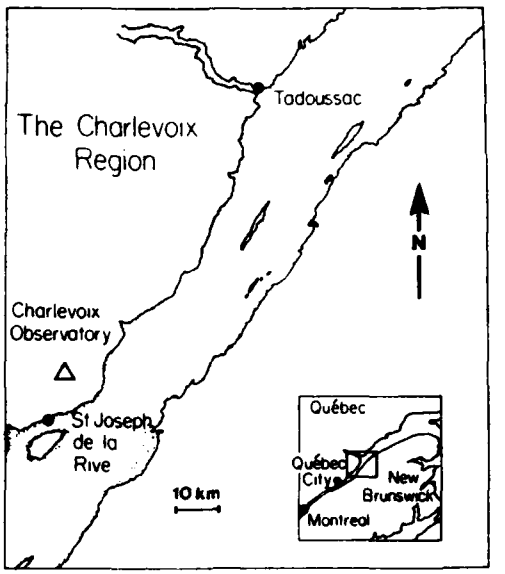

Fig. 1. Map of the St. Lawrence estuary near the Charlevoix observatory. The *stippled areas* are beaches. The location of the observatory is 47° 32.9′N, 70° 19.3′W

An adaptation of the Goertzel algorithm (Goertzel, 1958) was used to compute the amplitude spectra. Unlike the fast Fourier transform, the Goertzel method permits the rapid calculation of the direct Fourier transform for arbitrary frequencies for a time series of any length, without the need to process frequencies over the entire spectrum. The computation was done on a bandpass-filtered time series which had been multiplied by the Hanning window, so that the spectral resolution is $dw = 4\pi/(NdT)$, where dT ($= 1$ h) is the sampling interval of the data and N the number of hourly data points. Distortions from data gaps were reduced by filling the gaps with harmonic constituents from a preliminary Fourier transform that was applied to data series with linearly interpolated gaps.

For the time-variant analysis, we have used the HYCON tidal harmonic analysis program of Schüller (1977). The data from 1983 were divided into overlapping 60-day subsets with the origin shifted for each set by 10 days. The output of the program is a sequence, for each tidal harmonic, of amplitude and phase estimates derived from ana-

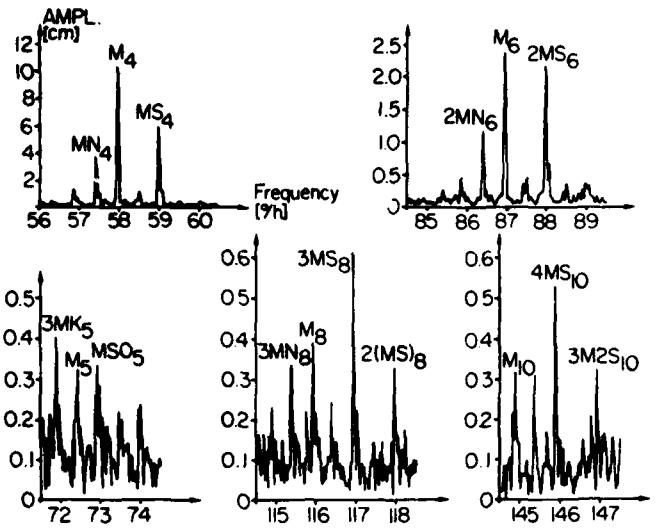

Fig. 2. High-resolution amplitude spectrum (0.05°/h bandwidth resolution) of St. Joseph de la Rive, showing the main non-linear tidal bands

lysis of the subsets, which together form a time-varying admittance function. A detailed description of the method is given in Peters and Beaumont (1985).

The marine tide

Spectrum of the marine tide

Figure 2 shows the amplitude spectrum for tidal frequencies greater than 56°/h (43 μHz) of the tide gauge at St. Joseph de la Rive for the period May 1, 1981 to December 31, 1982. Because of its close proximity to the site (Fig. 1), this tide gauge is representative of a major part of the loading at Charlevoix. The background noise level decreases from 0.3 cm within the quarter-diurnal band to 0.15 cm in the tenth-diurnal band.

Other tide gauge recordings in the estuary are shorter (in some cases less than 600 h), resulting in a lower spectral resolution. Adjacent frequencies then modulate one another, which for the shorter sets leads to biased estimates for the amplitudes and phases. Only M_4 and M_6 are free of significant interference within a bandwidth of 0.5°/h (0.386 μHz). It is for this reason that these frequencies were chosen for the comparison between the loading model and the observed mean amplitudes and phases; and for the time-variant analysis of 60-day (0.5°/h resolution) subsets of the 1983 data.

Tidal loading model

The load tilt calculations were made by the same method as Peters and Beaumont (1985) using the same triangular subdivision of the St. Lawrence estuary, but excluding the Saguenay River west of Tadoussac. The Green functions for the point load response of the Farrell Gutenberg Bullen Earth model (Farrell, 1972) were used and the integrated effect of the marine tide distribution found by convolving the Green functions with the in-phase and quadrature components of the discretized marine tide distribution. Calculations were made for the two extreme cases in which drying areas remain either wholly dry or wholly submerged. Realistic loading predictions will be affected by partial drying and should lie somewhere in between the extremes.

For the reasons mentioned above, empirical cotidal charts, based on observations from coastal tide gauges, were drawn for the non-linear constituents M_4 and M_6 only (Fig. 3a and b). Since the quarter- and sixth-diurnal tides are generally a localized shallow-water phenomenon, ocean areas beyond the mouth of the estuary were not included in the tidal distribution. Within the estuary, however, we have taken the liberty, in the absence of sufficient coastal gauges and the total lack of mid-stream stations, to freely interpolate co-amplitude and co-phase lines across the river. There is some justification for this. The across-stream depth profile is shallow on the south-eastern two-thirds (ranging from 0 to 5 m) throughout the middle part

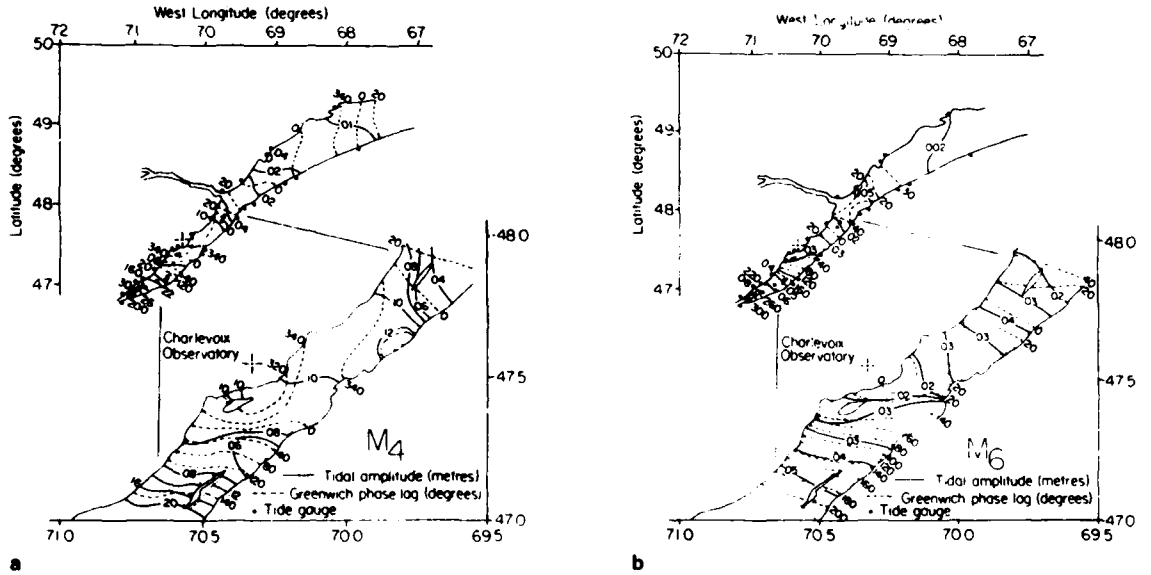

Fig. 3a and b. Empirical cotidal chart of **a** M_4 and **b** M_6 for the St. Lawrence estuary, with detail of the area adjacent to the Charlevoix site. *Dots* mark the location of tide gauge installations

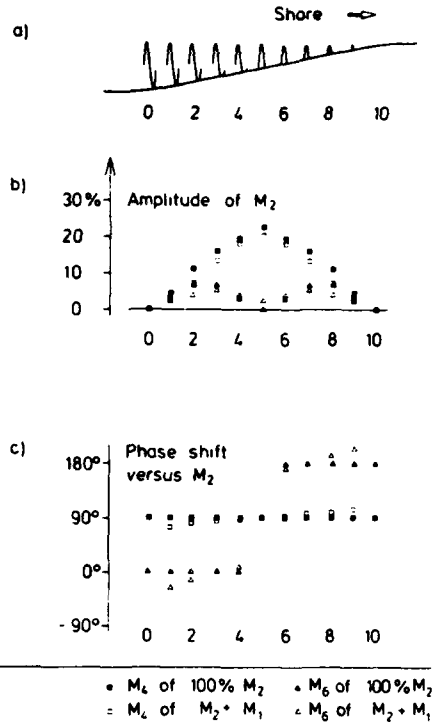

Fig. 4. **a** Schematic of a ramp-like beach showing the truncation of the linear tide as a function of position. **b** Relative amplitude of second- and third-order harmonics M_4 and M_6 of the simulated semi-diurnal M_2 tide plotted against position. **c** Phase shift of second- and third-order harmonics M_4 and M_6 of the simulated semi-diurnal M_2 tide plotted against position. Calculations were made for truncation of a single semi-diurnal wave of amplitude 1.0 (*full symbols*) and truncation of a combined 0.3-amplitude diurnal and 1.0-amplitude semi-diurnal wave series (*open symbols*), more closely resembling the real situation at Charlevoix

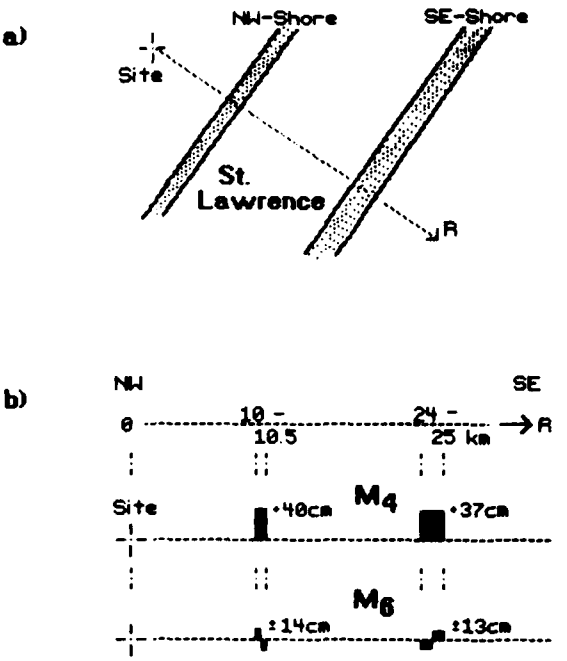

Fig. 5a and b. Geometry for loading calculations of rectified linear tide. **a** Strip-like beaches at 10.0–10.5 km and 24–25 km distance R from the site at the banks of the St. Lawrence River. **b** Maximum loading amplitudes over the whole beaches for the second-order harmonic M_4 and phase reversal midway up the beach for the third-order harmonic M_6

of the estuary, the deeper water being restricted to a channel along the north shore. We expect, therefore, non-linear interactions to occur throughout much of the shallow expanse. The least reliable part of the cotidal maps is in the area to the south of the Charlevoix site in which the steep gradient in amplitude and phase lag, for both constituents, is based on data from only two reliable tide gauges. This area clearly has the largest influence on the south tilt component, so that these results should be interpreted with caution.

Rectification of the linear tide

The non-linear tide loading model takes no account of rectification of the linear marine tide over drying areas. To estimate the effect on the loading, we simulated the truncation of the linear tide over a ramp-like beach (Fig. 4a). A set of 11 time series were synthesized to represent the tide at positions up the profile of the beach. Each series consisted of either a single sinusoid at semi-diurnal or two sinusoids at diurnal and semi-diurnal frequencies. Each series was then truncated using a gate function, the gate width determined according to position on the beach. The resulting series were Fourier transformed and amplitudes and phases of the second and third harmonics of the semi-diurnal tide (simulating M_4 and M_6) were plotted as a function of position on the beach (Fig. 4b and c). While the relative amplitudes of the harmonics, the second in particular, are quite high, there is a phase reversal of the third harmonics midway up the ramp, which results in a degree of cancellation. We will now use these results to arrive at a worst-case estimate of the effect of linear tide rectification on the non-linear loading at Charlevoix.

In the vicinity of the Charlevoix site, the width of the beaches, or drying areas, is small compared with their distance from the site. We calculated the loading tilt resulting from a 0.5-km-wide beach on the NW bank and a 1-km-wide beach on the SE bank of the St. Lawrence River (Fig. 5a). The amplitude of the marine M_2 amounts up to 2 m on the NW shore and up to 1.85 m on the SE shore (Peters and Beaumont, 1985). Taking 20% of this amplitude over the whole beach as a worst case for the second harmonic from Fig. 4b or 7% for the third harmonic, respectively, and considering partial cancellation due to phase reversal for the latter (Fig. 5b), we arrive at maximum effects of 30% of the loading model estimate of M_4 and 0.2% of the loading model estimate of M_6 (see next section). If, however, the whole drying areas were at heights represented by position 2 or 8 in Fig. 4a, no cancellation for the third-order harmonic would occur. The maximum effect could then be 40% of the loading model estimate of M_6. Therefore, a significant input from the rectification of linear tides over tidal flats cannot be excluded.

The tilt tide

Comparison of mean tidal estimates

The mean tidal estimates from the HYCON analysis of the 1983 data from boreholes 1 and 2 are compared with

Table 2. Comparison of M_4 and M_6 observations and loading model results

	Borehole 1	Borehole 2	Loading model	
			100%	0%
South				
M_4	2.19 (340.2) ±0.08 ±3.9	3.08 (339.5) ±0.11 ±3.1	3.16 (341)	3.76 (340)
M_6	0.40 (98) ±0.05 ±7	0.44 (77) ±0.06 ±7	0.79 (68)	0.93 (64)
East				
M_4	6.80 (352.7) ±0.17 ±1.9	7.77 (352.9) ±0.20 ±2.1	6.53 (345)	6.84 (346)
M_6	1.58 (25.4) ±0.08 ±3.8	1.87 (22.8) ±0.14 ±5.0	1.68 (23)	1.78 (24)

Amplitude in nanoradians, Greenwich phase lag (brackets), 95% confidence limits

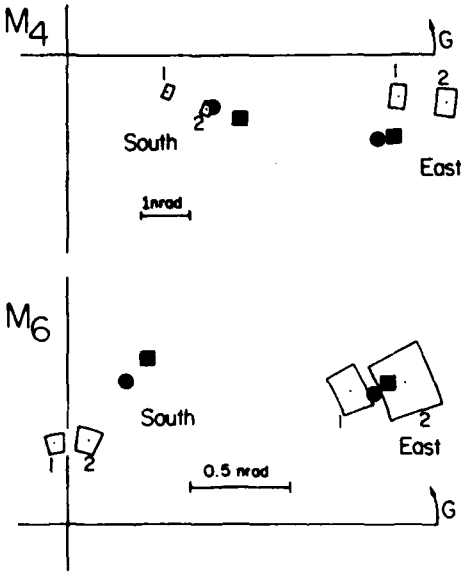

Fig. 6. Phasor plots of the M_4 and M_6 mean admittance estimates derived from the HYCON analysis of the south and east components of tilt measured in boreholes 1 and 2. The *solid dots* represent the loading model predictions for the two extreme cases in which there are no drying areas (*square dots*) and areas that do dry, doing so completely (*round dots*). Error sectors around each of the estimates are based on 95% confidence limits. *G* is Greenwich phase lag

the loading model predictions shown in Table 2. The results are displayed in the form of phasor diagrams in Fig. 6. Body tide amplitudes for M_4 are only 0.0059 nrad in EW and 0.0045 nrad in NS, using the development of Xi (1987), and even smaller for M_6. They are far beyond the resolution of the tilt measurements.

Apart from M_6 from the south direction, the borehole 1 results are systematically smaller in amplitude than those of borehole 2, but are consistent in phase. The loading model results are in reasonable agreement with the observations, except in the case of M_6 south. For M_4 east the model favours borehole 1, although both observations lag the theory by about 7°. For the south direction the model

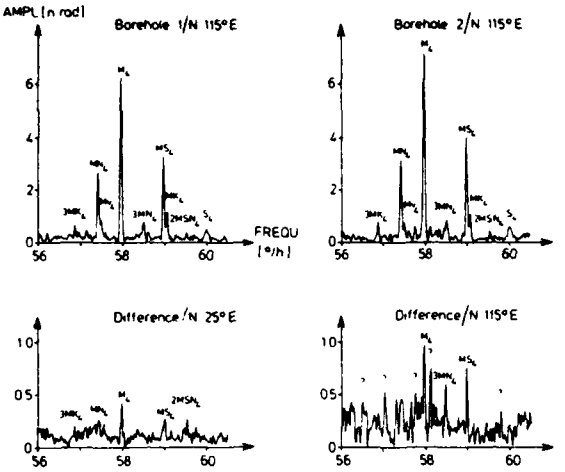

Fig. 7. High-resolution quarter-diurnal amplitude spectra (0.05°/h bandwidth resolution) of tilt in boreholes 1 and 2 and of the difference tilt signal at azimuth grossly parallel (N25°E) and perpendicular (N115°E) to the St. Lawrence River. N115°E is the azimuth at which most of the quarter-diurnal signal energy is observed

appears to overestimate the loading by as much as 100% for M_6 and by 70% and 20% for M_4 in boreholes 1 and 2, respectively, although we cannot rule out the possibility that local effects may be partly or wholly responsible for the disagreement.

Below, we examine more closely the coherency between the two borehole measurements to establish whether the differences are due to instrumental effects such as calibration or uncertainties in orientation.

Local tilt anomalies

Quarter-diurnal spectra of 20 months tilt recordings in boreholes 1 and 2 are plotted in Fig. 7. They essentially show the same tidal peaks as the tide gauge recordings in the St. Lawrence River (Fig. 2). A significant difference, however, can be seen between the tilt signals from the two boreholes. Spectra of the difference tilt signal contain non-linear tidal energy that seems to be polarized close to the azimuth of strongest marine loading.

Using the south and east admittances determined from both boreholes, we can derive the observed and difference tilt ellipses for each constituent (Tomaschek and Groten, 1963). The difference tilt for each constituent is formed from the difference between the admittance observed in boreholes 1 and 2. The ellipses are shown for the linear tides O_1, K_1, S_2, M_2 and N_2 in Fig. 8a and for the non-linear constituents MS_4, M_4, MN_4, $2MN_6$ and M_6 in Fig. 8b.

The observed ellipses for all constituents are strongly polarized towards the loading and in all cases, except the diurnals, the major axis for borehole 2 is larger. The most striking feature of these data is the polarization of the difference tilt ellipses (or tilt anomalies). The major axes of the linear tide anomalies lie in the range 60°–80° azimuth, whereas those of the non-linear anomalies are confined to azimuths in the range 110°–140° (see Fig. 9). Obviously, the linear tide anomalies (composed of body and loading components) are polarized 45°–60° anticlockwise with respect to the azimuth of the forcing, and the non-linear tidal anomalies are polarized 15° 40° clockwise with respect to the load only forcing. Calibration errors would result in

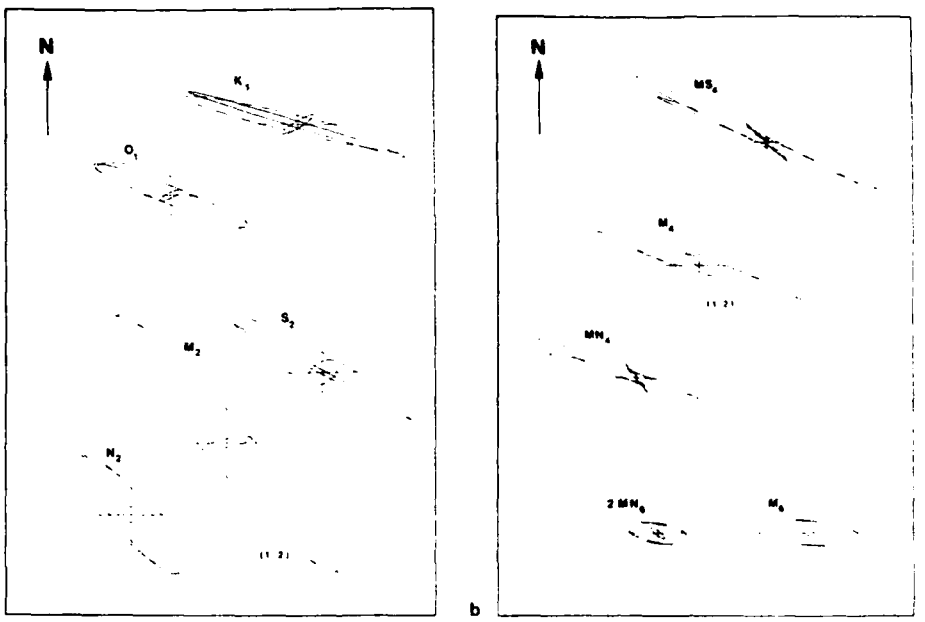

Fig. 8a and b. Tilt ellipses of the observed tilt in borehole 1 (*full line*) and borehole 2 (*dashed line*) and the difference tilt shown for **a** linear tidal constituents, and **b** non-linear constituents. M_2 and M_4 are plotted on a double scale relative to the other constituents. The lengths of the lines in the centres of the ellipses are 24 nrad (48 nrad for M_2) in **a** and 2.4 nrad (4.8 nrad for M_4) in **b**

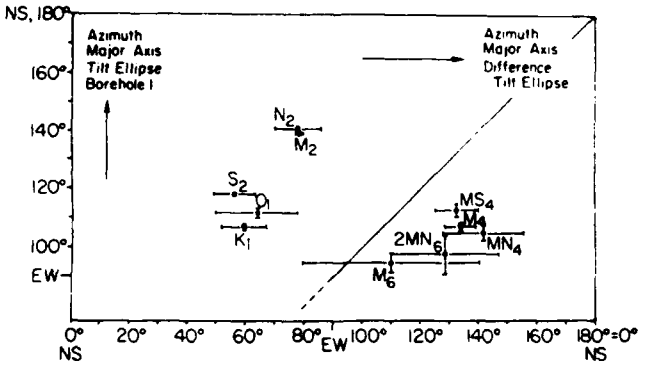

Fig. 9. Orientation of observed tilt ellipses for constituents measured in borehole 1 versus the orientation of the tilt ellipses for the same constituents of the difference between boreholes 1 and 2. Error bars reflect 95% confidence limits

anomalies aligned with the observed tilt ellipses (such anomalies would appear close to the oblique line running through the upper right corner in Fig. 9). Alignment errors of one or both tiltmeters would introduce anomalies characteristic of each tidal species, dependent on their frequency as well as their spatial distribution. Instead, we find a distinct grouping into linear and non-linear tidal components.

The alternative explanation for the observed anomalies involves the presence of a subsurface structural inhomogeneity (fault, fracture, geological contrast etc.) near one of the boreholes, through which strain-tilt coupling generates an anomaly governed by the nature and distribution of the forcing function. That the non-linear anomalies are polarized close to the azimuth of the loading is consistent with strain-tilt coupling arising from the non-linear load strain. In contrast, the linear tide, which has a body tide component, will produce an anomaly which is a function of both the body and the load strain. Furthermore, since the forcing distribution (load and body tide) for the diurnal and semi-diurnal constituents are different, strain-tilt coupling effects should also be different. Evidence for this is seen in Fig. 9 in which N_2 and M_2 form a subgroup separate from O_1 and K_1. That S_2 does not appear to fit into the scheme may reflect the influence of additional perturbing inputs, such as atmospheric tides, which are dominant within this frequency band.

The existence of subsurface inhomogeneities is known from a third borehole 80 m from the other two, in which a major water-bearing fracture was encountered at a depth of 130 m. Also, a subsurface discontinuity is inferred in the vicinity of boreholes 1 and 2 from a 90° shift in electric field polarization angle determined from magnetotelluric measurements at the site (R. Kurtz, personal communication).

Time variations in the M_4 and M_6 admittances

Because of the need for data continuity in time-variant analysis (Peters and Beaumont 1985), we have analysed tilt and tide gauge data recorded during 1983 in which relatively small data loss occurs (in the St. Joseph de la Rive data at a level of 13% and in borehole 1 at 2.7%). Figures 10 and 11 show the time-varying admittances in the form of trajectories in phasor space for M_4 and M_6, estimated from the HYCON analysis of the south and east components of tilt and the tide gauges at St. Joseph de la Rive and Tadoussac.

For the east direction M_4 traces out an almost circular path, perhaps indicative of an annual component, with a range of 12% in amplitude and 11° in phase. While the south component admittance shows larger fractional changes (30%) than the east, the absolute range of the changes is approximately the same. Variations in each component are coherent between boreholes, suggesting that the tiltmeters are responding to a regional process. Also, from analysis 10 on, the south and east series behave in a similar way and, in terms of the phase lag with respect to the mean, are coherent with the variations at Tadoussac. There is no obvious correlation between the tide gauge at St. Joseph de la Rive and the other M_4 admittance trajectories.

The variations in M_6 are also coherent between bore-

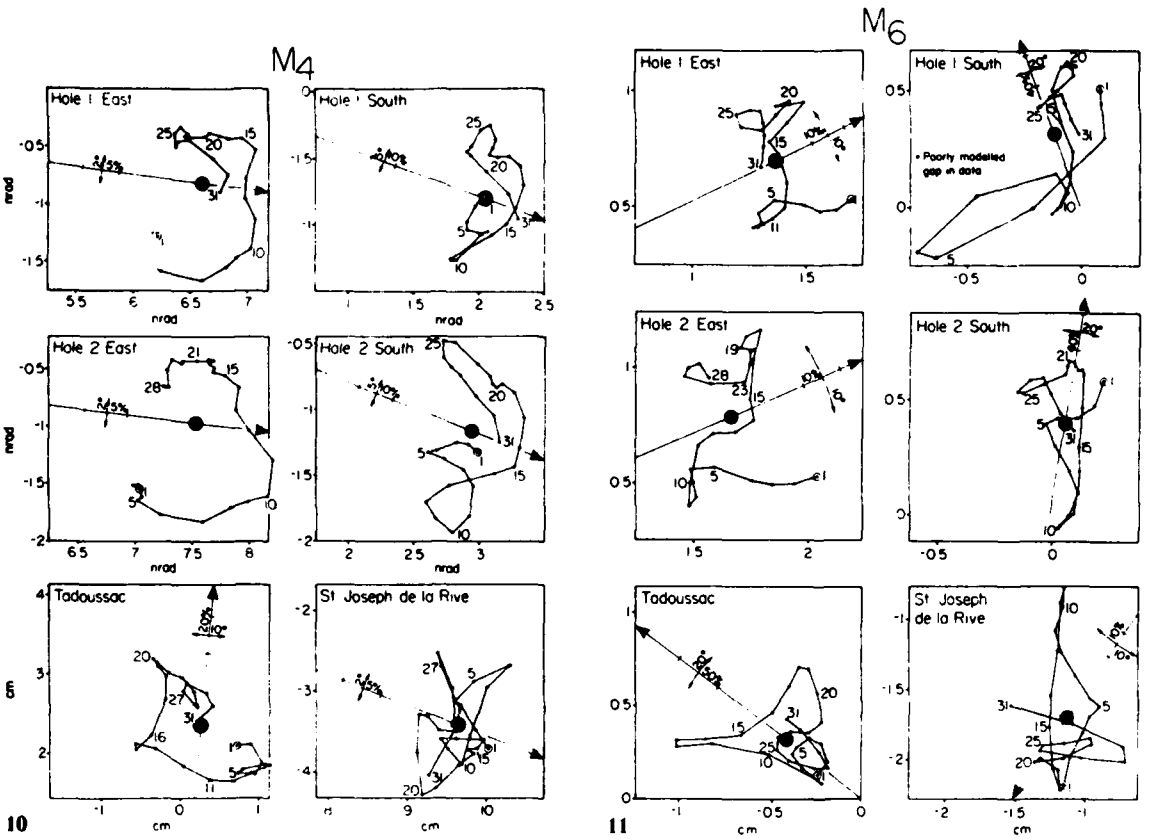

Fig. 10. Phasor trajectory plots of the M_4 admittance for tilt measured in boreholes 1 and 2 and tide gauges Tadoussac and St. Joseph de la Rive, estimated from HYCON sequential analysis. The mean admittance is indicated by the *round dot*. The *arrow* points in the direction of increasing amplitude. Fractional changes can be estimated from the amplitude and phase scales on the arrow which pertain to changes relative to the mean

Fig. 11. Phasor trajectory plots of M_6. Details as for Fig. 10

holes for each component direction. For the east direction the amplitude changes are mainly confined to the start and the end of the year, with the phase lag varying during the middle period. For the south direction, apart from an anomalous excursion in the borehole 1 curve caused by a gap, the variations are predominantly in amplitude and cover a range of 200% because of the small signal. Nevertheless, the essential features of the larger-amplitude east component remain, with the absolute changes being approximately the same in both directions. There is no clear correlation between the tide gauge at Tadoussac and the tilt. However, the sustained amplitude cycle dominating the tilt variations during the first 8 months (analyses 1–20) is also clear in St. Joseph de la Rive results.

Discussion and conclusions

Without embarking on a rigorous and probably futile investigation of the inhomogeneous local strain field geometry at the Charlevoix site, we have established that the differences in the mean values of the non-linear tidal results for the redundant tilt observations are probably due to strain-tilt coupling and are not associated with instrumental effects.

Unlike most tidal studies which are concerned with explaining small perturbations in the tilt response, we are trying to find the source of the entire signal. The only non-tectonic source of the non-linear M_4 and M_6 tidal signal is from tidal loading. Agreement between the observed mean admittance and the loading model results suggests that detectable tectonically induced non-linearities are not being generated in the Charlevoix area. The only major discrepancy occurs in the south component for M_6 in which the observed is about 50% smaller than predicted. It is likely that errors in the model due to the poorly constrained tide distribution south of the site are responsible for the disagreement.

In general, the level of agreement between the time-varying tide gauge admittances and the corresponding tilt results is only fair. This may be due to the small spatial scale of the shallow-water interactions, which makes a comparison between individual tide gauges and the tilt generally inappropriate. Also, in the case of St. Joseph de la Rive, the analysis results for data sets 21–27 were derived from data with gaps and were consequently heavily biased by the interpolation model. However, taken together, the mean admittance results and time-variant analysis results strongly indicate a marine origin for the non-linear harmonics in the tilt.

If the arguments of Beaumont (1978) are realistic, this result implies that the special condition in which the rate of change of the tectonic stress is equal to the mean tidal stress rate does not apply during the period covered by this study, or is not detectable within the prominent back-

ground of the non-linear loading. In their study of linear tidal admittance variations, Peters and Beaumont (1985) found no evidence for a high rate of stress accumulation in the region. Thus, from the combined evidence of both tidal response studies, the regional tectonic stress is stable or only slowly changing. These results are not unexpected considering the low level of earthquake activity during the period of the tiltmeter experiment. During 1983, the largest earthquake in the region was of magnitude 3.8, the epicentre of which was 38 km from the observatory.

Acknowledgements. This project was supported by the Air Force Geophysics Laboratory, Hanscom AFB under contracts F19628-80-C-0032 and F19628-83-K-0023, the Natural Sciences and Engineering Research Council through Operating and Equipment grants to C. Beaumont, and the Division of Geophysics, Geological Survey of Canada. The Marine Environment Data Service provided the tide gauge data. We would like to thank Chris Beaumont and Walter Zürn for helpful discussions and criticism, Tony Lambert and Don Bower for their interest and support throughout the program, and Jacques Lebrecque for his invaluable assistance with operations at the Charlevoix Observatory. Benoit Dostaler and Dianne Lemieux maintained the array on a daily basis and John Fahey assisted with data reduction and analysis. H.-J. Kümpel acknowledges the support from a Killam fellowship during a 1-year stay at Dalhousie University, Halifax, Nova Scotia.

References

Agnew, D.C.: Nonlinearity in rock: evidence from earth tides. J. Geophys. Res. **86**, 3969–3978, 1981

Beaumont, C.: Linear and nonlinear interactions between the earth tide and a tectonically stressed earth. In: Applications of geodesy to geodynamics. I. Mueller, ed.: pp 313–318. Ohio State University Press 1978

Brace, W.F., Paulding, B.W., Jr., Scholz, C.H.: Dilatancy in the fracture of crystalline rocks. J. Geophys. Res. **71**, 3939–3953, 1966

Farrell, W.E.: Deformation of the Earth by surface loads. Rev. Geophys. Space Phys. **10**, 761–797, 1972

Flach, D., Große-Brauckmann, W., Herbst, K., Jentzsch, G., Rosenbach, O.: Ergebnisse von Langzeitregistrierungen mit Askania-Bohrlochneigungsmessern – Vergleichende Analyse hinsichtlich der Gezeitenparameter und langperiodischer Anteile sowie instrumentelle Untersuchungen. Deutsche Geodät. Komm. **B211**, (M. Bonatz, ed.) 72–95, 1975

Gallagher, B.S., Munk, W.H.: Tides in shallow water: spectroscopy. Tellus **XXIII**, 346–363, 1971

Godin, G.: Eight years of observations on the water level at Quebec and Grondines 1962–1969. Manuscript Report Series **31**, Marine Sciences Directorate, Dept. Environment, Canada, 1973

Goertzel, G.: An algorithm for the evaluation of finite trigonometric series. Am. Math. Month. **65**, 34, 1958

Harrison, J.C.: Cavity and topographic effects in tilt and strain measurements. J. Geophys. Res. **81**, 319–328, 1976

Mjachkin, V.I., Sobolev, G.A., Dolbilkina, N.A., Morosov, V.N., Preobrazensky, V.B.: The study of variations in geophysical fields near focal zones of Kamchatka. Tectonophysics **14**, 287–293, 1972

Mjachkin, V.I., Brace, W.F., Sobolev, G.A., Dieterich, J.H.: Two models for earthquake forerunners. Pageoph. **113**, 169, 1975

Nersesov, I.L., Semenov, A.N., Simbireva, I.G.: Space time distribution of the travel time ratios of transverse and longitudinal waves in the Garm area. In: The physical basis of foreshocks, Moscow: Nauka Publ. 1969

Peters, J.A., Beaumont, C.: Borehole tilt measurements from Charlevoix, Quebec. J. Geophys. Res. **90**, 12791–12806, 1985

Rice, J.R., Rudnicki, J.W.: Earthquake precursory effects due to pore fluid stabilization of a weakening fault zone. J. Geophys. Res. **84**, 2177–2193, 1979

Rossiter, J.R., Lennon, G.W.: An intensive analysis of shallow water tides. Geophys. J.R. Astron. Soc. **16**, 275–293, 1968

Scholz, C.H., Kranz, R.: Notes on dilatancy recovery. J. Geophys. Res. **79**, 2132–2135, 1974

Schüller, K.: Tidal analysis by the hybrid least squares frequency domain convolution method. Proceedings of the Eighth International symposium on Earth Tides, M. Bonatz and P. Melchior eds., Institut für Theoretische Geodäsie der Univ. Bonn, FRG, 1977

Sobolev, G., Spetzler, H., Salov, B.: Precursors to failure in rocks while undergoing anelastic deformations. J. Geophys. Res. **83**, 1775–1784, 1978

Soga, N., Mizutani, H., Spetzler, H., Martin III, R.J.: The effect of dilatancy on velocity anisotropy in Westerly granite. J. Geophys. Res. **83**, 4451–4458, 1978

Stuart, W.D.: Diffusionless dilatancy model for earthquake precursors. Geophys. Res. Lett. **1**, 261–264, 1974

Tomaschek, R., Groten, E.: Die Residualbewegung in der horizontalen Gezeitenkomponente. Geofisica Pura e Applicata **56**, 1–15, 1963

Whitcomb, J.H., Garmany, J.D., Anderson, D.L.: Earthquake prediction: variation of seismic velocities before the San Fernando earthquake. Science **180**, 632–635, 1973

Xi, Qinwen: A new complete development of the tide-generating potential for the epoch J2000.0. Bull. Inf. Marées Terrestres **98**, 6744–6747, 1987

Zetler, B.D., Cummings, R.A.: A harmonic method for predicting shallow water tides. J. Marine Res. **25**, 103–114, 1967

Zschau, J.: Auflastgezeiten. Habilitation thesis, Kiel University, 1979

Received June 22, 1987; revised version September 10, 1987
Accepted September 10, 1987

NONTIDAL TILT AND WATER TABLE VARIATIONS IN A SEISMICALLY ACTIVE REGION IN QUEBEC, CANADA

H.-J. KÜMPEL, Institut für Geophysik, Olshausenstr. 40, D-2300 Kiel, FRG

J.A. PETERS, Department of Oceanography, Dalhousie University, Halifax, Nova Scotia, B3H 4J1, Canada

D.R. BOWER, Geophysics Division, Geological Survey of Canada, 3 Observatory Crescent, Ottawa, Ontario, K1A OY3, Canada

ABSTRACT

An array of three borehole tiltmeters was installed in 1981 in the Charlevoix region of Quebec, Canada, an area of high intraplate seismic activity. A magnitude 7.0 earthquake struck the area in 1925, and the last major event was a magnitude 5.0 which occurred in 1979. The nontidal tilt from two 47 m deep boreholes correlates strongly with transient and seasonal water table fluctuations. This suggests a dominant influence of pore pressure effects on that part of the tilt signal. The episodic nature of such effects makes it difficult to separate them from potential earthquake precursors during the build-up of tectonic stress.

We present both an empirical and a deterministic approach to overcome this problem. The former consists of removing pore pressure effects from the tilt signal by using simple empirical relations. The latter is an attempt to model the physical process through finite element calculations based on Biot's consolidation

theory for elastic porous media. Although in our case some boundary conditions are poorly known, it is believed that Biot's theory is adequate to describe the observed phenomena.

INTRODUCTION

Anomalous tilt preceding major earthquakes has been reported by several authors (e.g. Press, 1975; Mortensen and Johnston, 1976; Johnston et al., 1978; Gerard, 1978). Rainfall induced tilt, however, may obscure a possible precursory drift signal because of (a) its generally large amplitude, (b) its often step like onset which is likely to produce a wide disturbance spectrum and (c) because of its episodic occurrence (Wood and King, 1977). It has been demonstrated in many cases that among the various meteorologically induced tilt effects, rainfall induced tilt is the most pronounced and correlates best with local water table variations (e.g. Edge et al., 1981; Peters and Beaumont, 1985), or rather with variations in the local topography of the water table (Kümpel, 1982; Kümpel et al., 1987).

The present paper addresses the following problem: How can we remove the effects of water table variations from the tilt signal in order to make tectonically induced tilt more evident? The approach taken here is based on (a) monitoring the water table topography accurately, (b) performing a regression analysis of tilt on water table data, and (c) modelling the physical process involved. As a case study we present data from the Charlevoix seismic zone in Quebec, Canada, an area that has a history of large intraplate earthquakes occurring roughly every

60 to 90 years. The last major event occurred in 1979 and had a magntiude of 5.0 (Anglin and Buchbinder, 1981). Since 1974, geophysical measurements have been made by the Earth Physics Branch of the Department of Energy, Mines and Resources - since 1986 the Geophysics Division of the Geological Survey of Canada (Buchbinder et al., 1983). Peters and Beaumont (1985) have reported on details of the borehole tiltmeter experiment at the Charlevoix Observatory. The data for our study have been taken from their investigations. No prominent earthquakes occurred in the region during the period covered by the experiment.

PRESENTATION OF DATA

Tilt signals were recorded by three Bodenseewerk vertical pendulums operating in three boreholes, two at a depth of 47 m (B1 and B2) and the third (B3) at 110 m depth. The boreholes are located at the corners of a triangle of sides between 70 and 90 m (Fig. 1). The continuous water table recordings used in this study were obtained from pressure transducers in three observation wells: Wells 1 and 2 are 70 m deep and cased down to 30 m; Well 3 is 30 m deep and cased only to 10 m. The well level variations observed represent the integrated pressure variations in any separate aquifers along the uncased part of the wells. The tiltmeter boreholes and the wells were drilled into the granite country rock that is covered by 1 to 4 m of overburden. Thus, the water table heights in Wells 1 and 2 represent groundwater pressure regimes at the same depth in the fractured granite, while Well 3 responds to a regime nearer to the surface. The average depths of the well levels are about 20 m in Wells 1 and 2, and 9

m in Well 3. The pressure in Well 2 exceeds the one in Well 1 by only 10 to 20 cm water column. Precipitation data was taken from daily cumulative readings of the Meteorological Service at Les Eboulements, 7 km SE of the site.

The lower part of Figs. 2 to 5 show observed data series for various periods in 1982, 1983, and 1984 with large changes in the water table which are reflected in the tilt recordings. Strong water table variations occurred during the thaw in spring or after heavy rainfalls in autumn. Tilt in B3 has only been observed since late 1983. Superimposed on the tilt drift signals are earth tides and marine loading tides from the St. Lawrence River. Snow in the precipitation series has been converted to rain by applying a factor of 0.1 on the measured height of the snow.

EMPIRICAL ANALYSIS

The similarity between well level variations and tilt in B1 and B2 is obvious for all periods. However, while the well level variations are almost the same in Wells 1 and 2, the tilt response in the two 47 m deep boreholes is quite different. Well 3 responds to the unconfined water table. Variations in it are roughly 30% greater than in Wells 1 and 2 which penetrate partially confined aquifers. Wells 1 and 2 respond much more to tidal and barometric stresses than Well 3 but this response is much smaller than the water table changes we are discussing here. For the regression analysis described below, data from Wells 1 and 2 were combined to maximise continuity.

We tried to correct the tilt curves for the groundwater effect by establishing simple empirical relationships between the available series in the time domain. This was done in two steps:

(a) The cross correlation technique was applied to determine both the azimuth of the tilt signal which is most sensitive to the water table variation in the deep wells and the phase shift between the tilt and water table series. Prior to the correlation process, tides were removed by filtering (Pertsev, 1959) and gaps were interpolated linearly. The best-defined, most-sensitive tilt azimuth was the one perpendicular to the azimuth at which no correlation occurs (i.e. normalized crosscorrelation coefficient below 0.05). At the most sensitive azimuth, correlation coefficients were greater than 0.95 with the tilt signal lagging behind the water table variation by about 1 day (2 days).

(b) The least squares technique was used to find suitable regression coefficients for the tilt signals (at their most sensitive azimuth) and the water table variations in Wells 1 (or 2) and 3, allowing for a linear drift term in the tilt signal. Prior to the least squares fit tides were removed by lowpass filtering, gaps linearly interpolated, and significant phase shifts - as detected by the cross correlation - were applied. While hourly data series were used with the correlation procedure, 4-hourly series were taken for the regression analysis to reduce computer time.

In the case of the Charlevoix tiltmeter experiment, different regression parameters seem to be valid for water table variations dominated by the thaw and those produced by pure rainfall events (see most sensitive tilt azimuth in Figs. 2 to 5). Regression of

tilt signals on water table variations in the deep wells yielded coefficients for thaw (rainfall) events of 0.32 (0.52) μrad/m for the tilt in B1, 0.66 (0.76) μrad/m for the tilt in B2, and 0.09 μrad/m for the tilt in B3. The residual tilt in B2 for thaw events reduces significantly when the difference between the water table variations in the deep and shallow wells was taken into account (namely, 0.59 μrad/m due to the variation in Well 2 and 0.16 μrad/m due to the difference between the variations in Wells 2 and 3).

Through the empirical approach, the nontidal variations in the tilt series have been lowered to about the same level as the observed in the least sensitive azimuth. However, most of the residual tilt still seems to be related to pressure variations in the groundwater regime, which indicates an imperfect regression model. Better corrections may have been applied if these pressure variations were known from more locations in the vicinity of the tiltmeters. Furthermore, it is evident from Fig. 5 that tilt at the Charlevoix site at 110 m depth is much less influenced by water table variations than at 47 m depth. This was not expected since a major water bearing fracture was encountered at 135 m during the drilling of B3. (The hole was subsequently refilled with concrete to a depth of 110 m).

MODELLING THE GROUNDWATER EFFECT

A deterministic approach to relate tilt to pressure variations in the groundwater regime was tried using Biot's theory of consolidation (Biot, 1941). The theory relates stresses in the

matrix to pressure in the pores of a porous medium. It has previously been applied to simulate air pressure and rainfall induced tilt observed in unconsolidated soil in the Northern FRG (Zschau, 1979; Kümpel, 1987). Since neither the alignment nor the size of the groundwater-bearing fractures in the granite, nor the change in the topography of the water table during the thaw or after rainfalls are well known at the Charlevoix site, modelling yields at most a coarse quantitative estimate of the physical process. Other mechanisms like temperature effects from the infiltrating water, air pressure effects, extension of clay minerals, or geochemical alterations are unlikely because of the high correlation coefficients between tilt signals and water table variations. Loading effects from the rainwater or the change in the gravitational attraction due to the seepage of the rain or melted snow are too feeble to explain the observed tilt amplitudes (Kümpel, 1982).

Assuming a two-dimensional plane strain configuration the set of partial differential equations that has to be solved is :

$$\begin{aligned}
\mu \nabla^2 u + (\lambda + \mu) \frac{d\varepsilon}{dx} - \alpha \frac{d\sigma}{dx} &= 0 \\
\mu \nabla^2 w + (\lambda + \mu) \frac{d\varepsilon}{dz} - \alpha \frac{d\sigma}{dz} &= 0 \qquad (1) \\
\frac{\alpha}{\lambda + \mu} \frac{d}{dt} \left(\frac{\sigma_x + \sigma_z}{2} \right) + \left(\frac{\alpha^2}{\lambda + \mu} + S \right) \frac{d\sigma}{dt} &= \frac{k}{\eta} \nabla^2 \sigma
\end{aligned}$$

with variables

u = horizontal displacement,

w = vertical displacement,

σ = excess pore pressure (with respect to hydrostatic)

of coordinates

x = horizontal distance from left boundary,

z = depth, positive below surface,

t = time > 0s,

and soil constants

μ = shear modulus,

λ = Lamé constant,

$\alpha = 1 - c_g / c_m$ with c_g = grain compressibilty

and $c_m = (\lambda + 2\mu/3)$ = compressibility of the porous matrix (Nur and Byerlee, 1971),

$S = \rho c_f + (1-\rho)\, c_m$ i. e. the hydraulic capacity or storage coefficient

with ρ = volume porosity

and c_f = compressibility of the fluid filling the pores (Bodvarsson, 1970),

k = intrinsic permeability,

η = dynamic viscosity of the pore fluid.

$\nabla^2 = \partial^2/\partial x^2 + \partial^2/\partial z^2$ is the Laplacian operator,

$\varepsilon = \partial u/\partial x + \partial w/\partial z$ is the volume strain, and

$(\sigma_x + \sigma_z)/2$ is the average total stress.

Several assumptions have been made: strains are infinitesimal, deformation is elastic, the size of the water bearing fractures in the granite is small compared to the baselength of the tiltmeters, the fractures are fully saturated with water, flow in the fractures is laminar, inertia forces are negligible. The effective baselength of the tiltmeters is somewhere between

1.5 m, i.e. the distance between the points at which the upper and lower ends of the tiltmeters are clamped to the boreholes, and 6 m, which is the length of the stainless steel pods that host the tiltmeters at the bottom of the boreholes. The last of Eqs. (1) is further simplified by assuming the average stress term to be constant with time. Christian and Boehmer (1970) have analysed the effect of this simplification on various geometrical configurations. They did not find severe divergences when external loads were constant. This simplification turns the last of Eqs.(1) into the form of a heat conduction relation

$$\frac{d\sigma}{dt} = D \nabla^2 \sigma \qquad (2)$$

with $D = k/\eta / [\alpha^2(\lambda+\mu)^{-1} + S]$ being the diffusivity. Tilt Ψ of a vertical subsurface element at location (x, z) and time t is obtained from

$$\tan^{-1} \Psi(x,z,t) = \frac{u(x,z_2,t) - u(x,z_1,t)}{z_1 - z_2} \qquad (3)$$

if $|z_1 - z_2|$ is much larger than vertical displacements, $z = (z_1 + z_2)/2$, and Ψ positive for clockwise rotation of the vertical element. (Respective relations hold for strain and tilt of arbitrarily oriented elements).

The finite element grid used is shown in Fig. 6. Variables at lower and right boundaries are held at zero and no horizontal displacements are allowed along the left boundary. These conditions have been found to generate small distortions of the variables in the central part of the model if it is activated as

follows: At time t = 0s, the upper boundary is loaded by the weight of the additional groundwater, as indicated by the shaded area. At the base of the load, the pore pressure is instantaneously raised by the hydrostatic pressure of the additional groundwater when it saturates the available pore space. Of course, no tilt would arise from a uniform change of the water table over the entire upper boundary. By the plane strain type formulation tilt is modelled in the plane of strongest change in water table height i.e. in the azimuth where the tilt is most sensitive to water table variations. A laterally non-uniform rise of the water table could be caused by surface topography, anisotropic permeability in the granite, or lateral variation in surface run-off or seepage conditions. The overall length and depth of the model are chosen to allow simulation of the dominating deformation pattern in the centre of the model as inferred from the active boundary conditions.

Two extreme parameter sets were adopted to accomodate the possible depth dependence of the physical parameters of the granite. Model A follows a rough generalization of Davis (1969) who notes that due to weathering, both porosity and permeability of originally dense rocks are about 10 times greater at a depth of 10 m than at a depth of 100 m. Respectively, a depth dependence for Young's modulus $E = 2\mu(1 + \nu)$ and Poisson ratio $\nu = 0.5\lambda/(\lambda + \mu)$ is assumed in Model A (see Fig. 7). Because of the strong change of the parameters below the surface in this model, the thickness of the finite element layers need to decrease at shallow depths (Fig. 6). Model B represents a homogeneous layer

from top to bottom of the grid, adopting the values of Model A at 40 m depth. All values fall in the range of parameters observed by Brace (1965), Simmons and Brace (1965), Walsh (1965) and Davis (1969). Other parameters used are $c_g = 2 \cdot 10^{-12}$ $cm^2 dyn^{-1}$, $c_f = 5 \cdot 10^{-11}$ $cm^2 dyn^{-1}$ and $\eta = 0.0165$ g $s^{-1} cm^{-1}$ as for water at 20°C.

The solution of the consolidation problem is found in two steps. First, the instantaneous deformation from the loading at t = 0s is calculated from

$$\begin{aligned} \mu \nabla^2 u + (\lambda + \mu + \alpha^2/S)\, \partial \varepsilon_o / \partial x &= 0 \\ \mu \nabla^2 w + (\lambda + \mu + \alpha^2/S)\, \partial \varepsilon_o / \partial z &= 0 \end{aligned} \qquad (4)$$

when the medium is in equilibrium for t < 0 s. Eqs.(4) follow from the first two of Eqs.(1), setting

$$\sigma_o = -\alpha \varepsilon_o / S \qquad \text{for} \quad t = 0 \text{ s}, \qquad (5)$$

because the pore pressure diffuses with finite velocity into the medium. Eq.(5) yields the pore pressure distribution immediately after loading. Secondly, the system of Eqs. (1) with Eq. (2) is simultaneously solved for times $t = 2^{2n}$ s and n = 1, 2, 3 . . . . Initial values for the variables u, w, and σ are obtained from the first step and are denoted u_o, w_o, and σ_o. Given the step-like excitation of the model, the time iteration chosen provides numerical stability in the sense of Booker and Small (1975). Finite elements are of quadratic order, i.e. quadratic fits are exerted on the variables along each line segment combining two

nodes of the grid. Further tests on the reliability of the numerical results have been made for similar problems (Kümpel, 1987; Kümpel and Lohr, 1985). The program package used for the computations was TWODEPEP (IMSL, 1983). The number of elements (128) was restricted by computer capacity.

Fig. 8 shows the increase of pore pressure with time in a vertical column for both models. Note that the pore pressure is kept to zero at depth 180 m and that the steady state solutions of both models are obtained about 12 days after the step-like increase of the pore pressure at the surface. Due to greater permeability in its upper part, Model A yields somewhat higher pore pressures than Model B for the same times and depths. The well level observations confirm the quick response of the pore pressure to water input from the surface at 10 m depth (Well 3), but also show a stronger delay below 30 m depth than predicted by both models (Wells 1, 2; see nearly step-like evnts in 1982, Figs. 2, 3). This suggests the possible existence of a less permeable zone at depths below 10 m.

Horizontal displacements for an additional water column of 75 mm are plotted in Fig. 9. The water is assumed to infiltrate into a formation of 0.75% porosity, thereby generating a rise of the water table by 10 m. (In fact, this holds for Model A only at 40 m depth.) In each case the water level rise decays over 280 m because of lateral inhomogeneity in seepage conditions. Displacements resulting from pure loading of the additional water mass are much smaller than those generated immediately after loading by the pore pressure rise at the base of the load. The two models behave differently in some points. Ignoring the first hours after

loading, Model A predicts largest displacements at the surface while Model B predicts largest displacements at depths around 60 m. Model A - unlike Model B - predicts a change in the sign of the tilt with time, although not with depth, in its steady state response. Both models produce submillimeter horizontal displacements.

The tilt variations for the given boundary conditions, computed from the horizontal displacement field, are shown in Fig. 10. For some fixed time (18h in Fig. 10), the time axis that holds for a Model-B-permeability of $2.5 \cdot 10^{-10}$ cm^2 may be replaced by a permeability axis indicating how the tilt at that time depends on the permeability parameter. Or, tilt curves for a possibly less permeable zone below 10 m depth, as argued above, are obtained by shifting the time axis to the left until the 18h mark is opposite an alternative permeability. The time/permeability dependence of the process can also be described as a function of the dimensionless quantity

$$\varkappa = \frac{k\, t\, \vartheta\, g}{\eta\, L} \qquad (6)$$

where ϑ is the density of the pore fluid, g is the gravitational acceleration, and L is an arbitrary characteristic length dependent on the geometry of the problem, chosen to be 10 m here.

For the depth range analysed, Model A predicts depth dependent tilt only for $\varkappa$ values below about $3 \cdot 10^{-5}$ and a change in the sign of the tilt at $\varkappa \approx 6 \cdot 10^{-5}$. Model B predicts depth dependent tilt for all values of $\varkappa$ and about two times larger tilt amplitudes for small $\varkappa$ values than Model A. For $\varkappa$ greater than $5 \cdot 10^{-4}$,

tilt amplitudes at depths below 60 m are small. Although Model B suggests increasing positive tilt at depths below 90 m (see retrobending of steady state curve in lower part of Fig. 8), this is not realistic but reflects artefacts from the boundary conditions at 180 m depth.

The comparison of our calculations with the recorded tilt signals is impeded by the uncertainty of mainly three parameters:
(a) The effective porosity at the depth of the water table. It governs the rise of the water table for a certain amount of rain. From the strong event in Fig. 3 we may estimate that 75 mm of rain generate a water table rise of about 5 m at 10 m depth if surface run-off is neglegted. This means that the effective porosity could be up to 1.5% .

(b) The lateral pore pressure gradient that develops after the infiltration of water from the surface. It governs the tilt amplitude, together with the Young's modulus and the Poisson ratio of the formation. Neither the size of the gradient nor its direction are known from direct observation, but since brooks drain the ground at several hundred meters distance from the site we believe that a lateral decay of a water table variation of 10 m over 280 m distance is realistic. This is the situation adopted for the boundary conditions cited above, with the tiltmeters placed in the middle of the asymmetric water table rise. We may assume that the direction of the pore pressure gradient is the azimuth at which the respective tilt signal is most sensitive to well level variations. For tilt in B1 and B2 this is, in fact, the direction roughly perpendicular to the alignment of Wells 1

and 2 that both show almost the same water table height.

(c) The permeability. It governs the velocity of the propagation of a pore pressure anomaly into the formation and, therefore, the rise time of the tilt response. We can reduce this uncertainty when we restrict our discussion on the steady state part of the calculated tilt response (rightmost part of curves in Fig. 10). Note that the reduction of pore pressure gradients by fluid flow is not modelled.

From the two models calculated, the one with depth independent parameters agrees better with the tilt observations because the groundwater induced tilt observed at 100 m depth is much less than at 47 m (Fig. 5), and perhaps also because the tilt signals observed with the two almost step-like water table events in 1982 give no hint of a tilt sign reversal as predicted by the depth dependent parameter model (Figs. 2 and 3). Such sign reversal, however, would probably only be detectable if the permeability was by one to two orders of magnitude less than $2.5 \cdot 10^{-10}$ cm^2 (see Fig. 10). Also, the computed Model-B-tilt amplitudes at 47 m depth for the boundary conditions given are of the same magnitude than observed along with the strong rainfall event in Fig. 3, or with the thaw events in Figs. 2, 4, 5. Since in Model A the porosity at 10 m depth is assumed to be 3%, the water table variations and the tilt amplitudes for this model would be about four times weaker than for Model B, when the same amount of infiltrating water adds to the water table at that depth.

The different tilt response of the installations at 47 m depth to groundwater effects is probably due to local inhomogeneities in the porous rock. Evidence for such inhomogeneities has

also been found in the analysis of tidal tilt (Peters and Kümpel, 1987). Modelling of these anomalies has not been tried because of the multiplicity of possible parameters and the lack of control.

DISCUSSION

We draw the following conclusions from this investigation :

Applying Biot's theory of consolidation on the water saturated part of the granite at the Charlevoix Observatory we are able to predict the tilt amplitudes resulting from the pore pressure variations in the groundwater regime. The prediction is based on a strong lateral pore pressure gradient that develops after rainfall or during the thaw at springtime. The gradient may arise from inhomogeneous seepage conditons, locally varying surface run-off, or from topography, If the pore pressure gradient was by some numerical factor weaker than assumed, the Young's modulus E of the granite needs to be less by essentially the same factor.

There is no doubt that the best way to obtain meaningful tilt recordings in earthquake prone areas is to choose a site with a time invariant water table. Since this is generally not the case results from the Charlevoix experiment suggest tilt should be measured at least 100 m below the groundwater level. Even if this is not done, most of the tilt signal that is due to water table variations can still be removed by empirical analyses provided those variations are known from continuous observations of preferably more than one well in the vicinity. Although some drastic approximations are made, Biot's theory is felt to adequately

describe the physical process involved. Model calculations of this type provide valuable constraints on elastic and hydrologic parameters of the porous rock in which the tiltmeter is installed.

ACKNOWLEDGEMENTS

The tiltmeter experiment was supported by the Air Force Geophysics Laboratory, Hanscom AFB (under contracts F19628-80-C-0032 and F19628-83-K-0023), the Natural Sciences and Engineering Research Council and the Gravity, Geothermics and Geodynamics Division of the Earth Physics Branch (now Geophysical Division of the Geological Survey of Canada). H.-J. Kümpel received a Killam postdoctoral fellowship during a one-year-stay at the Dalhousie University in Halifax, Nova Scotia. We are grateful to Chris Beaumont and Jochen Zschau for numerous fruitful discussions and to Jacques Labrecque for his assistance in operations at the Charlevoix Observatory. Jim Covill assisted with data reduction, Kathleen Helbig, Jutta Pettke and Georg Lohr helped preparing the manuscript and drafting the diagrams.

REFERENCES

Anglin, F.M. and Buchbinder, G.G.R., 1981. Microseismicity in the mid-St. Lawrence Valley Charlevoix Zone, Quebec. Bull. Seism. Soc. Am., 71: 1553-1560.

Biot, M.A. 1941. General Theory of Three-dimensional Consoldiation. J. Appl. Phys., 12: 155-164.

Bodvarsson, G., 1970. Confined Fluids as Strainmeters. J. Geophy. Res., 75: 2711-2718.

Booker, J.R. and Small, J.C., 1975. An Investigation of the Stability of Numerical Solutions of Biot's Equation of Consolidation. Int. J. Solids Structures, 11: 907-917.

Brace, W.F., 1965. Some New Measurements of Linear Compressibility of Rocks. J. Geophys. Res., 70: 391-398.

Buchbinder, G.G.R., Kurtz, R. and Lambert, A., 1983. A Review of Time-Dependent Geophysical Parameters in the Charlevoix Region, Quebec. Earthquake Prediction Res., 2: 149-166.

Christian, J.T. and Boehmer, J.W., 1970. Plane Strain Consolidation by Finite Elements. J. Soil Mech. and Found. Div. ASCE, 96: 1435-1457.

Davis, S.N., 1969. Porosity and Permeability of Natural Materials. In: R.J.M. De Wiest (Editor), Flow through Porous Media. Academic Press, New York, pp. 54-89.

Edge, R.J., Baker, T.F. and Jeffries, G., 1981. Borehole Tilt Measurements: Aperiodic Crustal Tilt in an Aseismic Area. Tectonophysics, 71: 97-109.

Gerard, V.B., 1978. Earthquake Precursors from Earth Tilt Observations corrected for Rainfall. Nature, 276: 169-170.

IMSL, Inc., 1983. TWODEPEP, 5th ed. Manual, IMSL Inc., Houston.

Johnston, M.J.S., Jones, A.C., Danl, W. and Mortensen, C.E., 1978. Tilt near an Earthquake (ML = 4.3), Briones Hills, California. Bull. Seism. Soc. A., 68: 169-173.

Kümpel, H.-J., 1982. Neigungsmessungen zwischen Hydrologie und Ozeanographie. Ph.D. Thesis, University of Kiel, FRG, 165 pp.

Kümpel, H.-J., 1987. Model Calculations for Rainfall Induced Tilt and Strain Anomalies. Proc. 10th Int. Symp. on Earth Tides, Madrid 1985 (in print).

Kümpel, H.-J. and Lohr, G., 1985. In-situ Permeability from Non-dilatational Soil Deformation Caused by Groundwater Pumping - A Case Study. J. Geophys., 57: 184-190.

Kümpel, H.-J., Lohr, G. and Wang, R., 1987. Tilt Measurements at Various Depths in the Same Borehole. Proc. 10th Int. Symp. on Earth Tides, Madrid 1985 (in print).

Mortensen, C.E. and Johnston, M.J.S., 1976. Anomalous Tilt Preceding the Hollister Earthquake of November 28, 1974. J. Geophys. Res., 81: 3561-3566.

Nur, A. and Byerlee, J.D., 1971. An Exact Effective Stress Law for Elastic Deformation of Rocks with Fluids. J. Geophys. Res., 76: 6416-6419.

Pertsev, B.B., 1959. Sur la Dérive dans les Observations des Marrées Elastiques. IZV. Acad. Sc. URSS, Ser. Geoph., 4: 547-548.

Peters, J. and Beaumont, C., 1985. Borehole Tilt Measurements from Charlevoix, Quebec. J. Geophys. Res., 90: 12,791-12,806.

Peters, J. and Kümpel, H.-J., 1987. Nonlinear Tilt Tides from the Charlevoix Seismic Zone in Quebec. Submitted to Geophys. J. R. astr. Soc.

Press, F., 1975. Earthquake Prediction. Scientific American, 232: 15-23.

Simmons, G. and Brace, W.F., 1965. Comparison of Static and Dynamic Measurements of Compressibility of Rocks. J. Geophys. Res., 70: 391-398.

Walsh, J.B., 1965. The effect of Cracks on the Compressibility of Rock. J. Geophys. Res., 70: 381-389.

Wood, M.D. and King, N.E., 1977. Relation between Earthquakes, Weather, and Soil Tilt. Science, 197: 154-156.

Zschau, J., 1979. Air Pressure Induced Tilt in Porous Media. Proc. 8th Int. Symp. on Earth Tides, Bonn 1977: 418-433.

Publication No. 327 of Institute of Geophysics, Kiel

FIGURE CAPTIONS

Fig. 1: Plan view of the Charlevoix tiltmeter array in Québec showing the locations of the tiltmeter boreholes (B1, B2, B3) and the groundwater observation wells. Contour lines mark local topography.

Fig. 2: Set of precipitation, water table, and tilt data recorded at Charlevoix Observatory in spring 1982. The individual series are :

A - Rainfall (blank) or snow (shaded)

B - Difference between levels in Well 3 and Well 1 (or 2)

C, D, E - Water table variations in Wells 1, 2, 3

F, G - Tilt in B1, B2 at azimuth of highest sensitivity to water table variations in Well 1 (or 2)

H, J - Tilt in B1, B2 like series F, G, but corrected

I, K - Tilt in B1, B2 at azimuth of lowest sensitivity to water table variations

Fig. 3: Set of precipitation, water table, and tilt data recorded at Charlevoix Observatory in autumn 1982. Individual series as described in Fig. 2 .

Fig. 4: Set of precipitation, water table, and tilt data recorded at Charlevoix Observatory in spring 1983. Individual series as described in Fig. 2 .

Fig. 5: Set of precipitation, water table, and tilt data recorded at Charlevoix Observatory in spring 1984. Individual series as described in Fig. 2, except:

L - Tilt in B3 at azimuth of highest sensitivity to water table variation in Well 1 (or 2)

M - Tilt in B3 like series L, but corrected

N - Tilt in B3 at azimuth of lowest sensitivity to water table variations.

Fig. 6: Eight-layer model of 128 triangular elements for simulation of water table induced tilt at the Charlevoix site. Rectangular elements are subdivided into 4 triangles each, as indicated in left column. Layer boundaries are at 0.6, 1.8, 4.2, 9, 20, 40, and 80 m depth.

Fig. 7: Depth dependence of physical parameters that mostly control the deformation of the rock. Model A: curved lines, Model B: straight lines crossing Model A-lines at 40 m depth.

Fig. 8: Pore pressure increase versus depth over time after application at t = 0 s at the surface, for Model A (full lines) and Model B (broken lines).

Fig. 9: Horizontal displacements in vertical column at centre of finite element grid, using Model-A (full lines) or Model-B parameters (broken lines). L-curves denote the displacements due to surface load of 75 mm water, time indexed curves denote the displacements due to surface pore pressure increase of 1 bar corresponding to a rise of the water table of 10 m (i.e. 75 mm infiltrating into medium of 0.75% porosity). Both load and pres-

sure are applied at time t = 0 s and decay laterally from full amplitude at distance -140 m from the tiltmeters to zero values at + 140 m as indicated in Fig. 6.

Fig. 10: Tilt over time, permeability, or dimensionless $\mathcal{H}$ for three different depths at centre of finite element grid. Full lines hold for Model-A parameters, broken lines for Model-B parameters. Boundary conditions are as given in Fig. 9 .

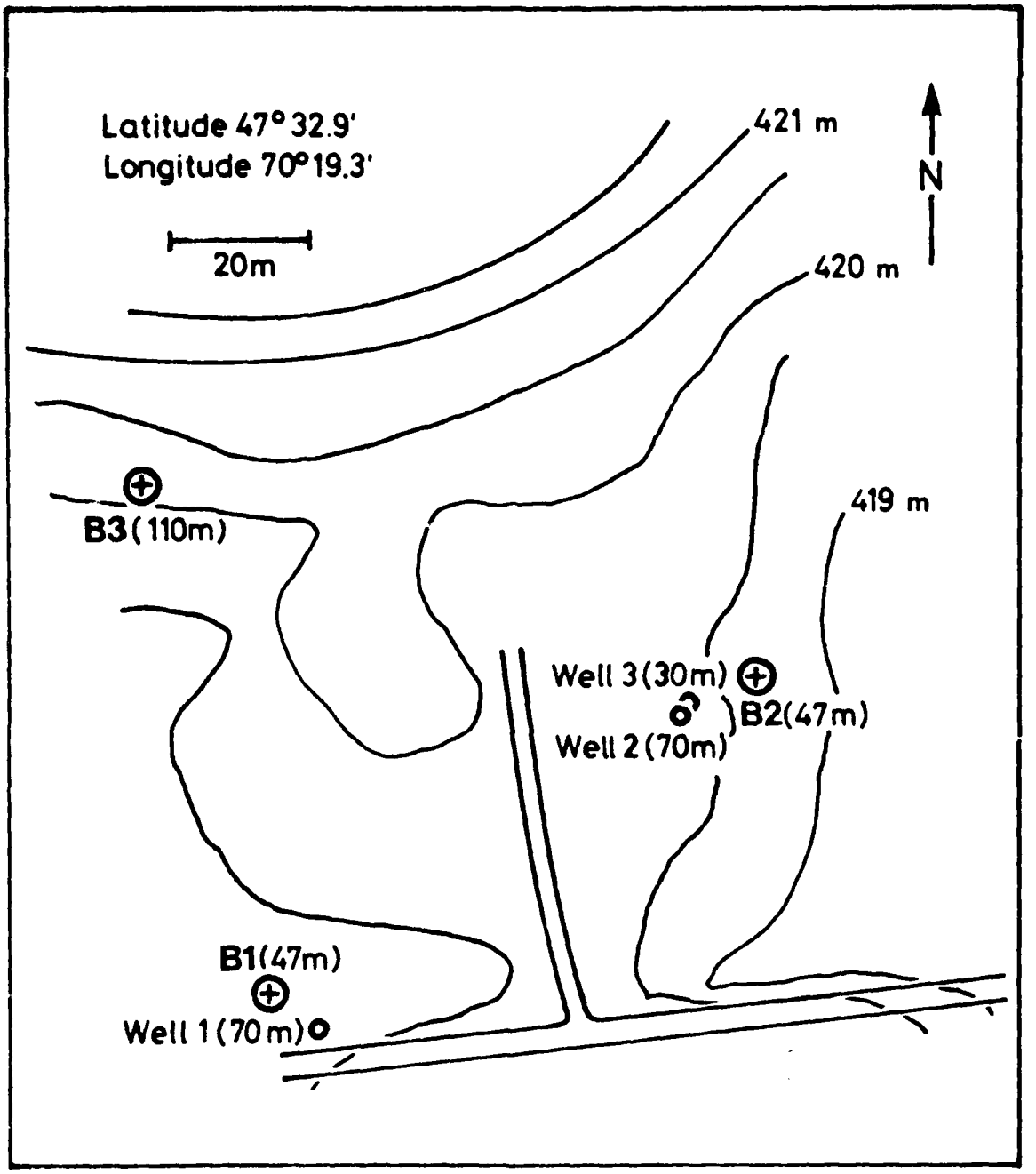
Latitude 47° 32.9'
Longitude 70° 19.3'
20m
421 m
420 m
419 m
N
B3 (110m)
Well 3 (30m)
B2(47m)
Well 2 (70m)
B1(47m)
Well 1 (70 m)

FIGURE 1

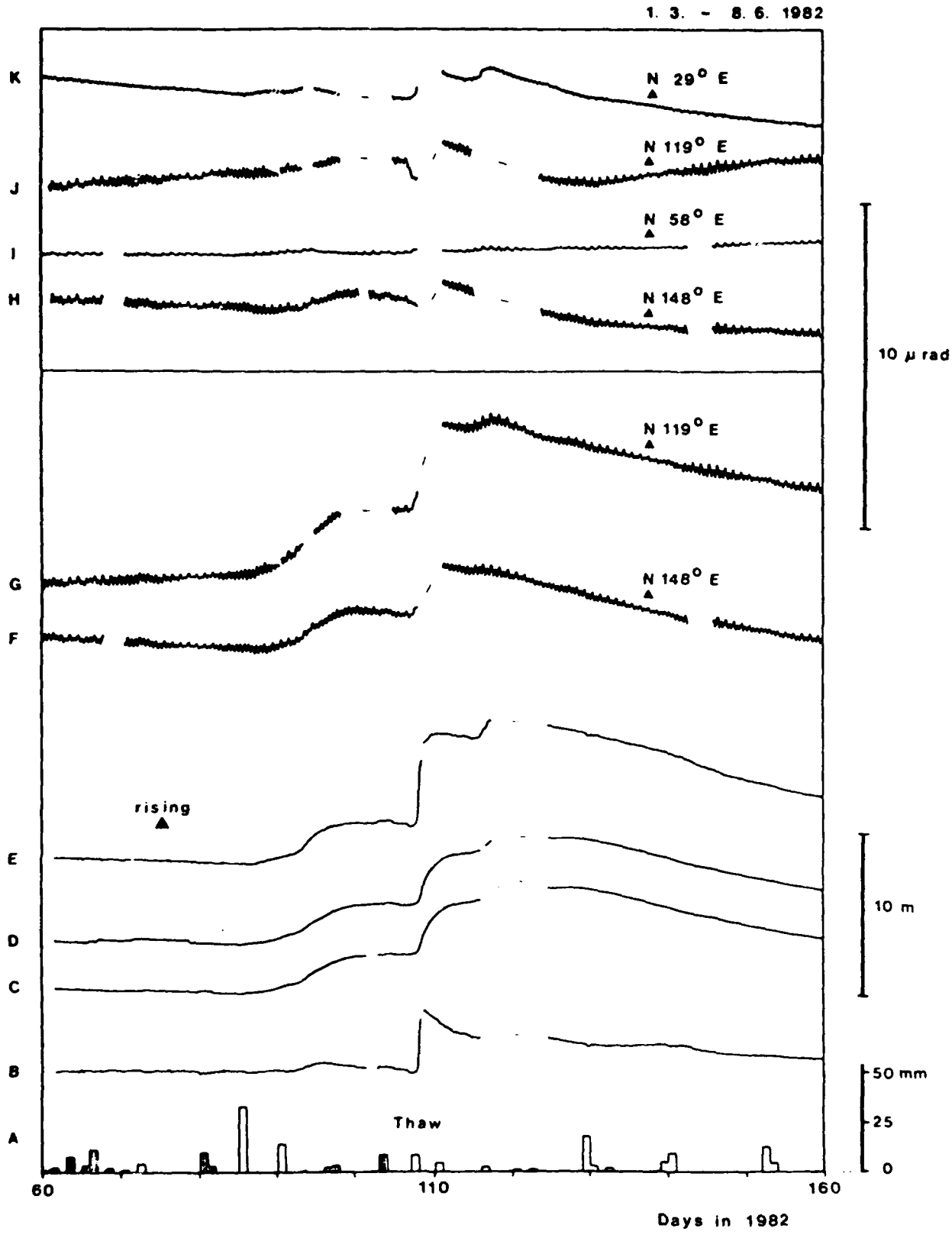
1. 3. - 8. 6. 1982
K
N 29° E
N 119° E
J
N 58° E
I
H
N 148° E
10 μ rad
N 119° E
G
N 148° E
F
rising
E
D
C
10 m
B
50 mm
25
0
A
Thaw
60
110
160
Days in 1982

FIGURE 2

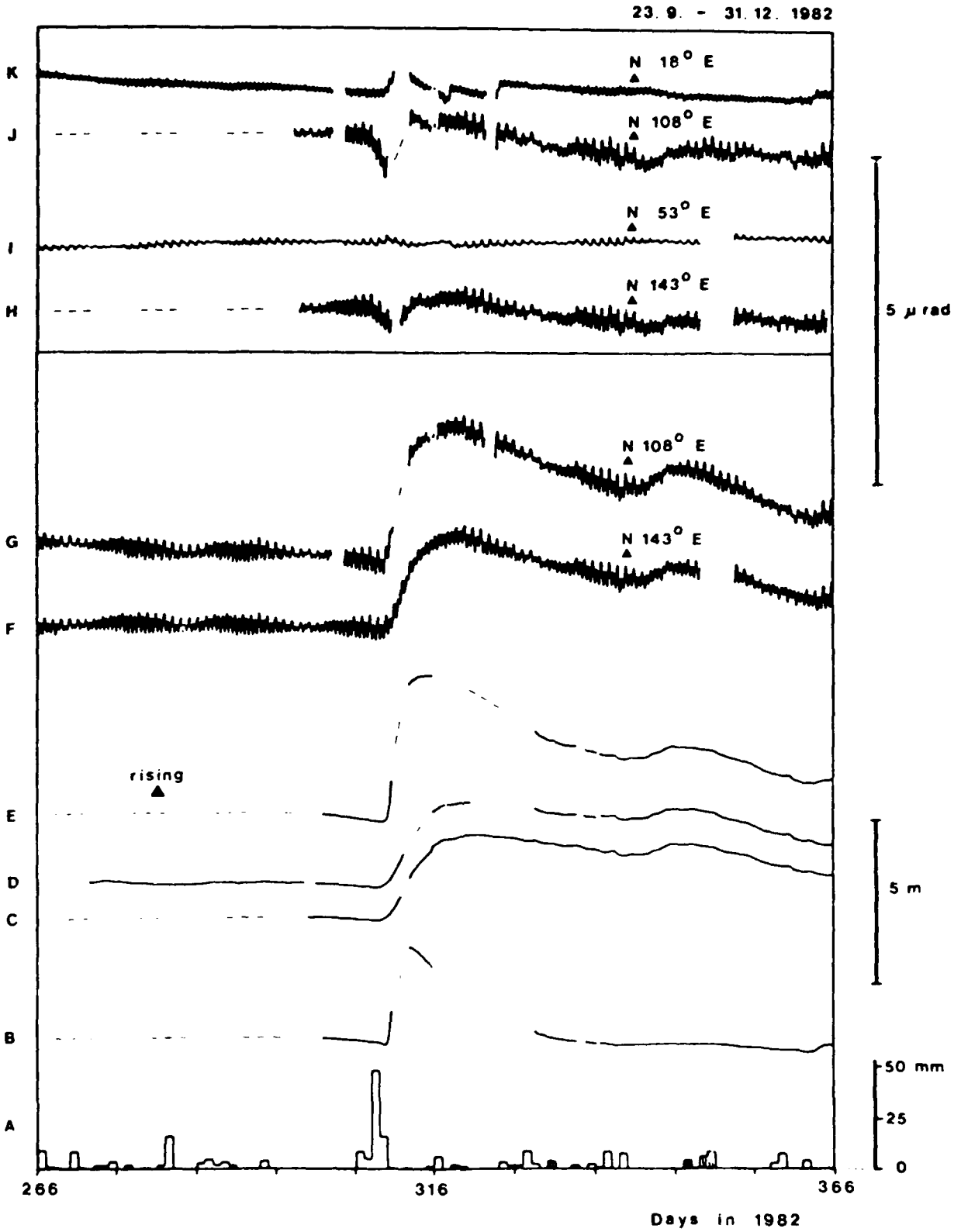
23. 9. - 31. 12. 1982
K
J
I
H
N 18° E
N 108° E
N 53° E
N 143° E
5 μ rad
G
F
N 108° E
N 143° E
rising
E
D
C
B
A
5 m
50 mm
25
0
266
316
366
Days in 1982

FIGURE 3

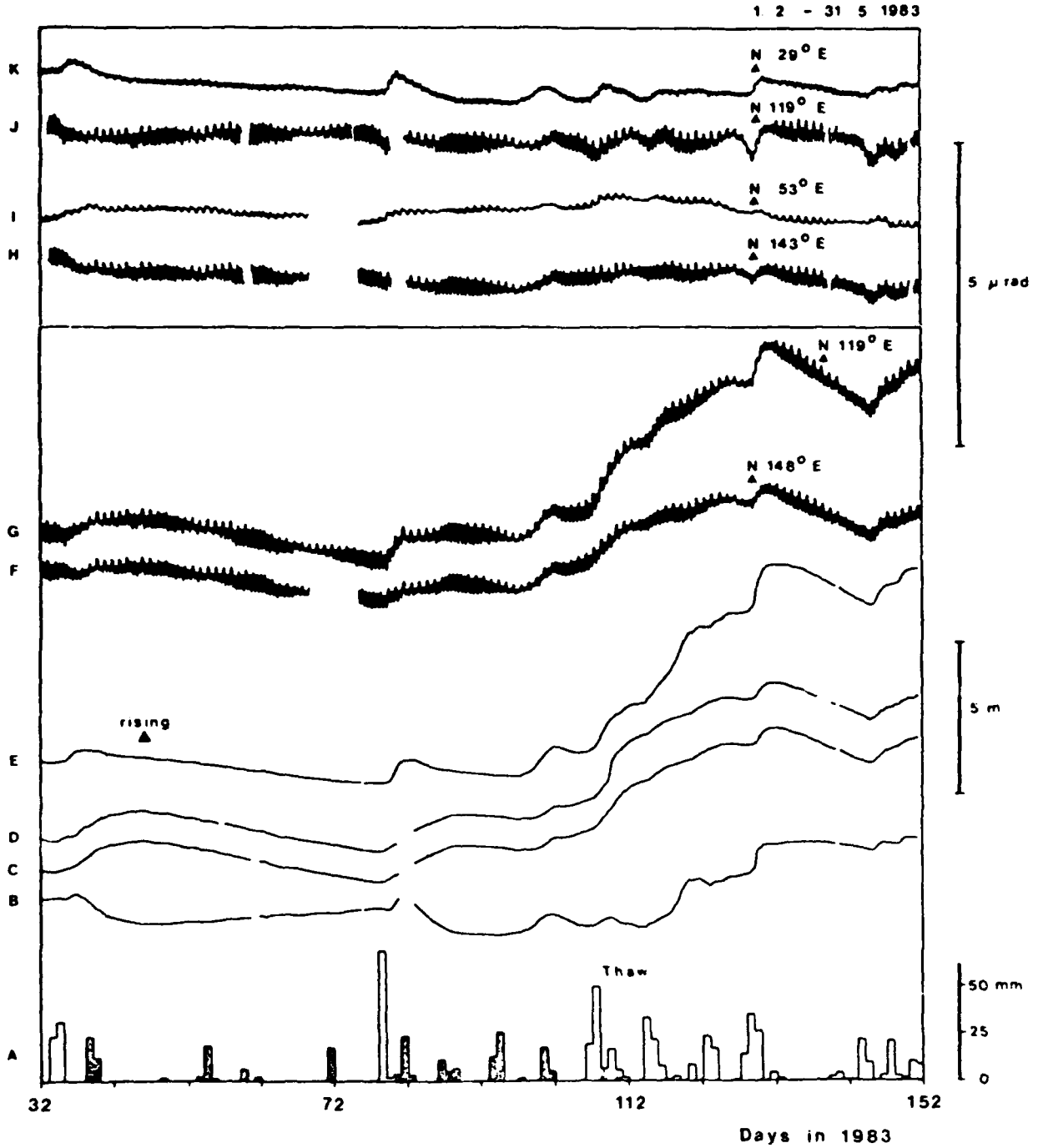
1 2 - 31 5 1983
K
N 29° E
J
N 119° E
I
N 53° E
H
N 143° E
5 μ rad
N 119° E
N 148° E
G
F
5 m
rising
E
D
C
B
Thaw
50 mm
25
0
A
32
72
112
152
Days in 1983

FIGURE 4

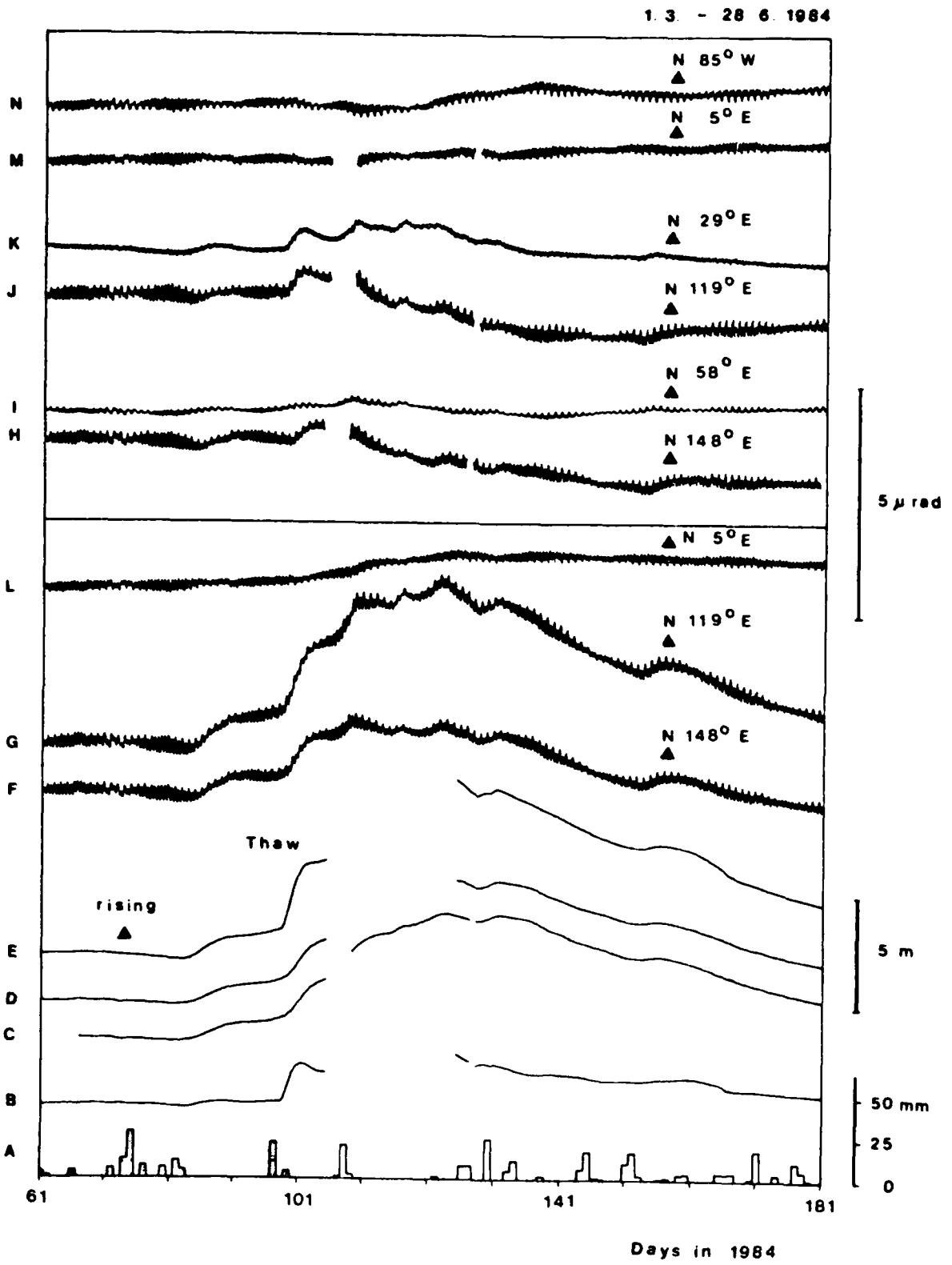
1. 3. - 28 6. 1984
N 85° W
N 5° E
N 29° E
N 119° E
N 58° E
N 148° E
N 5° E
N 119° E
N 148° E
N
M
K
J
I
H
L
G
F
E
D
C
B
A
5 μ rad
5 m
50 mm
25
0
Thaw
rising
61
101
141
181
Days in 1984

FIGURE 5

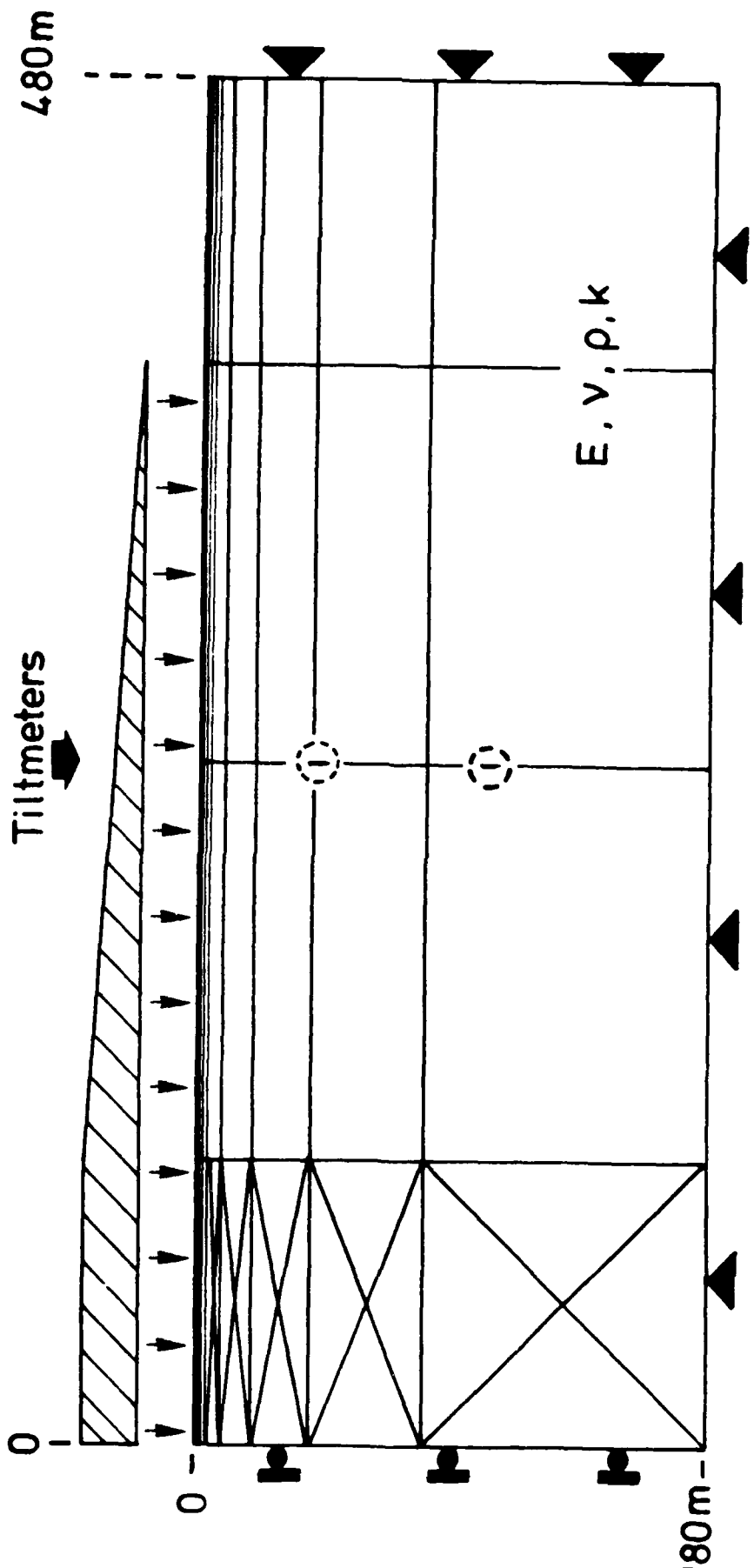

FIGURE 6

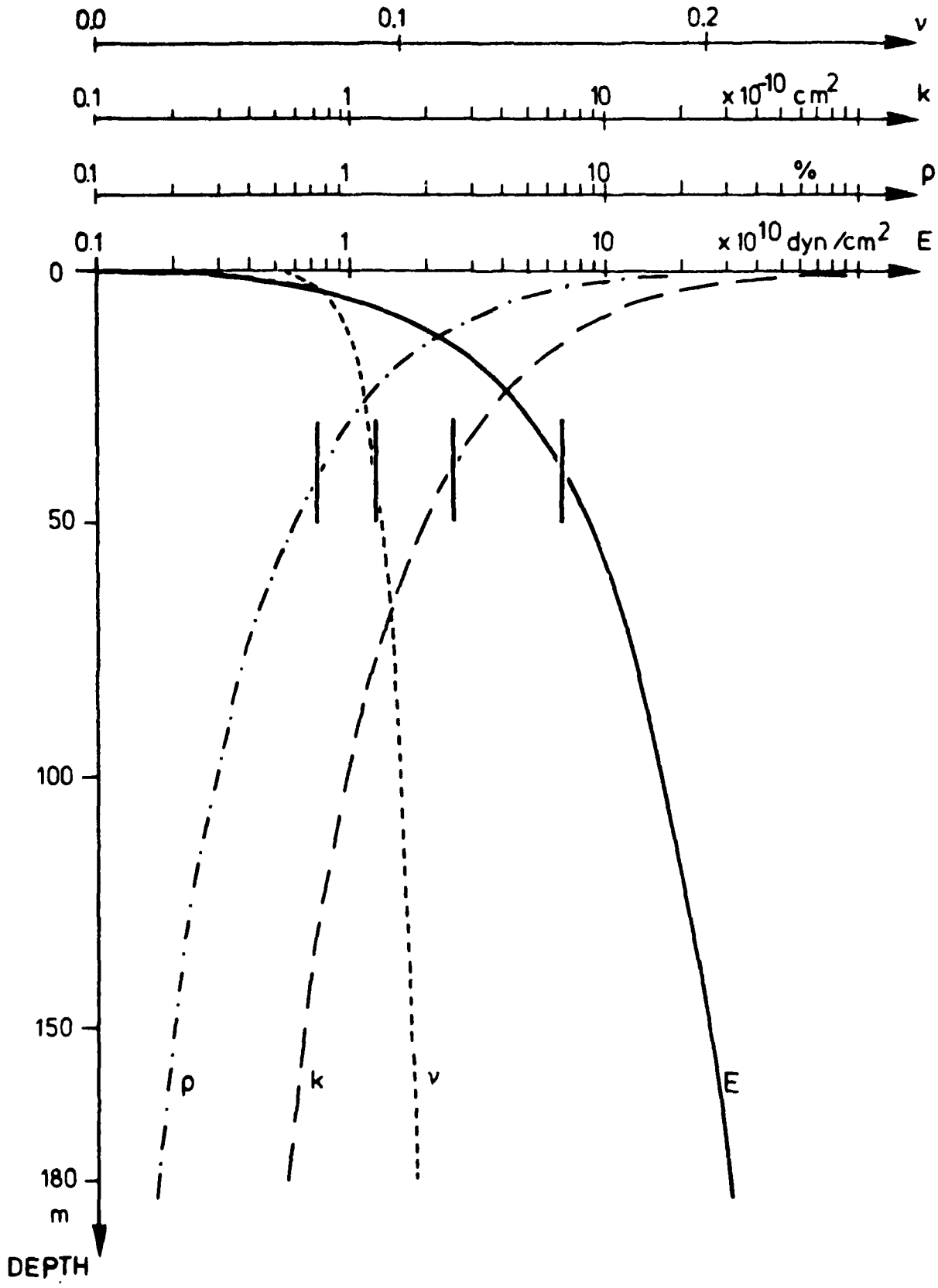
0.0
0.1
0.2
ν
0.1
1
10
x 10⁻¹⁰ cm²
k
0.1
1
10
%
ρ
0.1
1
10
x 10¹⁰ dyn /cm²
E
0
50
100
150
180
m
DEPTH
ρ
k
ν
E

FIGURE 7

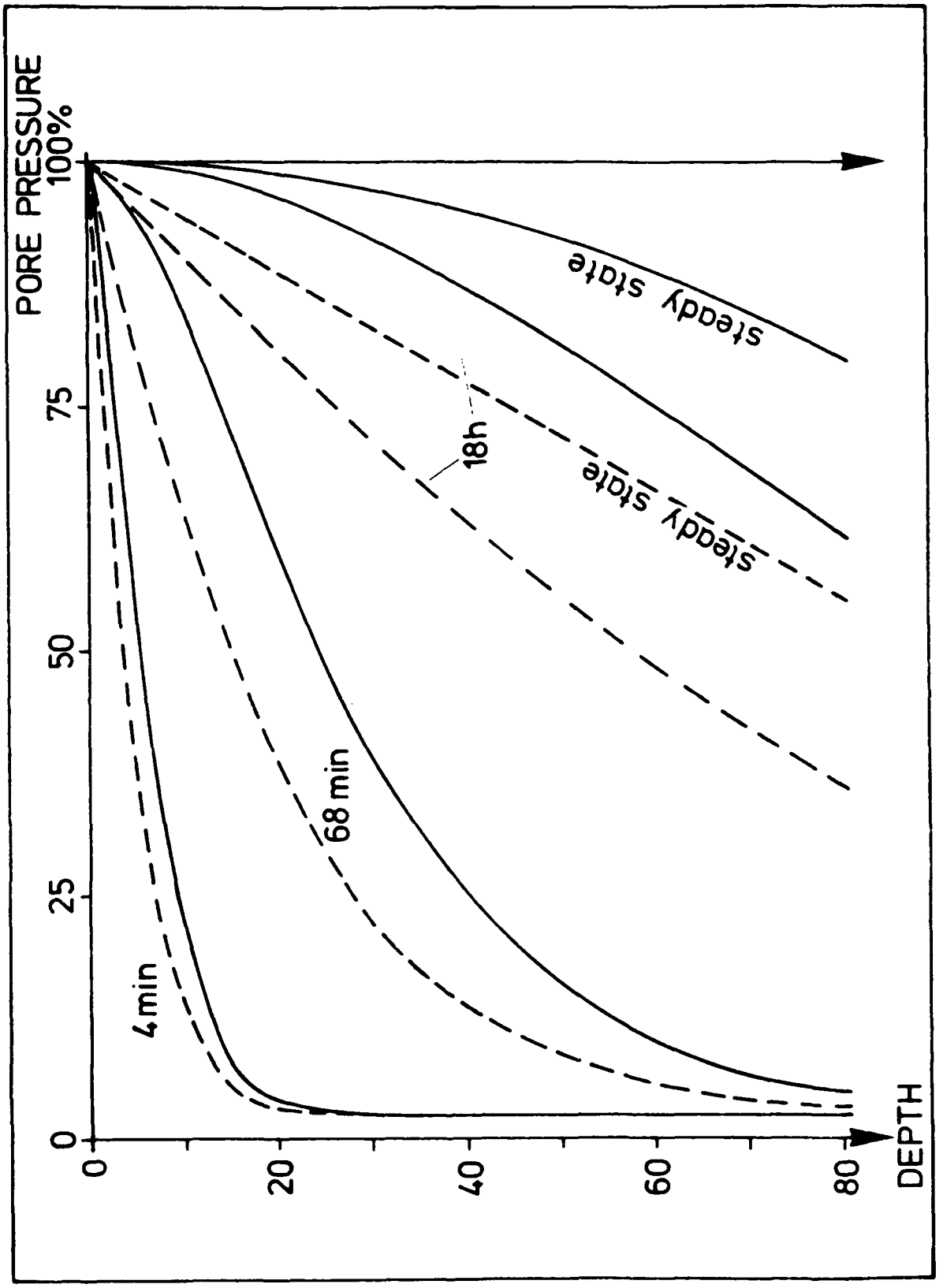
PORE PRESSURE
100%
75
50
25
0
0
20
40
60
80
DEPTH
4 min
68 min
18h
steady state
steady state

FIGURE 8

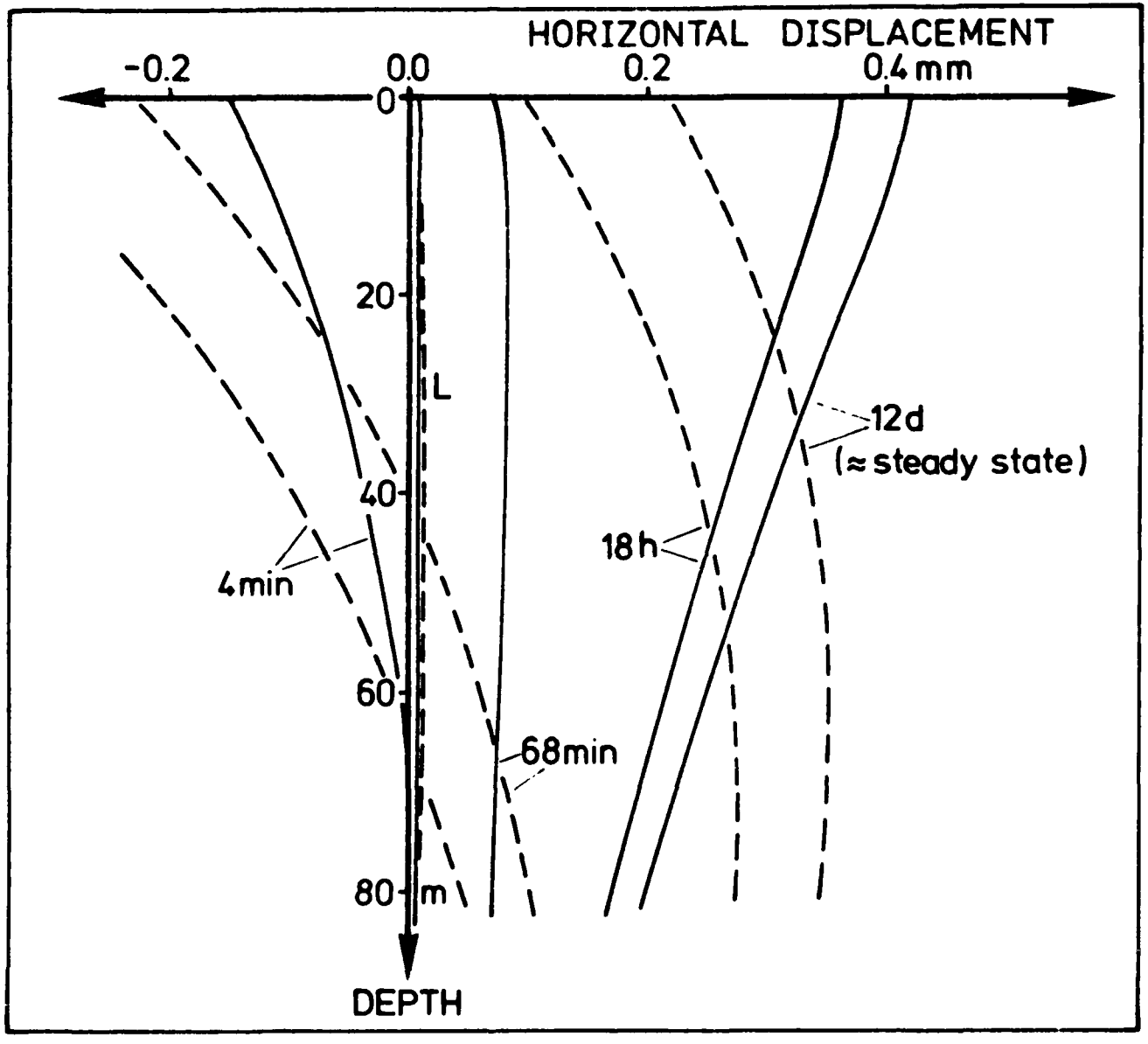
HORIZONTAL DISPLACEMENT
-0.2
0.0
0.2
0.4 mm
0
20
40
60
80
m
L
DEPTH
4min
68min
18h
12d
(≈ steady state)

FIGURE 9

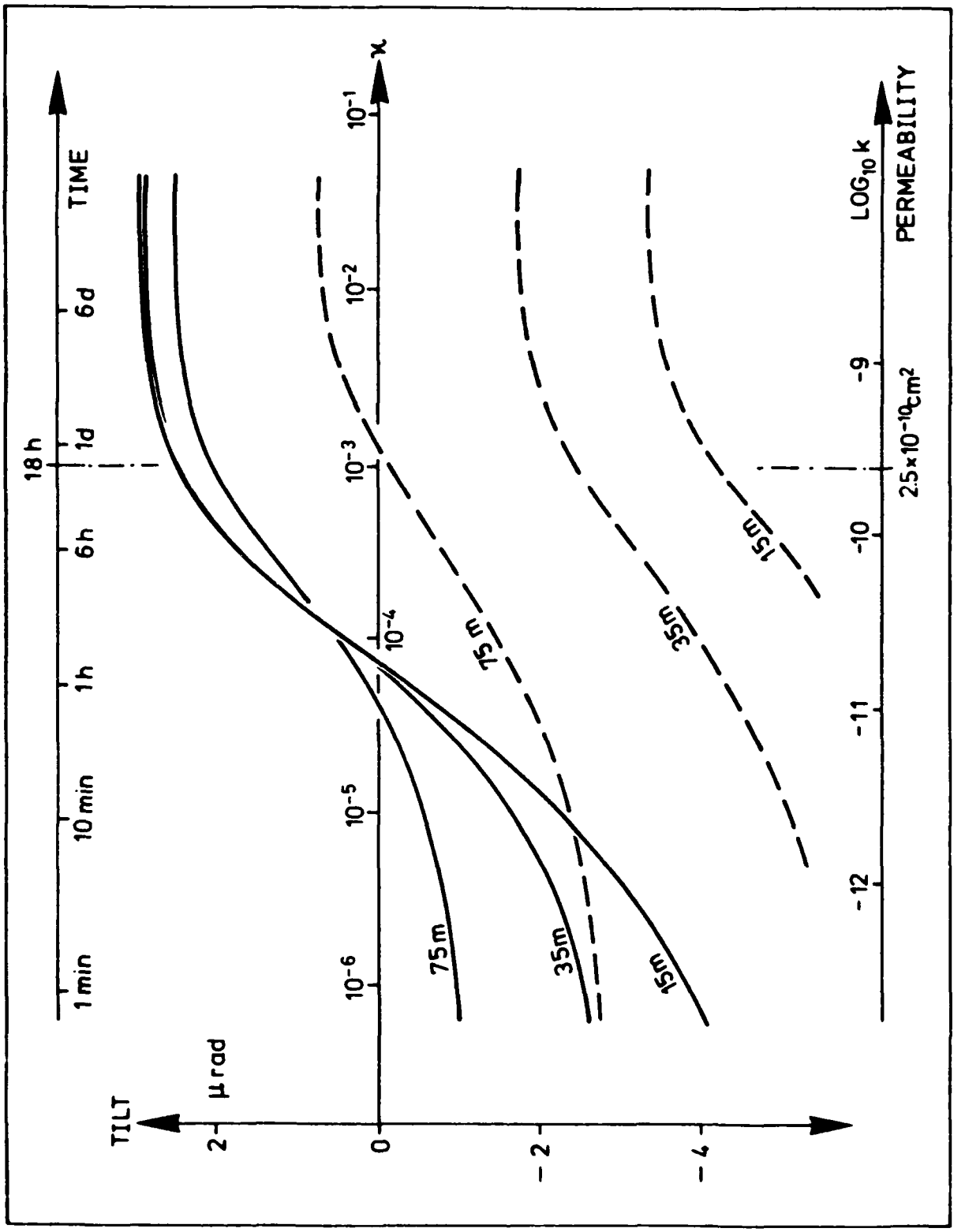
TILT
μrad
2
0
-2
-4
1 min
10 min
1 h
6 h
18 h
1 d
6 d
TIME
10⁻⁶
10⁻⁵
10⁻⁴
10⁻³
10⁻²
10⁻¹
κ
75m
35m
15m
75m
35m
15m
-9
-10
-11
-12
LOG10 k
PERMEABILITY
2.5×10⁻¹⁰cm²

FIGURE 10